GEOLOGICAL SURVEY OF CANADA
COMMISSION GÉOLOGIQUE DU CANADA

Current Research 1998-D
Recherches en cours 1998-D

EASTERN CANADA AND NATIONAL AND GENERAL PROGRAMS

EST DU CANADA ET PROGRAMMES NATIONAUX ET GÉNÉRAUX

Natural Resources Canada
Ressources naturelles Canada

Canada

NOTICE TO LIBRARIANS AND INDEXERS

The Geological Survey's Current Research series contains many reports comparable in scope and subject matter to those appearing in scientific journals and other serials. Most contributions to Current Research include an abstract and bibliographic citation. It is hoped that these will assist you in cataloguing and indexing these reports and that this will result in a still wider dissemination of the results of the Geological Survey's research activities.

AVIS AUX BIBLIOTHÉCAIRES ET PRÉPARATEURS D'INDEX

La série Recherches en cours de la Commission géologique contient plusieurs rapports dont la portée et la nature sont comparables à ceux qui paraissent dans les revues scientifiques et autres périodiques. La plupart des articles publiés dans Recherches en cours sont accompagnés d'un résumé et d'une bibliographie, ce qui vous permettra, on l'espère, de cataloguer et d'indexer ces rapports, d'où une meilleure diffusion des résultats de recherche de la Commission géologique.

GEOLOGICAL SURVEY OF CANADA
COMMISSION GÉOLOGIQUE DU CANADA

CURRENT RESEARCH 1998-D

EASTERN CANADA AND NATIONAL AND GENERAL PROGRAMS

RECHERCHES EN COURS 1998-D

EST DU CANADA ET PROGRAMMES NATIONAUX ET GÉNÉRAUX

1998

Catalogue No. M44-1998/4E
ISBN 0-660-17301-8

Available in Canada from
Geological Survey of Canada offices:

601 Booth Street
Ottawa, Ontario K1A 0E8

3303-33rd Street N.W.
Calgary, Alberta T2L 2A7

101-605 Robson Street
Vancouver, B.C. V6B 5J3

or from

Canadian Government Publishing
Public Works and Government Services Canada
Ottawa, Ontario K1A 0S9

A deposit copy of this publication is also available for reference
in selected public libraries across Canada

Price subject to change without notice

Cover illustration

Limestone beds of the Rivière Ouelle Formation in the Grande Vallée area. See paper by Chi and Lavoie, this volume. Photograph by D. Lavoie. GSC 1997-85

Photo en page couverture

Couches de calcaire de la Formation de Rivière Ouelle dans la région de Grande Vallée. Cette photographie se rapporte à l'article de Chi et Lavoie dans le présent volume. Photo : D. Lavoie, GSC 1997-85

Separates

A limited number of separates of the papers that appear in this volume are available by direct request to the individual authors. The addresses of the Geological Survey of Canada offices follow:

Geological Survey of Canada
601 Booth Street
Ottawa, Ontario
K1A 0E8
(FAX: 613-996-9990)

Geological Survey of Canada (Calgary)
3303-33rd Street N.W.
Calgary, Alberta
T2L 2A7
(FAX: 403-292-5377)

Geological Survey of Canada (Pacific)
101-605 Robson Street
Vancouver, British Columbia
V6B 5J3
(FAX: 604-666-1124)

Geological Survey of Canada (Pacific)
P.O. Box 6000
9860 Saanich Road
Sidney, British Columbia
V8L 4B2
(FAX: 604-363-6565)

Geological Survey of Canada (Atlantic)
Bedford Institute of Oceanography
P.O. Box 1006
Dartmouth, Nova Scotia
B2Y 4A2
(FAX: 902-426-2256)

Quebec Geoscience Centre/INRS
2535, boulevard Laurier
C.P. 7500
Sainte-Foy (Québec)
G1V 4C7
(FAX: 418-654-2615)

Tirés à part

On peut obtenir un nombre limité de «tirés à part» des articles qui paraissent dans cette publication en s'adressant directement à chaque auteur. Les adresses des différents bureaux de la Commission géologique du Canada sont les suivantes :

Commission géologique du Canada
601, rue Booth
Ottawa (Ontario)
K1A 0E8
(facsimilé : 613-996-9990)

Commission géologique du Canada (Calgary)
3303-33rd Street N.W.,
Calgary, Alberta
T2L 2A7
(facsimilé : 403-292-5377)

Commission géologique du Canada (Pacifique)
101-605 Robson Street
Vancouver, British Columbia
V6B 5J3
(facsimilé : 604-666-1124)

Commission géologique du Canada (Pacifique)
P.O. Box 6000
9860 Saanich Road
Sidney, British Columbia
V8L 4B2
(facsimilé : 604-363-6565)

Commission géologique du Canada (Atlantique)
Institut océanographique Bedford
P.O. Box 1006
Dartmouth, Nova Scotia
B2Y 4A2
(facsimilé : 902-426-2256)

Centre géoscientifique de Québec/INRS
2535, boulevard Laurier
C.P. 7500
Sainte-Foy (Québec)
G1V 4C7
(facsimilé : 418-654-2615)

CONTENTS

Characteristics of the Taconic orogenic front, northeastern Quebec Appalachians

Gregory Lynch
Quebec Geoscience Centre, Sainte-Foy

Lynch, G., 1998: Characteristics of the Taconic orogenic front, northeastern Quebec Appalachians; in Current Research 1998-D; Geological Survey of Canada, p. 1-9.

Abstract: The Taconic orogenic front in the Humber Zone of the northeastern Quebec Appalachians features large-scale fault propagation folds above blind thrust tips in synorogenic flysch of the Middle Ordovician Cloridorme Group. Out-of-sequence high-angle anticlinal breakthrough and thrust juxtaposition of upright units onto strongly overturned footwall units are characteristic. However, submarine fan progradation in the lower Cloridorme Group may be interpreted to reflect faulting in a regular forward-propagating thrust system during early flysch sedimentation. Underlying the southwest limit of the Cloridorme Group, the lowest exposed structural level (Logan's Line and Cap-Chat Mélange) contains a thick zone of extensional shear overprinting earlier thrust structures. The net excision of a substantial portion of the Ordovician stratigraphy along this fault is interpreted to indicate that a significant period of extension and tectonic backsliding occurred late in the evolution of the Taconic Orogen.

Résumé : Le front orogénique taconique dans la Zone de Humber, dans le nord-est des Appalaches du Québec, est caractérisé par de grands plis fortement déversés au-dessus de chevauchements aveugles situés dans les flyschs synorogéniques du Groupe de Cloridorme (Ordovicien moyen). Le recoupement d'anticlinaux par des chevauchements hors-séquence et la juxtaposition d'unités dressées au-dessus d'unités inversées sont caractéristiques. Par contre, une progradation de cônes sous-marins dans la partie inférieure du Groupe de Cloridorme refléterait la formation de failles dans un système de chevauchement à propagation normale au début de la sédimentation des flyschs. L'ensemble structural (Ligne de Logan et Mélange de Cap-Chat) sous la limite sud-ouest du Groupe de Cloridorme contient une zone épaisse de cisaillement par distension superposée sur les chevauchements. L'absence d'une grande portion de la série ordovicienne le long de cette faille témoignerait d'une importante période de distension vers la fin de l'orogénie taconique.

INTRODUCTION

The Appalachian Humber Zone forms a 1700 km long belt in Canada, extending along western Newfoundland, through Gaspésie to the southwest, and into the Eastern Townships of southeastern Quebec. Underlying this zone are Cambrian-Ordovician rift and passive margin shelf and slope depositional settings from the Laurentian margin of the ancient Iapetus Ocean. The belt is characterized by a fold-and-thrust style of deformation and deposition of thick successions of Late Ordovician syntectonic foreland flysch sedimentary rocks, in what is usually termed the Taconic Orogen. Recently, geological studies and research have concentrated on the southwestern Newfoundland segment of the Humber Zone (e.g. Stockmal and Waldron, 1993), and renewed hydrocarbon exploration has also been spurred on by success in this region (e.g. Cooper et al., 1997). Detailed cross-sections and stratigraphic analysis based on new mapping and seismic data have resulted in significant advances. In contrast to this, the Gaspé segment of the Humber Zone has received less attention lately. Although a comprehensive summary of the stratigraphic and geological framework was put forward by Slivitzky et al. (1991), only a few schematic cross-sections are presented and they are based on structural concepts developed over twenty years ago (e.g. St-Julien and Hubert, 1975). The objective of this research is to augment the structural database of the northeastern Quebec Humber Zone along a number of transects, in order to more accurately define the structural style of the region. Preliminary findings are presented from the Grande-Vallée, Marsoui, and Matane areas (Fig. 1). These results will better enable direct comparisons with southwestern Newfoundland, and with other well known foreland flysch basins and fold-thrust belts.

STRATIGRAPHY AND STRUCTURE

Northwest Grande-Vallée

The Grande-Vallée sheet (22H/03, 1:50 000 scale) in the northern Gaspésie region (Fig. 1), was mapped and compiled by Lachambre and Brisebois (1990), and the geology is described in Slivitzky et al. (1991), with modest revisions proposed by Lynch and Arsenault (1997). The area was chosen for study because it provides a relatively complete section of Humber Zone stratigraphy for this region, spanning the Neoproterozoic Shickshock Group, the Cambrian l'Orignal Formation and Trois-Pistoles Group, the Cambrian-Ordovician Romieu Formation, and a thick succession of Ordovician strata including the Rivière Ouelle, Tourelle, and Deslandes formations, and the Cloridorme Group at the top of the succession. Collectively these units define the Quebec Supergroup, which has a total thickness of approximately 10-12 km (Slivitzky et al., 1991). Three broad depositional regimes are recognized for the supergroup (e.g. Slivitzky et al., 1991; Lavoie, 1997; Lynch and Arsenault, 1997): (1) rift and passive margin continental slope clastic-dominated assemblages, defined by the Shickshock Group, l'Orignal Formation, and Trois-Pistoles Group; (2) passive margin upper- to lower-slope–basin-plain shale- and carbonate-dominated assemblages, comprising the Romieu and Rivière

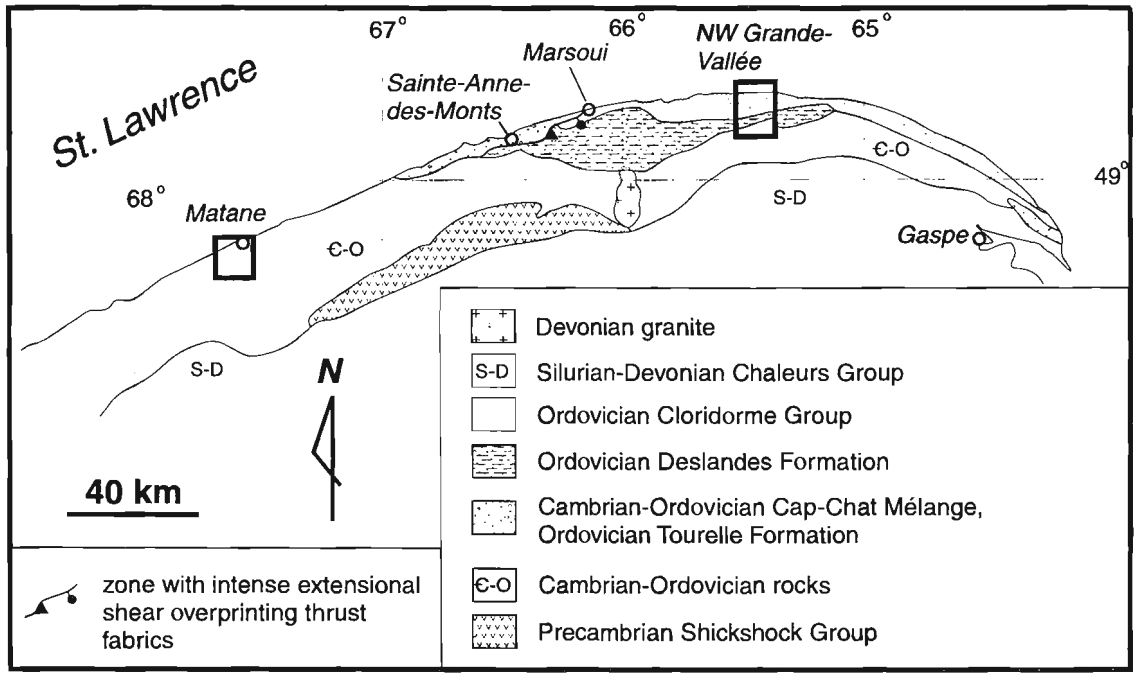

Figure 1. *Location map of the Humber Zone and study areas: Grande-Vallée, Marsoui, and Matane (modified from Slivitzky et al., 1991).*

Ouelle formations (e.g. Lavoie, 1997); and (3) a thick upper flysch package marking the onset of Taconic deformation, which includes the Tourelle and Deslandes formations, as well as the Cloridorme Group (e.g. Kessler et al., 1995). North-directed thrust imbrication and telescoping during the Late Ordovician Taconic Orogeny, likely along a ramp with a steep taper, resulted in the exposure of all these units at the same erosional level, with the oldest rocks to the south and the youngest to the north (Lynch and Arsenault, 1997).

Detailed mapping was undertaken in the northwest sector of the Grande-Vallée sheet (Fig. 2). A cross-section was constructed from the pretectonic carbonate rocks of the Rivière Ouelle Formation in the south, through the entire syntectonic flysch package and into the Cloridorme Group to the north (Fig. 3). The Rivière Ouelle Formation consists predominantly of interbedded carbonate rocks and shale, featuring thin beds of limestone or dolostone, including calcilutite, as well as minor fine-grained quartz-rich arenite. Thick carbonate beds are rare. Distinct horizons of 'in situ' carbonate conglomerate and breccia also occur but are widely scattered. Primary sedimentary structures may include crossbedding, load structures at shale-carbonate rock contacts, and mud rip-up clasts. Slivitzky et al. (1991) consider the Rivière Ouelle Formation in the Gaspé region to be well dated by Early Ordovician graptolites and estimate its thickness at approximately 1000 m.

The Tourelle Formation is the lowermost of the main flysch deposits (Kessler et al., 1995) and is reported to concordantly overlie the Rivière Ouelle Formation in the Rivière-du-Loup area to the southwest (Vallières, 1984). Detritus provenance studies for this formation in the type area suggest that sedimentation coincided with Arenig to Llanvirnian early Taconic deformation and ophiolite obduction (e.g. Hiscott, 1978). In the map area, the Tourelle Formation consists of thickly bedded lithic wacke, siltstone, and shale typically in approximately equal proportions. The base of the coarser grained beds features load structures and flute casts, and normal graded bedding is common. Clasts in the wackes range up to pebble size, and include quartz, feldspar, unidentified lithic fragments, chert, carbonate, and detrital mica (mostly biotite). Regionally the Tourelle Formation is considered to represent arc-derived gravity flow deposits on small foreland slope basins (Hiscott, 1978; Kessler et al., 1995). It is apparently 500-1000 m thick (Hiscott, 1978; Slivitzky et al., 1991), and its thickness seems to vary significantly along strike. In the study area (Fig. 2), the surface covered by the Tourelle Formation was previously assigned to the Deslandes Formation (Lachambre and Brisebois, 1990); this however is inconsistent with the abundance of thickly bedded coarse-grained lithic wacke observed in the unit.

The Deslandes Formation (Slivitzky et al., 1991) features thinly bedded medium- to fine-grained quartz arenite or wacke, with siltstone and shale interbeds. Shale-dominated sections may contain thin chert horizons. Thin grey carbonate beds show well developed crosslamination in coarse-grained limestone as well as graded bedding. Map-scale patterns (Fig. 2) (Lynch and Arsenault, 1997) indicate that the Deslandes Formation overlies the Tourelle Formation. The contact may be gradational and some overlap seems likely; however the relationships are uncertain because of limited exposure. Graptolites from the Deslandes Formation in the map area indicate a middle Ordovician age, slightly younger than that recorded for the Tourelle Formation in its type area (Slivitzky et al., 1991). The total thickness of the Deslandes Formation east of the study area is 1380 m; work by Kessler et al. (1995) in this area suggests that the Deslandes Formation was deposited as thin basin-plain forebulge-derived turbidite.

Two of the six formations that define the Cloridorme Group according to Slivitzky et al. (1991) occur in the coastal area at the north end of the map (Fig. 2) (Lachambre and Brisebois, 1990). The Cloridorme Group is Middle to Late Ordovician (Caradoc) (Slivitzky et al., 1991). Note that a group designation for the Cloridorme agrees with the suggestion of Biron (1974), and that total thickness estimates for the group range from 3447 m (Kessler et al., 1995) to over 5700 m (Slivitzky et al., 1991). Coastal exposures and steep stream sections provide good access to both the Gros Morne and Manche-d'Épée formations. The Gros Morne Formation is characterized by the dominance of thickly bedded coarse-grained wacke (60-80 per cent) and subordinate thin interbeds of shale and siltstone (20-40 per cent). Sandstone beds are typically 0.5-2 m thick, and show graded bedding with pebbly bases and well developed flutes. Load structures, tool marks, and crossbedding also occur. Some clastic units contain a carbonate matrix, and minor dolostone occurs. Measured sections and map pattern estimates suggest a minimum thickness of 245 to 450 m for the Gros Morne Formation (Slivitzky et al., 1991), and in the study area it may be as much as 600 m (Fig. 3). The Manche-d'Épée Formation is dominated by mudstone, siltstone, and homogeneous fine-grained clastic units. The clastic rocks are variably carbonate bearing, and calcilutite or dololutite occurs locally. The rocks are typically thinly bedded, and silty horizons usually show well developed crossbedding. Measured sections of the Manche-d'Épée Formation in the type area are at least 829 m thick (Slivitzky et al., 1991). In the type section immediately to the southwest, the Gros Morne Formation conformably overlies the Manche-d'Épée Formation with a gradual contact (Slivitzky et al., 1991). However, in the Grande-Vallée area (Fig. 2), upright beds of the Gros Morne Formation occur above strongly overturned beds of the Manche-d'Épée Formation; clearly, beds of the Gros Morne Formation have been thrust over the Manche-d'Épée Formation (Fig. 2, 3). The contact between the two is not exposed in the immediate area; however a small syncline with upright beds (Fig. 2) suggests that the Gros Morne Formation occurs stratigraphically above the Manche-d'Épée Formation. It should be stressed at this point that some formations in the Cloridorme Group overlap laterally (e.g. Manche-d'Épée and Pointe-à-la-Frégate formations, Slivitzky et al., 1991), and it is proposed here on the basis of field and map observations that the Gros Morne and Manche-d'Épée formations may overlap laterally and represent facies changes within a submarine fan setting. Furthermore, Slivitzky et al. (1991) consider that the Cloridorme is a formation rather than a group because they acknowledge difficulties in tracing units laterally. The apparent climb or progradation of the Gros Morne Formation from a position below the Manche-d'Épée Formation to a position

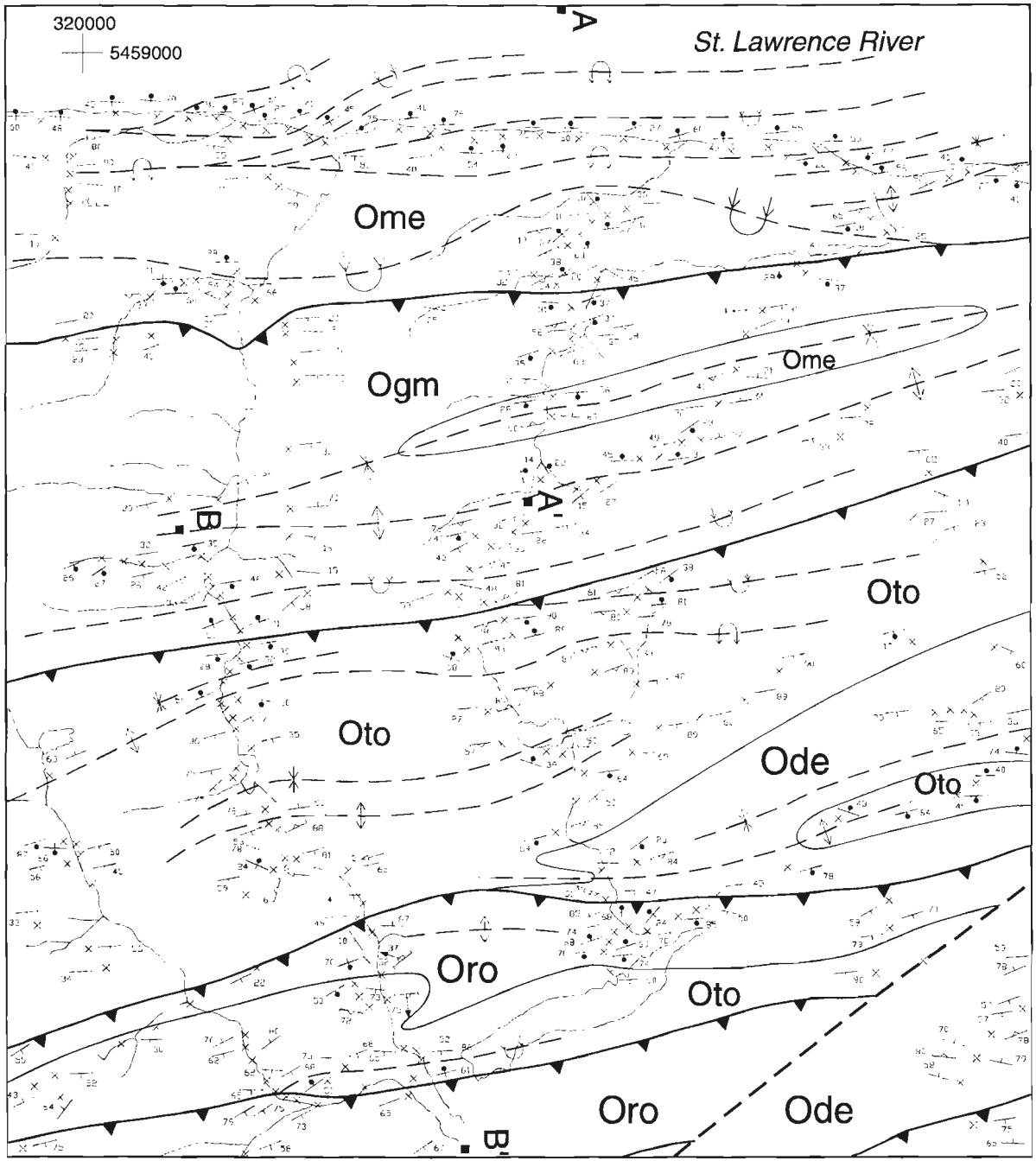

Figure 2. *Geology of the northwest Grande-Vallée map sheet (22H/3), updated from Lynch and Arsenault (1997) and Lachambre and Brisebois (1990). Units are described in detail in the text, and cross-section A-A'–B-B' is shown in Figure 3.*

above towards the west is consistent with regional paleocurrent measurements from the lower Cloridorme Group that indicate general westward transportation (Slivitzky et al., 1991; Kessler et al., 1995) and overall major westward submarine fan progradation (Kessler et al., 1995).

The north-south cross-section in Figure 3 shows the structure in the northwestern Grande-Vallée map area. A significant new thrust is now recognized within the Cloridorme Group north of Logan's Ligne, which in this area marks the southern margin of the Cloridorme Group. Overturned beds, and overturned axial planes to inclined folds, dip predominantly to the south and are widespread in all flysch deposits (Fig. 2), indicating a strong northward vergence for the folds and thrusts. As mentioned above, the thrust within the Cloridorme Group can be traced by the juxtaposition of upright beds onto overturned beds in the footwall units. This basic geometry is characteristic of anticlinal breakthrough where thrusts propagate upwards into the overturned limbs of fault propagation folds, which are genetically linked to the thrusting (Suppe and Medwedeff, 1990). This key geometric relationship is recorded at several places within the Grande-Vallée map area (Lachambre and Brisebois, 1990; Lynch and Arsenault, 1997), as well as within the Cloridorme Group in the surrounding region, and along segments of Logan's Line (Slivitzky et al., 1991), suggesting that this structural style is widespread. In addition, strongly overturned fold limbs are characteristic of fault propagation folds that occur above blind thrust tips; thus, the widespread occurrence of large panels of overturned flysch may suggest that blind thrust tips occur in the subsurface beneath the Cloridorme Group, such as in Figure 3.

Marsoui

Outcrops were mapped along Highway 132 between Marsoui and Saint-Anne-des-Monts, to investigate the nature of the transition between the Cloridorme Group and the Cap-Chat Mélange (Logan's Line). The two units are in fault contact in this area (Logan's Line), and the contact is exposed along the coast immediately east of Marsoui. The fault has been described as a thrust that transported overturned upper Cloridorme Group rocks towards the northwest above the Cap-Chat Mélange (Slivitzky et al., 1991). However, the nature of this fault is enigmatic as it places younger units over older rocks. The complete characterization of this apparently significant structure requires further investigation.

Here the Cloridorme Group consists of the Roches Penchées Formation, the highest stratigraphic unit within the group. It is composed predominantly of thick beds of coarse-grained wacke, with thinner interbeds of shale and minor silty limestone and calcilutite. A variety of sedimentary structures indicate gravity flow during deposition and likely turbidity currents. The Roches Penchées Formation is similar to the Gros Morne Formation found lower in the Cloridorme Group in that thickly bedded wacke clearly predominates over shale. However, the Roches Penchées Formation is distinct from

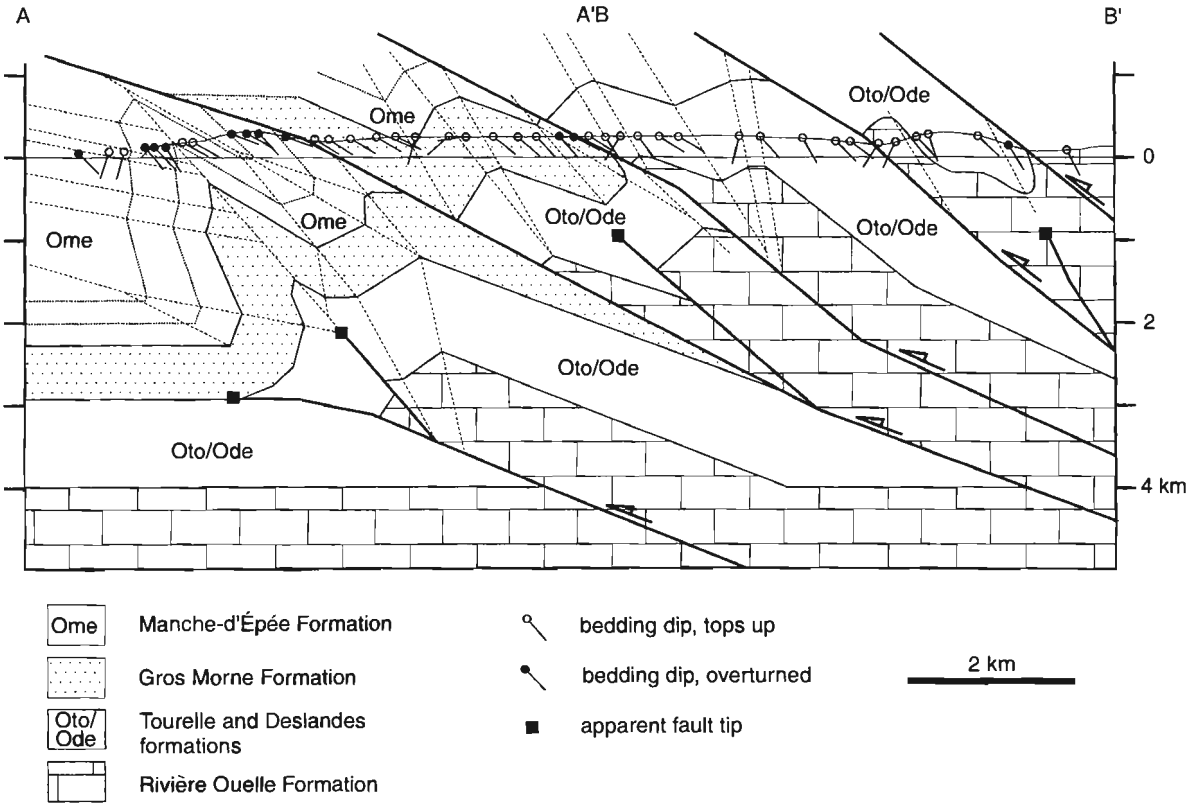

Figure 3. *North-south cross-section through the northwest corner of the Grande-Vallée map sheet (22H/3), with location of A-A'–B-B' shown on Figure 2.*

other formations within the Cloridorme Group since paleocurrent indicators are consistently towards the east, marking an abrupt reversal of the direction of transportation and the sediment source region (Slivitzky et al., 1991; Kessler et al., 1995). Bedding attitudes define large north-verging folds (Lachambre and Brisebois, 1990). Intraformational imbricate thrust faults and duplex structures also demonstrate north-northwest transportation and structural thickening within the unit (Fig. 4a). The Roches Penchées Formation is estimated to be approximately 1900 m thick (Slivitzky et al., 1991; Kessler et al., 1995).

As a regional map unit, the Cap-Chat Mélange remains a loosely defined unit and is somewhat problematical as both primary sedimentary structures and secondary tectonic structures have been used to define and outline it extent (see discussion in Slivitzky et al., 1991). Stratigraphically, the Cap-Chat Mélange is comprised of rocks derived predominantly from the Upper Cambrian Ladrière or upper Grosses Roches formations (see Lavoie, 1998) and the conformably overlying Ordovician Tourelle Formation (Hiscott, 1978, 1980), and may also include rocks from the Rivière Ouelle and Deslandes formations (Slivitzky et al., 1991). The Tourelle Formation has been extensively studied in this area (Hiscott, 1978, 1980) and is dominated by coalesced marine mid-fan deposits accumulated along an unstable foredeep trough during early development of the Taconic Orogeny. Olistoliths and olistostromes with spectacular soft-sediment deformation features are described by Hiscott (1980) from coastal exposures; however, transported slabs are tens of metres in size and do not form mapple units for possible subdivision of the Tourelle Formation.

Although the fault (Logan's Line) that separates the Cap-Chat Mélange from the Roches Penchées Formation is a sharp boundary, deformation features relating to it extend well into the footwall unit, defining a broader shear zone (Fig. 4b, c, d). Immediately west-southwest of Marsoui, interbedded sandstone and shale are intensely sheared and have

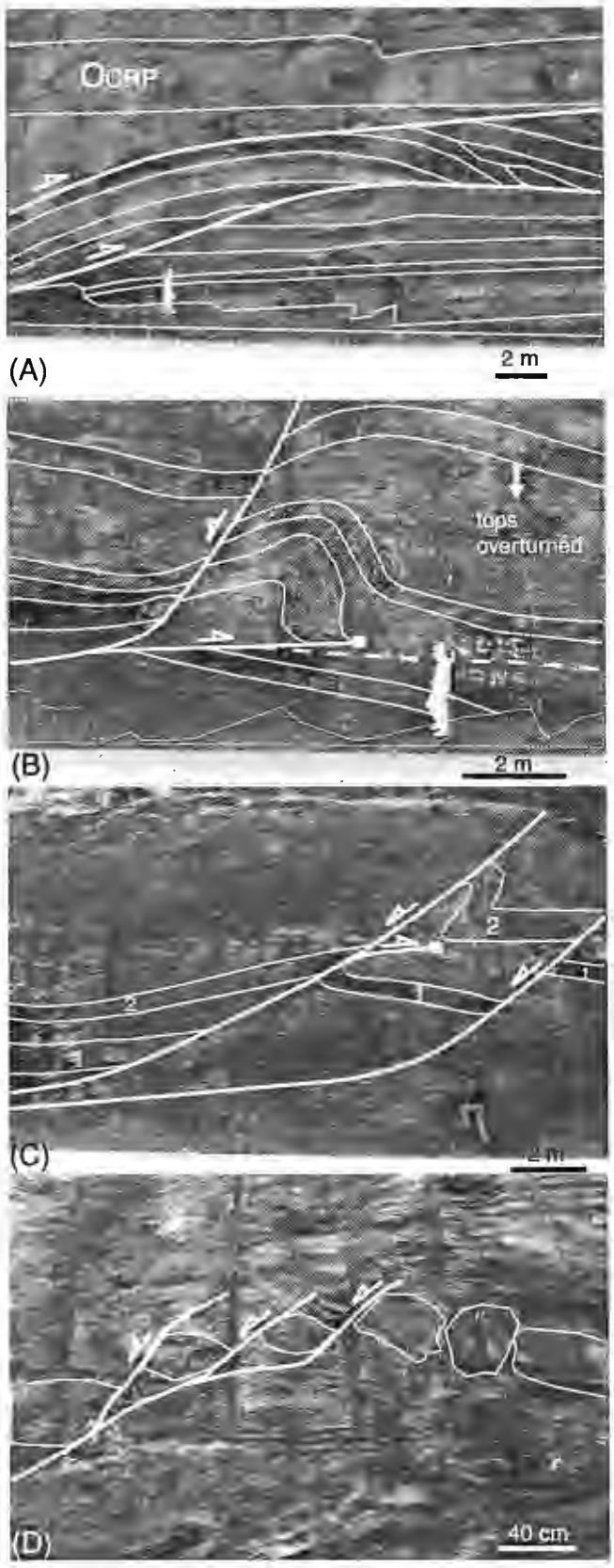

Figure 4.

(A) Outcrop of Roches Penchées Formation along Highway 132, 3.5 km east of Marsoui, showing ramp-and-flat imbricate thrust geometry and fault-bend folding, from a site in the immediate hanging wall of Logan's Line (view towards the southwest). ***(B)*** *Overturned Cap-des-Rosiers Group along Highway 132, 1.6 km west of Marsoui, showing a short thrust segment and a fault propogation fold above a fault tip, truncated by a listric normal fault rooted in an earlier thrust, from a site in the immediate footwall of Logan's Line (view towards the southwest).* ***(C)*** *Extension of outcrop in (b), showing a short thrust segment and a fault propogation fold above a fault tip, truncated by a listric normal fault rooted in an earlier thrust (beds 1 and 2 highlighted to show offset).* ***(D)*** *The intense boudinage of beds due to bedding-parallel extensional shear has resulted in segmentation and the creation of detached blocks.*

been affected by two distinct phases of deformation. Sandstone consists of well sorted medium- to coarse-grained quartz arenite and arkosic sandstone in 10-100 cm thick beds with well developed planar and trough cross-stratification, indicating that the units are overturned. Interbedded siltstone and shale are subordinate to the sandstone. Bitumen-coated fractures are locally concentrated in the outcrops, and thin, black, impregnated, bituminous beds also occur. Units are difficult to assign because of deformation, but the sandstone resemble that from the upper Grosses Roches Formation (see Lavoie, 1998, for regional correlations). Outcrop-scale north-northwest-verging fault propagation folds at the tips of small thrust faults are preserved within the shear zone (Fig. 4b, c). Their juxtaposition onto the overturned limb of a much larger fold structure argues for anticlinal breakthrough of the propagating thrust (e.g. Suppe and Medwedeff, 1990). However, roadside exposures show that these thrusts and fold structures are truncated by a later set of listric normal faults that merge with and are rooted in the earlier thrust structures. Extensional features include the offsetting of adjacent beds demonstrating normal offset, as well as intense boudinage and segmentation of beds throughout much of the outcrop, highlighting bedding-parallel shear (Fig. 4d). Listric bends in normal faults have locally generated roll-over in the truncated sandstone. These late features record south-southwest-directed extension. The fault propogation folds and short thrust segments are the only remnant features diagnostic of the original thrusting event, as most of the remaining structural fabrics relate to extension. The combined effects of early thrusting and later extension or backsliding have resulted in a thick zone of highly sheared rocks along the upper contact of the Cap-Chat Mélange that defines the Logan's Line in this area. If stratigraphic observations were used to assess the relative importance of the two shearing events, then the

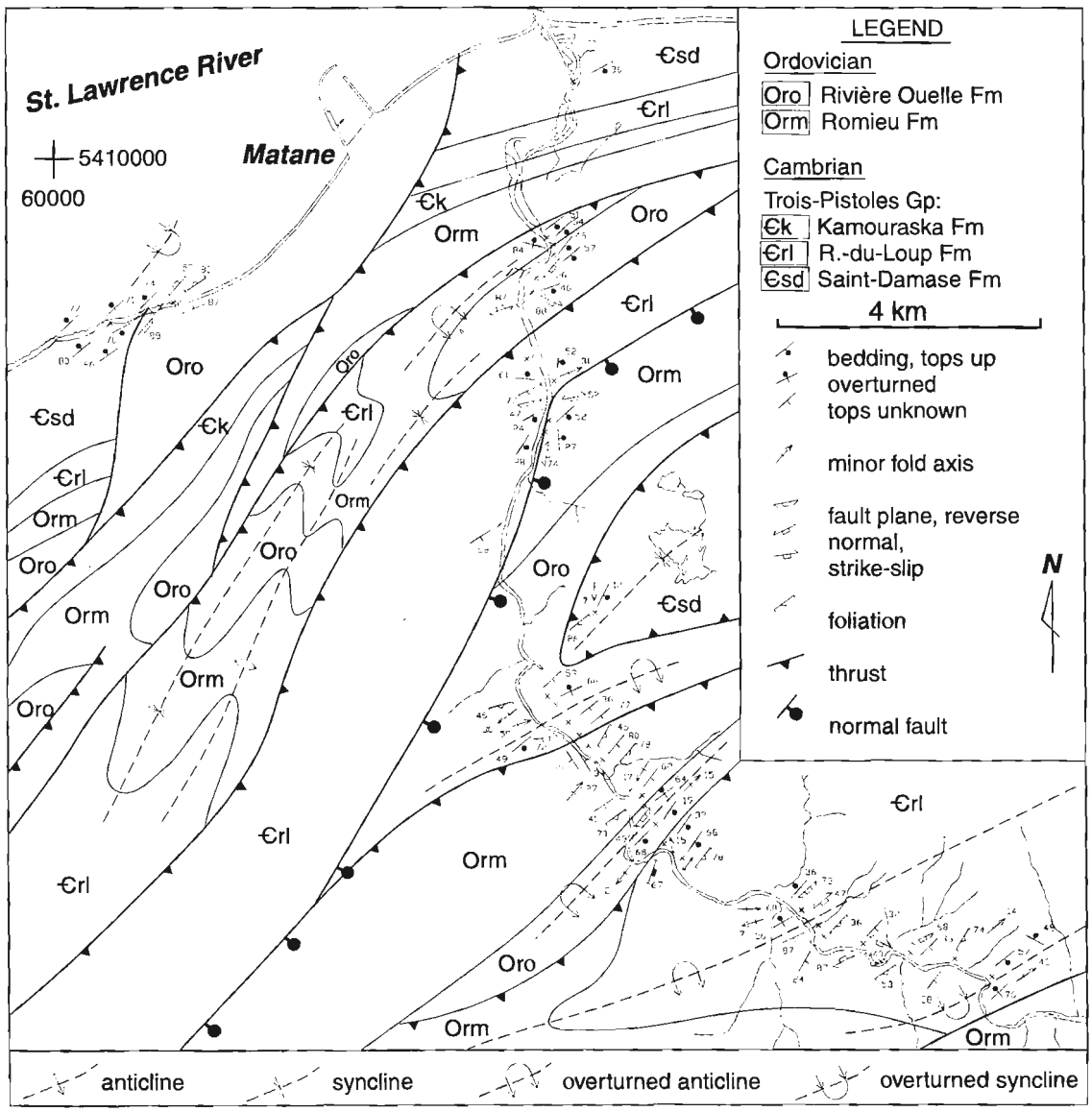

Figure 5. *Geological map of the Matane area (modified from Slivitzky et al., 1991), showing structural data from the transect along the Matane River. Rock units are described in the text.*

creation of a large stratigraphic gap with most of the very thick Cloridorme Group missing, and the apparent excision of part or all of the Ordovician stratigraphy from the surrounding region, would indicate that extensional shear at this site was more significant than compressional shear and thrusting.

Matane

Preliminary results are presented from a north-south transect of roadside outcrops along the Matane River (Fig. 5). Low-lying outcrops from the intertidal zone along the coast were also investigated. Two stratigraphic groupings are recognized: the clastic-dominated Cambrian Trois-Pistoles Group and the overlying carbonate- and shale-dominated Lower Ordovician Romieu and Rivière Ouelle formations. The lowest stratigraphic unit in the Trois-Pistoles Group is the Saint-Damase Formation, which consists of massive coarse-grained wacke that is thickly bedded, or that forms a distinct massive sandstone unit at least 10 m thick in a quarry in the central part of the study area (Fig. 5). This unit was previously assigned to the Tourelle Formation (e.g. see compilation in Slivitzky et al., 1990). However, its very thick massive nature is characteristic of the Saint-Damase Formation. Thick channel forms are also common, particularly along coastal exposures, but here the distinction from the Tourelle Formation is less certain. The Rivière-du-Loup Formation is predominantly shale, with minor limestone and siltstone as well as scattered thin beds of distinct white orthoquartzite; it separates the Saint-Damase Formation from the overlying Kamouraska Formation. The Kamouraska Formation is very distinct and regionally extensive, and consists of thick, white, massive orthoquartzite; it occurs immediately west of the transect (Fig. 5). The overlying Romieu Formation is also shale dominated but contains a higher proportion of siltstone and thinly bedded silty limestone and calcilutite. The Rivière Ouelle Formation consists of abundant calcilutite, some grainstone and rudite or carbonate breccia, and shale and quartz arenite.

Outcrop-scale folds along the transect are strongly overturned and verge consistently towards the north-northwest, while overturned beds at several sites dip southward. Exposed fold hinges show tight folding with steeply to moderately inclined axial planes and moderately east-plunging axes. Outcrop-scale thrusts and apparent map-scale thrust imbrication indicate north-northwest transportation during thrusting. However, numerous outcrops show evidence of late-stage brittle faulting, including sets of normal faults or strike-slip faults. The normal faults dip steeply and show normal offset of adjacent beds and bedding drag along the faults, and contain small breccia zones and shear planes. The strike-slip faults are characterized by subhorizontal striae along shear planes, bedding drag along the faults, sets of conjugate fractures with dextral and sinistral offsets, and bedding boudinage and segmentation. The importance of these late faults is unclear, although the map pattern and the intensity of shear textures observed locally at outcrops indicate that a prominent sinistral fault is present immediately southwest of Matane and that a prominent normal fault exists at the centre of the transect (Fig. 5).

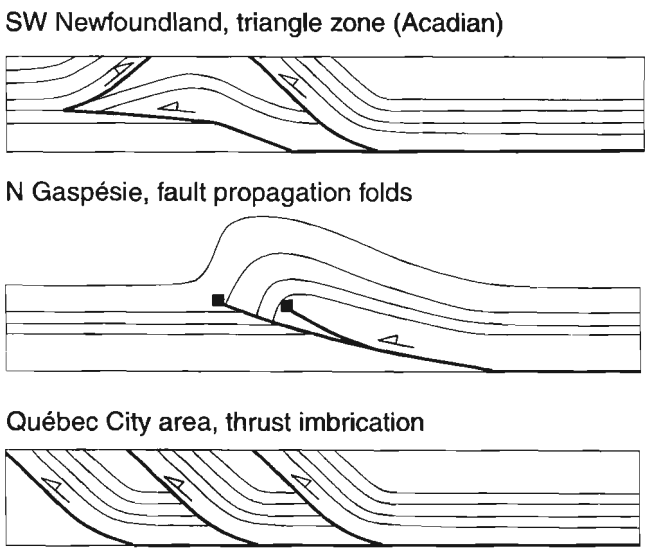

Figure 6. *Schematic representation of different structural styles for mountain fronts (adapted from Vann et al., 1986), applied to the foreland of the Humber Zone, from southwestern Newfoundland to Gaspésie and to the Québec City area.*

DISCUSSION

Orogenic shortening is balanced in foreland domains by the creation of positive relief, denudation, and flysch sedimentation. Movement along individual thrusts dissipates into large fault propagation folds, or into imbricate thrust fans with movement partitioned onto several smaller thrusts, or into triangle zones containing opposite-facing thrusts (Fig. 6). These create a structural style characteristic of mountain fronts (e.g. Vann et al., 1986). The objective of the research presented here was to begin characterizing the style of deformation in the Taconic foreland of the northeastern Quebec Appalachians, and to establish possible links with sedimentation. In Grande-Vallée and the surrounding area, deformation in the flysch package (Tourelle and Deslandes formations, Cloridorme Group) features large-scale fault-propagation folds characterized by strongly overturned north-verging fold limbs, and anticlinal breakthrough juxtaposing upright hanging-wall units onto the overturned footwall limbs. The recognition of this geometric relationship has led to the recognition of a significant new thrust within the Cloridorme Group, north of the Logan's Line. Other blind thrust tips in the subsurface are also inferred to exist from domains of overturned stratigraphy. This style of foreland deformation in this segment of the Humber Zone is distinct from that in other foreland segments; in southwestern Newfoundland, the dominant structural feature is a large, apparently younger, triangle zone (Stockmal and Waldron, 1993), whereas the imbricate thrust system or duplexing in the foreland domain

near Québec City is characterized by closely spaced imbricate thrusts and the absence of overturned bedding (e.g. see maps of Lebel and Hubert, 1995) (Fig. 6).

The age of the thrusting documented here is poorly constrained. Thrusts crosscut the Middle Ordovician (Caradoc) Cloridorme Group. South of the study area, Silurian rocks of the Chaleurs Group are not affected by this deformation event, thus providing an apparent upper limit for the deformation. It should also be noted that the mappable thrusts that crosscut the flysch are probably not the thrusts originally related to flysch sedimentation. Flysch deposits and turbidity currents can travel significant distances, and thrust faults that may be related to the generation of these deposits are likely found south of the exposed flysch. However marine-fan progradation and west-northwest-directed transportation for early flysch units may indicate a predominantly in-sequence forward propagating thrust system that eventually crosscut the flysch package.

During this study, important penetrative extensional shear fabrics that overprinted earlier thrust fabrics were recognized along the upper contact of the Cap-Chat Mélange and the overlying Cloridorme Group (Logan's Ligne); this is likely significant for understanding the area's structural evolution and regional tectonics. The missing units along this fault indicate that extension may have been considerable. Furthermore, the listric nature of the extensional faults and their spatial association with earlier fold and thrust structures show that the thrusts were a controlling factor of the extension that resulted in an episode of postorogenic backsliding, possibly similar to that documented in tectonically active regions in Wyoming and Utah (West, 1993). It is tempting to associate this tectonic reversal with sedimentation in the Roches Penchées Formation in the fault's hanging wall, since the formation is characterized by a reversal in sediment source regions in the late stages of deposition of the Cloridorme Group. However, such an association is unlikely given that the Roches Penchées Formation has also been affected by thrusting (Fig. 4a), which predates extension. Alternatively, extension may be related to extension responsible for the deposition of the Chaleurs Group to the south, beginning in the Silurian. Important Silurian extension is recorded along faults and in higher grade rocks of the Taconian internal zone in the southeastern Quebec Appalachians (Pinet et al., 1996), and may be the hinterland expression of the extension recorded in the foreland domain of the Marsoui area and the Cap-Chat Mélange.

ACKNOWLEDGMENTS

D. Lavoie, R. Bertrand, and G. Gasbarro are thanked for their collaboration during field work. K. Lauzière helped with the preparation of some of the figures. This manuscript benefited from a review by D. Lavoie.

REFERENCES

Biron, S.
1974: Géologie de la région des Mechins; ministère des Richesses naturelles, Québec, DP-244.

Cooper, M., Weissenberger, J., Hostad, D., Gillespie, D., Rae, D., Clark, E., and Knight, I.
1997: Exploring for giant oilfields in the Cambrian-Ordovician of Western Newfoundland; the story so far...; Canadian Society of Petroleum Geologists, Reservoir, v. 24, p. 6.

Hiscott, R.N.
1978: Provenance of Ordovician deep-water sandstones, Tourelle Formation, Quebec, and implications for the initiation of the Taconic orogeny; Canadian Journal of Earth Sciences, v. 15, p. 1579-1597.
1980: Depositional framework of sandy mid-fan complexes of Tourelle Formation, Ordovician, Quebec; American Association of Petroleum Geologists Bulletin, v. 64, p. 1051-1077.

Kessler, G. II, Prave, A.R., Malo, M., and Bloechl, W.V.
1995: Mid-Upper Ordovician flysch deposition, northern Gaspé peninsula, Québec: a synthesis with implications for foreland and successor basin evolution in the northern Appalachian orogen; Society for Sedimentary Geology (SEPM), Pacific Section, v. 77, p. 251-255.

Lachambre, G. et Brisebois D.
1990: Géologie de la Gaspésie, Grande Vallée, 22H/3 et 22H/6; ministère de l'Énergie et des Ressources du Québec, carte n° 2152, DV 91-02 (échelle 1:50 000).

Lavoie, D.
1997: Cambrian-Ordovician slope conglomerates in the Humber Zone, Quebec reentrant; in Current Research 1997-D; Geological Survey of Canada, p. 9-20.
1998: Along strike Upper Cambrian–Lower Ordovician stratigraphic nomenclature and framework for the external Humber Zone, from Quebec City to Gaspé; in Current Research 1998-D; Geological Survey of Canada, p. XX-XX.

Lebel, D. et Hubert, C.
1995: Géologie de la région de Saint-Raphaël (Chaudière-Appalaches); ministère de l'Énergie et des Ressources du Québec, ET 93-02.

Lynch, G. and Arsenault, O.
1997: Stratigraphy and deformation of the Humber Zone in Gaspésie, Quebec; in Current Research 1997-D; Geological Survey of Canada, p.1-8.

Pinet, N., Tremblay, A., and Sosson, M.
1996: Extension versus shortening models for hinterland-directed motions in the southern Québec Appalachians; Tectonophysics, v. 267, p. 239-256.

Slivitzky, A., St-Julien, P. et Lachambre, G.
1991: Synthèse géologique du Cambro-Ordovicien du nord de la Gaspésie; ministère de l'Énergie et des Ressources du Québec, ET 88-14, 61 p.

St-Julien, P. and Hubert, C.
1975: Evolution of the Taconian orogen in the Quebec Appalachians; American Journal of Science, v. 275-A, p. 337-362.

Stockmal, G.S. and Waldron, J.W.F.
1993: Structural and tectonic evolution of the Humber Zone, western Newfoundland, 1. Implications of balanced cross-sections through the Appalachian structural front, Port au Port Peninsula; Tectonics, v. 12, p. 1056-1075.

Suppe, J. and Medwedeff, D.A.
1990: Geometry and kinematics of fault-propagation folding; Eclogae Geologicae Helvetiae, v. 83, p. 409-454.

Vallières, A.
1984: Stratigraphie et tectonique de l'orogénie taconique de la région de Rivière-du-Loup; thèse de doctorat, Université Laval, 302 p.

Vann, I.R., Graham, R.H., and Hayward, A.B.
1986: The structure of mountain fronts; Journal of Structural Geology, v. 8, p. 215-227.

West, M.W.
1993: Extensional reactivation of thrust faults accompanied by coseismic surface rupture, southwestern Wyoming and north-central Utah; Geological Society of America Bulletin, v. 105, p. 1137-1150.

Geological Survey of Canada Project 960012ZH

Along-strike Upper Cambrian–Lower Ordovician stratigraphic nomenclature and framework for the external Humber Zone, from Quebec City to Gaspé

Denis Lavoie
Quebec Geoscience Centre, Sainte-Foy

Lavoie, D., 1998: Along-strike Upper Cambrian–Lower Ordovician stratigraphic nomenclature and framework for the external Humber Zone, from Quebec City to Gaspé; in Current Research 1998-D; Geological Survey of Canada, p. 11-18.

Abstract: The Upper Cambrian–lowermost Ordovician succession in the Humber Zone (eastern Quebec) is a coarse-grained interval that contrasts with adjacent stratigraphic units. Our understanding of this interval is hampered by a complex stratigraphic framework that reflects the local perspective of previous studies as well as depositional facies variations. The name 'Trois-Pistoles Group' is proposed for this succession. At the base of the succession, the Saint-Damase Formation consists of limestone conglomerate and thickly bedded arkosic sandstone and overlies fine-grained siliciclastic rocks of the Saint-Roch and l'Orignal formations. The Saint-Damase Formation is overlain by a succession of turbidite (Ladrière Formation and upper part of the Lauzon and Grosses-Roches formations), mudrock (Rivière-du-Loup Formation), and quartzite (Kamouraska Formation). The upper part of the succession reflects facies zonation developed on the continental slope after the major lowstand recorded in the Saint-Damase Formation.

Résumé : La succession de la Zone de Humber (Québec oriental) du Cambrien supérieur–base de l'Ordovicien est un interval à grain grossier qui fait contraste avec les unités stratigraphiques adjacentes. Notre compréhension de la succession est limitée par le cadre stratigraphique complexe qui reflète la nature locale des études antérieures et les variations dans les faciès sédimentaires. Le nom «Groupe de Trois-Pistoles» est proposé pour cette succession. À sa base, la Formation de Saint-Damase comporte des conglomérats calcaires et des grès arkosiques en lits épais; elle surmonte les roches silicoclastiques à grain fin des formations de Saint-Roch et de l'Orignal. Vient ensuite une succession de turbidite (Formation de Ladrière et partie supérieure des formations de Lauzon et de Grosses-Roches), de mudrock (Formation de Rivière-du-Loup) et de quartzite (Formation de Kamouraska). La partie supérieure de la succession réflète une zonation de faciès développée sur le talus continental après l'important bas niveau marin dont témoigne la Formation de Saint-Damase.

INTRODUCTION

Cambro-Ordovician continental-slope sedimentary rocks in the external domain of the Humber Zone of the Quebec Reentrant outcrop over some 600 km along the south shore of the St. Lawrence River in eastern Québec (Fig. 1). These rocks are the only significant record of a Cambrian passive margin in the Quebec Reentrant, the coeval shallow platform being buried beneath the Appalachians (Hubert et al, 1970; Davies and Walker, 1974; Hendry, 1978; Lajoie, 1979; Hein and Walker, 1982; Slivitzky et al., 1991; Bernstein et al., 1992; Lynch and Arsenault, 1997; Lavoie, 1997a, b). The succession consists of siliciclastic-dominated Cambrian strata and mixed siliciclastic/carbonate Ordovician strata. The current passive-margin stratigraphy is complex because of the use of locally-defined units (Table 1), even though fine local sedimentological and biostratigraphic analyses are available. The regional significance of these rocks, their along-strike correlations within the Canadian Humber Zone and with the coeval unexposed shallow-marine platform, and their thermal history are largely unknown.

This continental slope succession is similar to the Cow Head Group in western Newfoundland (James and Stevens, 1986) along the St. Lawrence Promontory (Fig. 1). There, correlations between slope and shallow platform sedimentary records are well established and have led to the proposal of a coherent paleogeographic scenario (James et al., 1989). The integration of this regional paleogeographic picture with detailed tectonic studies (Waldron and Stockmal, 1994; Stockmal et al., 1995) was instrumental in the discovery of and ongoing exploration for oil reservoirs in western Newfoundland (Cooper et al., 1997).

In light of recent interest in the hydrocarbon potential of eastern Canadian Paleozoic basins and particularly the Cambro-Ordovician tectonostratigraphic Humber Zone (Williams, 1979), an integrated stratigraphic, sedimentological, maturation, and structural study of the Humber Zone in the Quebec Reentrant was initiated. Its goal is to propose an up-to-date paleogeographic, tectonic, thermal, and hydrocarbon synthesis incorporating specific transects for this largely unknown area stretching from Quebec City to Gaspésie.

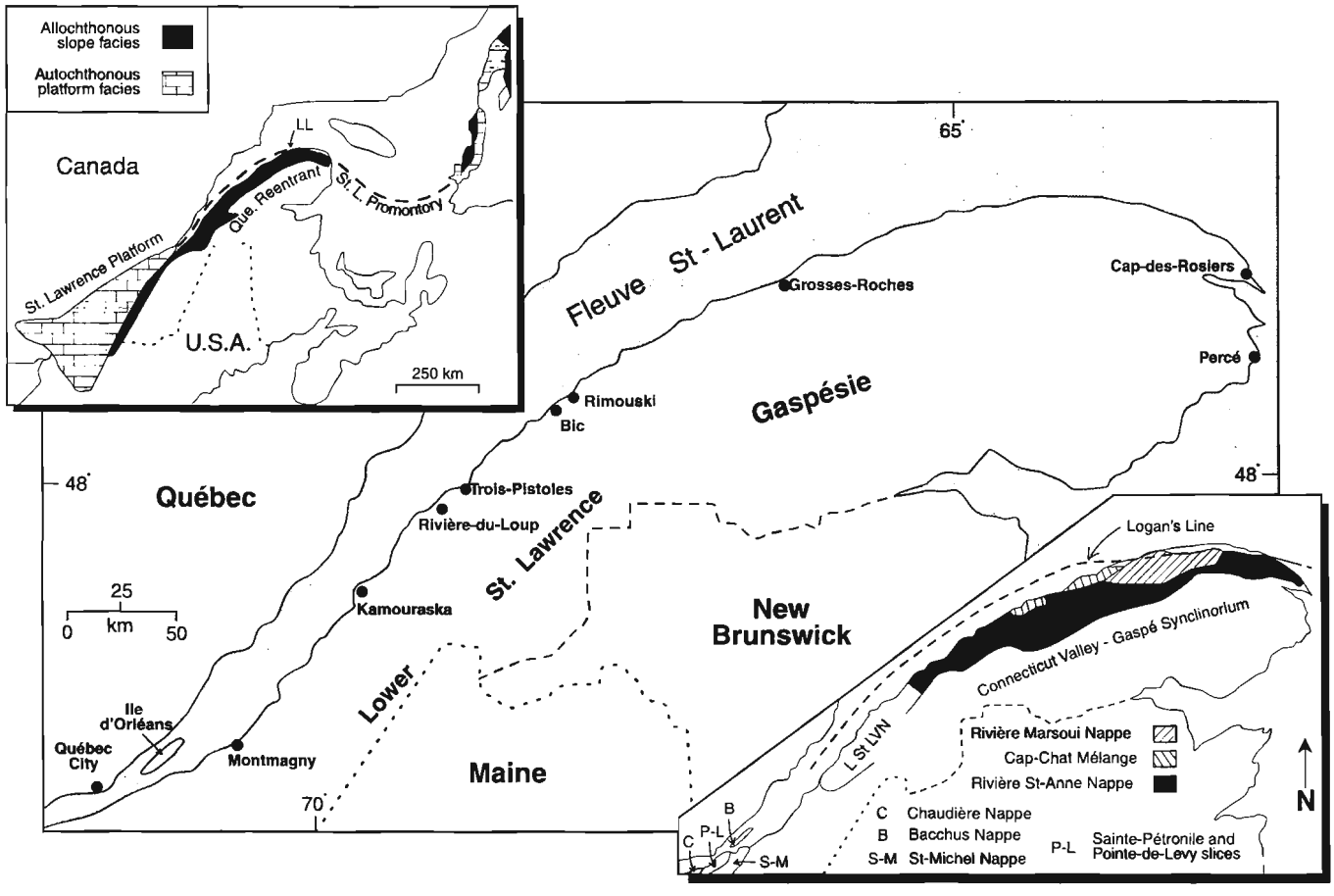

Figure 1. Location map for eastern Québec with inset map showing distribution of Cambro-Orodvician allochthonous slope and autochthonous platform sedimentary rocks in the Quebec Reentrant and St. Lawrence Promontory. L.L. = Logan's Ligne; LStVN = Lower St. Lawrence Valley North. Modified from Lavoie (1997a).

Table 1. Stratigraphic nomenclature for Cambrian to Ordovician passive margin sedimentary rocks of the Humber Zone. Î.O. = Île d'Orléans, R.d.L. = Rivière-du-Loup. All units are formations unless otherwise noted.

	Î.O.	Kamouraska		R.d.L.	Rimouski	Grosses-Roches		Gaspé
	Slivitzky et St-Julien (1987)	Hubert (1973)		Vallières (1984)	Lajoie (1972)	Hendry (1978) Bernstein et al. (1992)		Slivitzky et al. (1991)
Lower Ordovician	Pointe-de-la-Martinière	Rivière Ouelle		Rivière Ouelle		l'Anse-du-Crapaud		Rivière Ouelle
Upper Cambrian	Trou Saint-Patrice (Lauzon)	Kamouraska		Kamouraska		Grosses-Roches	Upper Mbr.	Kamouraska
		Saint-Damase	Sainte-Anne Mbr.	Rivière-du-Loup	Ladrière			Rivière-du-Loup
			La Pocatière Mbr.	Saint-Damase	Cap Enragé		Lower Mbr.	Saint-Damase
			Des Aulnaies Mbr.					
Middle Cambrian	l'Anse Maranda	Saint-Roch		Saint-Roch	l'Orignal	l'Orignal		l'Orignal

Such detailed studies rely heavily on coherent conventional and sequence stratigraphic frameworks. The Upper Cambrian–lowermost Ordovician coarse-grained sedimentary rocks are a significant marker unit in the predominantly fine-grained succession. Over the years, various stratigraphic designations have been introduced that reflect either the local perspective of some studies or the internal variations in the stratigraphy of these rocks (Table 1). A simplified nomenclature for these correlative units is required.

This paper proposes a regionally coherent stratigraphic framework for the Upper Cambrian–lowermost Ordovician succession in the external domain of the Humber Zone that is based on a compilation of available information and on detailed field studies. Five critial localities are examined: Île d'Orléans, Kamouraska, Rivière-du-Loup–Trois Pistoles, Bic–Rimouski, and Grosses-Roches (Fig. 1). The resulting framework not only takes into account regional variations in the internal stratigraphy of the succession, but also provides a baseline for integrating adjacent successions.

GEOLOGICAL SETTING

Cambro-Ordovician continental slope deposits of the external domain of the Humber Zone of the Québec Reentrant are part of the Québec Supergroup that outcrops from Quebec City to Gaspésie (Fig. 1). These predominantly fine-grained, poorly fossiliferous, and locally poorly exposed sedimentary rocks are preserved in southeasterly dipping thrust slices of the external tectonic domain, as defined by St-Julien and Hubert (1975). These slices were emplaced over the Cambrian-Ordovician shelf during the Middle Ordovician Taconian orogeny (St-Julien and Hubert 1975; St-Julien et al., 1983).

The Cambro-Ordovician succession of the external domain of the Humber Zone in the Quebec Appalachians was deposited in an evolving tectono-sedimentary basin (Lavoie, 1997a, b). Late Precambrian–Early Cambrian rift-related sedimentary and volcanic rocks (Shickshock Group and correlative units) are followed by Early Cambrian–Late Ordovician passive margin continental-slope sedimentary rocks (Saint-Roch Group/l'Orignal Formation [previously published incorrectly as 'Orignal Formation'], Trois-Pistoles Group [see herein], and Rivière Ouelle Formation). This succession is overlain by Middle to Late Ordovician foreland basin sedimentary rocks (Tourelle and Deslandes formations and Cloridorme Group, the latter being part of the parautochtonous domain, *sensu* St-Julien and Hubert, 1975).

STRATIGRAPHY

The lack of a coherent stratigraphic framework for the Humber Zone in eastern Quebec and particularly for passive margin stage sedimentary rocks is largely due to the structural complexity of the zone and to limited biostratigraphic data and the lack of marker beds. The present stratigraphy (Table 1) is based on large-scale mapping and a few regional thematic studies (e.g. Béland, 1957; Biron, 1971, 1974; Lajoie, 1972, 1974; Hubert, 1973; Liard, 1973; Vallières, 1984; Slivitsky and St-Julien, 1987; Slivitzky et al., 1991; Lebel and Hubert, 1995; Lavoie, 1997a), and has proven to be

inadequate at finer scales (Bernstein et al., 1992). The age of these units is loosely defined. Local paleontological studies have revealed the presence of graptolites (Erdtmann, 1967; Riva, 1972; Landing et al., 1986; Slivitzky et al., 1991; Maletz, 1992), trilobites and brachiopods (Landing and Ludvigsen, 1984), chitinozoans (Achab, 1980, 1982, 1989), and conodonts (Uyeno and Barnes, 1970; Barnes, 1984). Moreover, the age of the slope conglomerate is mostly constrained by the youngest fossils in limestone clasts (Rasetti, 1943, 1944, 1945a, b, 1946a, b, 1948a, b).

Regionally, the succession can be divided into broad stratigraphic packages consisting of fine-grained sedimentary rocks separated by or interbedded with coarse-grained units (Lavoie, 1997a, b). The lowest package consists of Lower Cambrian siliciclastic rocks capped by conglomerate units. The next package is defined by Middle Cambrian fine-grained siliciclastic rocks capped by lowest Upper Cambrian conglomerate. The third package, the subject of this report, consists of Upper Cambrian–lowermost Ordovician mixed siliciclastic and limestone conglomerate, sandstone, and shale. The last package consists of Lower to Middle Ordovician fine-grained successions of siliciclastic rocks and limestone with local conglomerate.

UPPER CAMBRIAN–LOWERMOST ORDOVICIAN SEDIMENTARY ROCKS

These rocks are an important marker succession owing to their coarse-grained nature and their regional persistence along the entire external Humber Zone. Moreover, similar-aged coarse-grained units occur in adjacent areas of the Appalachians (e.g. western Newfoundland, James and Stevens, 1986). Age constraints on this succession are relatively good and based on shallow-water platformal fossils in limestone conglomerate clasts (see Rasetti 1943, 1944, 1945a, b, 1946a, b, 1948a, b), on pelagic fossils in the overlying Rivière Ouelle Formation (and correlative units), and on current micropaleontological research. Five specific localities in the Quebec Humber Zone are examined (Fig. 2; Table 1).

Île d'Orléans

The most recent geological synthesis of this area is that of Slivitzky and St-Julien (1987), who introduced the term 'Île d'Orléans Group' for the Lower Cambrian to Lower Ordovician sedimentary rocks at that locality. This group consists of (in ascending order) the l'Anse Maranda (Lower to Upper Cambrian), Trou Saint-Patrice (Upper Cambrian to Lower Ordovician), and Pointe-de-la-Martinière (Lower Ordovician) formations.

The Trou Saint-Patrice Formation was assigned by St-Julien (1995) to the Lauzon Formation as initially defined by Logan (1866), which abruptly overlies the variably coloured mudstone of the l'Anse Maranda Formation. Its general internal stratigraphy consists of a lower limestone conglomerate and/or massive feldspar-rich sandstone, capped by interbedded mudstone and calcarenite/sandstone. Red mudstone marks the transition to the overlying Pointe-de-la-Martinière Formation.

Kamouraska

The Kamouraska area in the lower St. Lawrence Valley is the type area of the Saint-Damase and Kamouraska formations initially defined by Hubert (1973). Although both units are strikingly different from stratigraphically adjacent units, the were not included in a formal group.

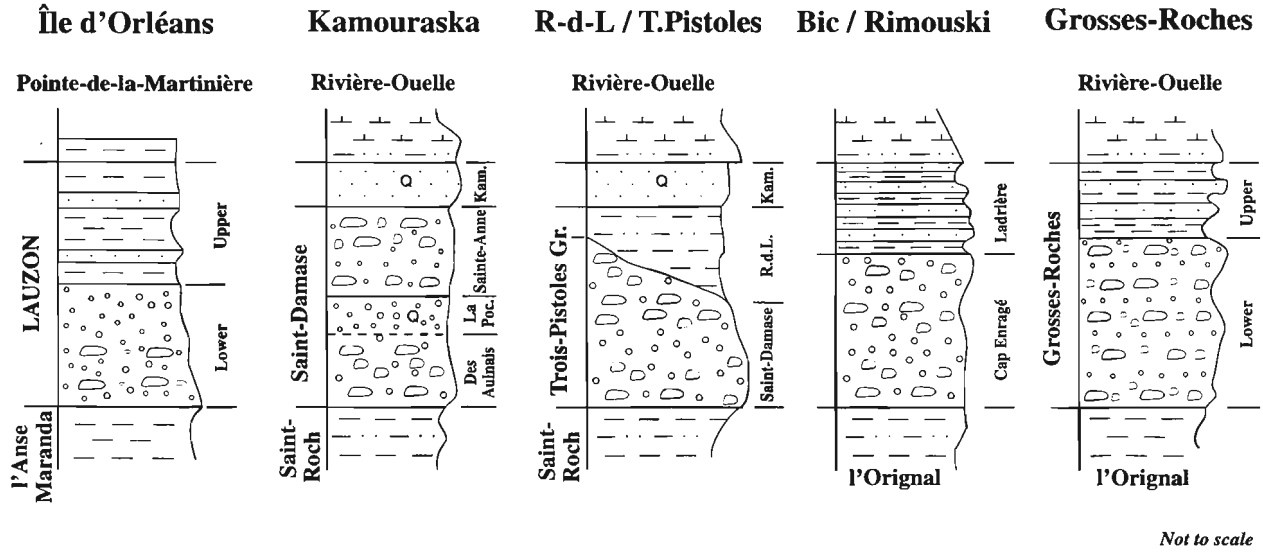

Figure 2. General stratigraphy and facies distribution of Upper Cambrian to lowermost Ordovician succession for locations discussed in text. R-d-L = Rivière-du-Loup; T.Pistoles = Trois-Pistoles; La Poc. = La Pocatière; Kam. = Kamouraska.

The Saint-Damase Formation abruptly overlies mudstone and siltstone of the Saint-Roch Formation (Hubert, 1965, 1973). In the type area, the Saint-Damase Formation has been divided into three formal members (in ascending order): the Des Aulnaies, La Pocatière, and Saint-Anne members. It is very significant that the tripartite division of the Saint-Damase Formation is not recognized outside the Kamouraska area. The Des Aulnaies and Saint-Anne members consist predominantly of thickly bedded arkosic and quartzitic sandstone and limestone conglomerate interbedded with minor thinly bedded mudstone. The coarse-grained facies are locally graded and crosslaminated and form metre- to decametre-thick fining- and thinning-upward intervals. The La Pocatière Member is sandwiched between the other members and consists predominantly of massive and thickly bedded quartzite with very minor limestone conglomerate; it has not been recognized outside the type area.

The Kamouraska Formation (Dresser, 1912; Hubert, 1973) overlies the Saint-Damase Formation. It is certainly the most distinctive sedimentary unit along the entire external domain of the Humber Zone. It consists predominantly of thickly bedded fine- to medium-grained quartzite, and contains rare thin beds of arkosic sandstone and few beds of limestone conglomerate. Few to no sedimentary structures are visible except for some dish structures. The relatively well sorted sedimentary rocks of the Kamouraska Formation contain silica cement although some open pore space is still present and bitumen cement is locally abundant (Hubert, 1973; Chi and Lavoie, 1998). The Kamouraska Formation is abruptly overlain by the predominantly fine-grained mixed siliciclastic and limestone beds of the Rivière Ouelle Formation.

In the Montmagny area, Lebel and Hubert (1995) have included the Saint-Damase and Kamouraska formations in the Trois-Pistoles Group of Vallières (1984), although the group's middle unit (Rivière-du-Loup Formation, see below) is not present.

Rivière-du-Loup–Trois-Pistoles

The most recent study in this area is that of Vallières (1984), who introduced the term 'Trois-Pistoles Group' for the Upper Cambrian–lowermost Ordovician sedimentary rocks in the area. As defined, the Trois-Pistoles Group consists of (in ascending order) the Saint-Damase, Rivière-du-Loup, and Kamouraska formations.

The Saint-Damase Formation consists of thickly bedded, locally pebbly, arkosic sandstone and limestone conglomerate with minor thinly bedded mudstone; the middle La Pocatière Member recognized by Hubert (1973) in the Kamouraska area is not present. The Saint-Damase Formation (formerly the Cap Enragé Formation, Lajoie [1972]) is typified by the cyclic alternation of limestone-conglomerate-dominated and fine-grained to pebbly sandstone intervals. Each 'cycle' usually contains a lower conglomeratic zone that thins and fines upward and passes into the sandstone-rich interval that also thins and fines upward. In the Trois-Pistoles area, up to three of these cycles have been recognized (see Hein and Walker, 1982). Details about the conglomerate are given in Lavoie (1997a).

The very distinctive Rivière-du-Loup Formation (Vallières, 1984) is a mudstone and siltstone unit developed between the Saint-Damase and Kamouraska formations in the Rivière-du-Loup map area. Its distribution is erratic. It has not been recognized southwest of the type area but is reported at many localities to the northeast (Slivitzky et al., 1991). However, recent local detailed studies have shown some inconsistencies in the reported occurrences of the unit (Bernstein et al., 1992; Lavoie, 1997a; Lynch and Arsenault, 1997).

The typical quartzite of the Kamouraska Formation is well exposed at the top of the Trois-Pistoles Group in the Rivière-du-Loup area. Towards the northeast, however, it is locally stratigraphically replaced by impure turbidite of the Ladrière Formation (see below).

Bic–Rimouski

The most recent detailed study of this area is by Lajoie (1972, 1974). A relatively distinct stratigraphic succession has been proposed for the area. The name 'Cap Enragé Formation' (Hubert et al., 1970; Lajoie, 1972) was introduced for the coarse-grained Upper Cambrian succession that overlies, locally unconformably, the mudstone of the l'Orignal Formation. The Cap Enragé Formation has been divided into three informal members: a lower sand-sized to pebbly arkosic sandstone-dominated unit, a middle limestone conglomerate with minor sandstone, and an upper arkosic sandstone-dominated unit. This division is strongly reminiscent of the cyclic stratigraphic pattern of the Saint-Damase Formation in the Rivière-du-Loup–Trois-Pistoles area.

The Cap Enragé Formation is conformably overlain by the Ladrière Formation (Hubert et al., 1970; Lajoie, 1972), which consists predominantly of interbedded mudstone and arkosic sandstone. It is interesting to note that the Ladrière Formation is stratigraphically laterally equivalent to the Rivière-du-Loup Formation and possibly to part of the Kamouraska Formation. Some parts of it are indeed fairly similar to the Rivière-du-Loup Formation, although its stratigraphic correlation with the Kamouraska Formation is uncertain.

Grosses-Roches

The first detailed studies of the Upper Cambrian–lowermost Ordovician section in this area were those of Hendry (1973, 1976, 1978, 1979). The succession was originally described as a conglomerate and quartzite section (Béland, 1957) and was later named the 'Cap-des-Rosiers Formation' by Hendry (1978), who assumed that this coarse-grained section was correlative with the Lower Ordovician section at Cap-des-Rosiers in easternmost Gaspésie. Later, it was shown that most if not all of this section was Late Cambrian, and Hendry (1979) named it the 'Grosses-Roches Formation'. In their compilation map, Brisebois et al. (1991) assigned this succession to the Trois-Pistoles Group; this was later challenged by

Bernstein et al. (1992), who proposed retaining the name 'Grosses-Roches Formation' mostly because the section lacked a tripartite division and a clear Kamouraska Formation interval.

The base of the succession is clearly erosive into the fine-grained l'Orignal Formation (see Fig. 5a, Lavoie, 1997a). It consists of at least five 'cycles' of fining- and thinning-upward limestone conglomerate-arkosic sandstone, preliminary details of which are given by Lavoie (1997a). The upper part of the succession underlies the mixed limestone-siliciclastic rocks of the Rivière Ouelle Formation (or l'Anse-du-Crapaud Formation, Bernstein et al., 1992) and constitutes a thinly bedded, mixed sandstone-mudstone section (see Fig. 2, Bernstein et al., 1992) that in many ways resembles the Ladrière Formation as defined 125 km to the southwest.

REGIONAL STRATIGRAPHIC FRAMEWORK

Significant variations in the stratigraphic nomenclature of the Upper Cambrian–lowermost Ordovician succession are due in part either to the local nature of some studies or to changes in the internal stratigraphy of the succession (Fig. 2; Table 1). Briefly, the succession is invariably characterized by a lower thick unit of coarse-grained arkosic sandstone with limestone conglomerate, the Saint-Damase Formation (lower part of the Lauzon Formation, Cap Enragé Formation, and lower part of the Grosses-Roches Formation), that abruptly overlies Lower to Middle Cambrian predominantly fine-grained rocks (l'Anse Maranda, Saint-Roch, and l'Orignal formations). In Gaspésie, this interval is also correlative with informal units 2c and 2d of Liard (1973) and formation no. 3 of Biron (1974). The rest of the succession varies along strike of the orogen, being either a predominantly fine-grained succession (upper part of the Lauzon Formation, Rivière-du-Loup and Ladrière formations, upper part of the Grosses-Roches Formation) with minor sandstone (Île d'Orléans, Rivière-du-Loup, Rimouski, and Grosses-Roches areas), or a thickly bedded quartzite (Kamouraska Formation) with no intervening facies (Montmagny, Kamouraska, and some parts of Gaspésie). At many localities (Rivière-du-Loup and Gaspé), the fine-grained siliciclastic interval (e.g. the Rivière-du-Loup Formation correlative with units 3a and 3c of Liard [1973] and with parts of formation no. 4 of Biron [1974]) is overlain by the thickly bedded Kamouraska unit (unit 3b of Liard [1973] and unit 4a of Biron [1974]). Obviously, a major part of the problem with the stratigraphic nomenclature is due to variations in depositional facies along strike of the orogen.

It is beyond the scope of this paper to propose detailed paleogeographic scenarios for this time interval in the Humber Zone. It is obvious, however, that a major lowstand affected the continental margin in the Late Cambrian (Lavoie, 1997a, b). Significant erosion of the pre- to syn-Late Cambrian shallow-water siliciclastic and carbonate platform and underlying (?)Grenville basement is recorded in the lower part of the coeval continental-slope rocks and at all localities studied along strike of the orogen; this suggests a regional-scale collapse of the shallow-water margin of the continental shelf.

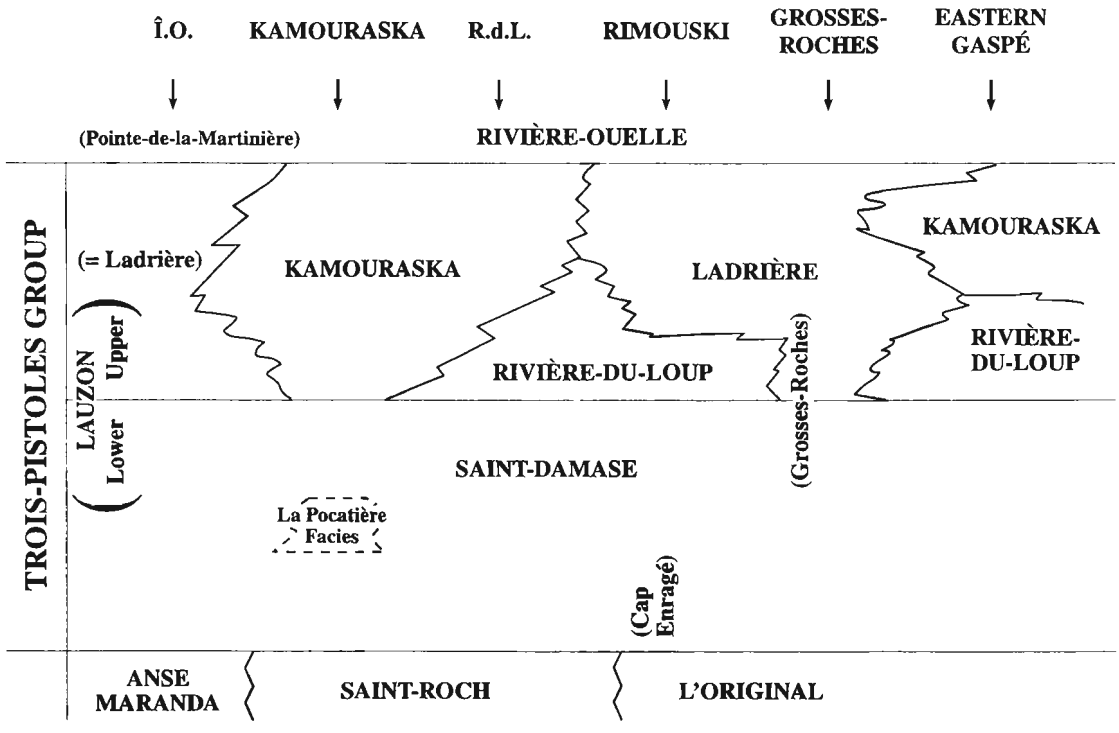

Figure 3. Schematic stratigraphic framework for the Upper Cambrian to lowermost Ordovician succession in the Humber Zone in eastern Quebec. Î.O. = Île d'Orléans; R.-d.-L. = Rivière-du-Loup.

Next comes a laterally complex succession of fine-grained mudrock (upper part of the Lauzon Formation, Rivière-du-Loup Formation), or classical turbidite (Ladrière Formation, upper part of the Grosses-Roches Formation), or well sorted thickly bedded quartzite (Kamouraska Formation). The critical unit is the Kamouraska Formation, which is interpreted to represent continental-slope channel-fill sandstone that was deposited initially as shallow-water siliciclastic material trapped in nearshore settings during a transgressive event and later exported basinward in submarine channels during the late highstand. This restricted paleoenvironment scenario would explain the unit's lateral variations in thickness, its absence at some localities, and its replacement by fine-grained hemipelagic mudrock and turbidite at many localities.

Thus, the proposed regional stratigraphic scenario must take into account the presence of significant paleoenvironmental variations (Fig. 3). It is proposed that the name 'Trois-Pistoles Group' be retained for the entire Upper Cambrian–lowermost Ordovician succession. The regionally persistent limestone conglomerate–massive arkosic sandstone interval at the base of the group is designated the 'Saint-Damase Formation'; it contains a local quartzite-rich facies, the La Pocatière facies. Thus, the Saint-Damase Formation would be correlative with the lower part of the Lauzon Formation (formerly the Trou Saint-Patrice Formation on Île d'Orléans), the Cap Enragé Formation, and the lower part of the Grosses-Roches Formation (as described by Bernstein et al., 1992). The overlying stratigraphic unit is the laterally interfingering Rivière-du-Loup (predominantly mudstone), Ladrière (correlative with the upper part of the Lauzon and Grosses-Roches formations, e.g. predominantly classical turbidite), and the Kamouraska (quartzite) formations. Locally, mudrock of the Rivière-du-Loup Formation is overlain by thickly bedded quartzite of the Kamouraska Formation, although such a relationship is unknown in the classical turbidite of the Ladrière Formation (and correlative units).

ACKNOWLEDGMENTS

Research was funded by the Geological Survey of Canada. Thanks are expressed to L. Bernstein, who carried out detailed work on the Cambrian-Ordovician passive margin succession in the Quebec Humber Zone. G. Gasbarro, R. Bertrand, E, Asselin, and G. Lynch are thanked for their help, their discussions, and the sharing of information. This manuscript benefited from a review by G. Lynch.

REFERENCES

Achab, A.
1980: Chitinozoaires de l'Arenig inférieur de la Formation de Lévis (Québec, Canada); Review of Palaeontology and Palynology, v. 31, p. 219-239.
1982: Chitinozoaires de l'Arenig supérieur (Zone D) de la Formation de Lévis, Québec; Canadian Journal of Earth Sciences, v. 19, p. 1295-1307.
1989: Ordovician chitinozoan zonation of Quebec and western Newfoundland; Journal of Paleontology, v. 63, p. 14-24.

Achab, A. (cont.)
1984: Early Ordovician eustatic events in Canada; in Aspects of the Ordovician System, (ed.) D.L. Bruton; Paleontological Contributions from the University of Oslo, no. 295, Universitetsforlaget, p. 51-63.

Béland, J.
1957: Région de Sainte-Félécité–Grosses-Roches; ministère des Mines, Québec, RP 339.

Bernstein, L., James, N.P., and Lavoie, D.
1992: Cambro-Ordovician stratigraphy in the Quebec Reentrant, Grosses-Roches–Les Méchins area, Gaspésie, Québec; in Current Research, Part E; Geological Survey of Canada, Paper 92-1E, p. 381-392.

Biron, S.
1971: Géologie de la rive du Saint-Laurent de Cap-Chat à Gros-Morne; ministère des Richesses naturelles, Québec, DP-240.
1974: Géologie de la région des Méchins; ministère des Richesses naturelles, Québec, DP-299.

Brisebois, D., Lachambre, G. et Piqué, D.
1991: Carte géologique de la Gaspésie; ministère des Ressources naturelles, Québec (échelle 250 000).

Chi, G. and Lavoie, D.
1998: Porosity evolution and evidence of hydrocarbon migration in the Kamouraska and Rivière Ouelle formations, Humber Zone, Québec - a fluid-inclusion approach; Current Research 1998-D; Geological Survey of Canada, p. XX-XX.

Cooper, M., Weissenberger, J., Hostad, D., Gillespie, D., Rae, D., Clark, E., and Knight, I.
1997: Exploring for giant oil fields in the Cambro-Ordovician of Western Newfoundland; the story so far...; Canadian Society of Petroleum Geologists, Reservoir, v. 24, no. 8, p. 6.

Davies, I.C. and Walker, R.G.
1974: Transport and deposition of resedimented conglomerates: the Cap Enragé Formation, Gaspé, Québec; Journal of Sedimentary Petrology, v. 44, p. 1200-1216.

Dresser, J.A.
1912: Reconnaissance along the National Transcontinental Railway in southern Québec; Geological Survey of Canada, Memoir 35, 40 p.

Erdtmann, B.D.
1967: A new fauna of Early Ordovician graptolites from St. Michel, Québec; Canadian Journal of Earth Sciences, v. 4, p. 335-355.

Hein, F.J. and Walker, R.G.
1982: The Cambro-Ordovician Cap Enragé Formation, Québec, Canada: conglomeratic deposits of submarine channel with terraces; Sedimentology, v. 29, p. 309-329.

Hendry, H.E.
1973: Sedimentation of deep water conglomerates in Lower Ordovician rocks of Quebec - composite bedding produced by progressive liquefaction of sediment?; Journal of Sedimentary Petrology, v. 43, p. 125-136.
1976: The orientation of discoidal clasts in resedimented conglomerates, Cambro-Ordovician, Gaspé, Québec; Journal of Sedimentary Petrology, v. 46, p. 48-55.
1978: Cap des Rosiers Formation at Grosses Roches, Quebec - deposits of the midfan region on an Ordovician submarine fan; Canadian Journal of Earth Sciences, v. 15, p. 1472-1488.
1979: Grosses-Roches - Early Ordovician mid-fan conglomerates and sandstones; in Cambro-Ordovician submarine channels and fans, l'Islets to Sainte-Anne-des-Monts, (ed.) G.V. Middleton, R.G. Walker, P. Strong, F.J. Hein, H.E. Hendry, and R.V. Hiscott; Geological Association of Canada, Field Trip Guidebook A-6, Québec City, p. 26-32.

Hubert, C.
1965: Stratigraphy of the Quebec Complex in the l'Islet–Kamouraska area, Quebec; Ph.D. thesis, McGill University, Montréal, 192 p.
1973: Kamouraska, La Pocatière, and Saint-Jean-Port-Joli area; Quebec Department of Natural Resources, Geological Exploration Service, Geological Report 151, 205 p.

Hubert, C., Lajoie, J., and Léonard, M.A.
1970: Deep sea sediments in the lower Paleozoic Québec Supergroup; in Flysch Sedimentation in North America, (ed.) J. Lajoie; Geological Association of Canada, Special Paper No. 7, p. 103-126.

James, N.P. and Stevens, R.K.
1986: Stratigraphy and correlation of the Cambro-Ordovician Cow Head Group, western Newfoundland; Geological Survey of Canada, Bulletin 366, 143 p.

James, N.P., Stevens, R.K., Barnes, C.R., and Knight, I.
1989: Evolution of a Lower Paleozoic continental-margin carbonate platform, northern Canadian Appalachians; in Controls on Carbonate Platform and Basin Development, (ed.) P.D. Crevello, J.L. Wilson, Sarg, J.F., and Read, J.F.; Society of Economic Paleontologists and Mineralogists, Special Publication No. 44, p. 123-146.

Lajoie, J.
1972: Géologie des régions de Rimouski et de Lac-des-Baies (moitié ouest), Comtés de Rimouski et Rivière-du-Loup; ministère des Richesses naturelles, Québec, DP-64, 40 p.
1974: Région de Rimouski: ministère des Richesses naturelles, Québec, Dossier public 64, 45 p.
1979: Origin of megarythms in flysch sequences of the Québec Appalachians; Canadian Journal of Earth Sciences, v. 16, p. 1518-1523.

Landing, E., Barnes, C.R., and Stevens, R.K.
1986: Tempo of earliest Ordovician graptolite faunal succession: conodont-based correlations from the Tremadocian of Quebec; Canadian Journal of Earth Sciences, v. 23, p. 1928-1949.

Landing, E. and Ludvigsen, R.
1984: Classification and conodont-based age of the Ordovician trilobite *Ellsaspis* (middle Arenigian, Ville Guay, Québec); Canadian Journal of Earth Sciences, v. 21, p. 1483-1490.

Lavoie, D.
1997a: Cambrian-Ordovician slope conglomerates in the Humber Zone, Quebec Reentrant, Québec; in Current Research 1997-D; Geological Survey of Canada, p. 9-20.

1997b:
The Sauk-Tippecanoe Sequences along the Iapetus continental margin in eastern Canada: facies evolution and sea level history from Newfoundland to southern Québec; Canadian Society of Petroleum Geologists–Society for Sedimentary Geology, Joint Meeting, Calgary; Program with Abstracts, p. 163.

Lebel, D. et Hubert, C.
1995: Géologie de la région de Saint-Raphaël (Chaudière-Appalaches); ministère de l'Énergie et des Ressources du Québec, ET 93-02.

Liard, P.
1973: Cartes supplémentaires pour la région de Mont-Joli–Matane; ministère des Richesses naturelles, Québec, DP-290.

Logan, W.E.
1866: Geology of Canada; Geological Survey of Canada, Report of Progress 1863-1866.

Lynch, G. and Arsenault, O.
1997: Stratigrapby and deformation of the Humber Zone in Gaspésie Québec; in Current Research 1997-D; Geological Survey of Canada, p. 1-8.

Maletz, J.
1992: Yapeenain (Early Ordovician) graptolites in the Quebec Appalachians; Canadian Journal of Earth Sciences, v. 29, p. 1330-1334.

Rasetti, F.
1943: New Ordovician trilobites from Lévis, Québec; Journal of Paleontology, v. 17, p. 101-104.
1944: Upper Cambrian trilobites from the Lévis conglomerates; Journal of Paleontology, v. 18, p. 229-258.
1945a: Faunes cambriennes de conglomérats de la formation de Sillery; Naturaliste canadien, vol. 72, p. 53-67.

Rasetti, F. (cont.)
1945b: New Upper Cambrian trilobites from the Lévis conglomerate; Journal of Paleontology, v. 19, p. 462-478.
1946a: Cambrian and Early Ordovician stratigraphy of the Lower St. Lawrence Valley; Geological Society of America Bulletin, v. 57, p. 687-706.
1946b: Early Upper Cambrian trilobites from western Gaspé; Journal of Paleontology, v. 20, p. 442-462.
1948a: Lower Cambrian trilobites from the conglomerates of Quebec (*Ptychopariidea*); Journal of Paleontology, v. 22, p. 1-24.
1948b: Middle Cambrian trilobites from the conglomerates of Quebec (exclusive of *Ptychopariidea*); Journal of Paleontology, v. 22, p. 315-339.

Riva, J.
1972: Geology of the environs of Quebec City; 24th International Geological Congress, Montréal, Québec; Field Trip Guidebook B-19, 53 p.

Slivitzky, A. et St-Julien, P.
1987: Compilation géologique de la région de l'Estrie-Beauce; ministère de l'Énergie et des Ressources, Québec MM-85-04, 40 p.

Slivitzky, A., St-Julien, P. et Lachambre, G.
1991: Synthèse géologique du Cambro-Ordovician du nord de la Gaspésie; ministère de l'Énergie et des Ressources, Québec, ET 88-14, 61 p.

St-Julien, P.
1995: Géologie de la région de Québec; ministère de l'Énergie et des Ressources, Québec, MB 94-40.

St-Julien, P. and Hubert, C.
1975: Evolution of the Taconian Orogen in the Quebec Appalachians; American Journal of Science, v. 275-A, p. 337-362.

St-Julien, P., Slivitzky, A., and Feininger, T.
1983: A deep structural profile across the Appalachians of southern Québec; in Contributions to the Tectonics and Geophysics of Mountain Chains, (ed.) R.D. Hatcher, H. Williams, and I. Zietz; Geological Society of America, Memoir 158, p. 103-112.

Stockmal, G.S., Waldron, J.W.F., and Quinlan, G.M.
1995: Flexural modeling of Paleozoic foreland basin subsidence, offshore Western Newfoundland: evidence for substantial post-taconian thrust transport; Journal of Geology, v. 103, p. 653-671.

Uyeno, T.T. and Barnes, C.R.
1970: Conodont from tbe Lévis Formation (zone D1) (Middle Ordovician), Lévis, Québec; Geological Survey of Canada, Bulletin 187, p. 99-123.

Vallières, A.
1984: Stratigraphie et structure de l'orogénie taconique de la région de Rivière-du-Loup; thèse de doctorat, Université Laval, Québec, 302 p.

Waldron, J.W.F. and Stockmal, G.S.
1994: Structural and tectonic evolution of the Humber Zone, western Newfoundland, 2: geophysical and geological for Acadian thrust tectonics; Tectonics, v. 13, p. 1498-1513.

Williams, H.
1979: Appalachian Orogen in Canada; Canadian Journal of Earth Sciences, v. 16, p. 792-807.

Geological Survey of Canada Project 960012ZH

Porosity evolution and evidence of hydrocarbon migration in the Kamouraska and Rivière Ouelle formations, Humber Zone, Quebec – a fluid-inclusion approach

Guoxiang Chi and Denis Lavoie
Quebec Geoscience Centre, Sainte-Foy

Chi, G. and Lavoie, D., 1998: Porosity evolution and evidence of hydrocarbon migration in the Kamouraska and Rivière Ouelle formations, Humber Zone, Quebec – a fluid-inclusion approach; in Current Research 1998-D; Geological Survey of Canada, p. 19-24.

Abstract: Fluid inclusions in authigenic phases in quartzite of the Late Cambrian Kamouraska Formation and limestone of the Early Ordovician Rivière Ouelle Formation were studied in order to evaluate the evolution of porosity and look for evidence of hydrocarbon migration. Estimates of current quartzite porosity range from near zero to 5%. Paleoporosity occluded by quartz cement ranges from <5% to 15%. Quartz cementation likely started at temperatures <50°C. Some pores probably remained open until significant burial. Bituminous matter was observed along grain boundaries, coating residual pores, or cutting detrital quartz grains. Some quartz+calcite veins from the Montmagny area contain abundant light hydrocarbon inclusions. Limited fluid-inclusion data from the Rivière Ouelle Formation indicate that limestone pores were not occluded until burial temperatures reached about 100-120°C. Some calcite veins contain abundant high-density methane inclusions. Hydrocarbon inclusions and bituminous matter suggest relatively late hydrocarbon migration.

Résumé : On a étudié des inclusions fluides dans les minéraux authigènes du quartzite de la Formation de Kamouraska (Cambrien tardif) et du calcaire de la Formation de Rivière Ouelle (Ordovicien précoce) afin d'évaluer l'évolution de la porosité et de trouver des indices de la migration d'hydrocarbures. La porosité actuelle du quartzite est estimée à entre zéro et 5 %. Le volume de paléovides remplis de quartz varie de <5 % à 15 %. La cimentation par du quartz aurait commencé à des températures <50 °C. Certains vides sont probablement restés ouverts jusqu'à enfouissement de la roche. De la matière bitumineuse se rencontre aux contacts des grains, autour des vides ou recoupant les grains de quartz détritique. Des veines de quartz+calcite dans la région de Montmagny contiennent d'abondantes inclusions d'hydrocarbures légers. Un nombre limité de données tirées des inclusions fluides dans la Formation de Rivière Ouelle indique que les vides dans le calcaire n'ont été cimentés que lorsque les températures d'enfouissement avaient atteint environ 100-120 °C. Certaines veines de calcite contiennent d'abondantes inclusions de méthane de haute densité. La présence d'inclusions d'hydrocarbures et de matière bitumineuse suggère une migration tardive des hydrocarbures.

INTRODUCTION

The Cambrian-Ordovician Humber Zone of the Quebec Reentrant was a part of the Laurentian continental margin. It comprises slope and rise sedimentary rock that were thrust over the autochthonous rocks of the St. Lawrence Platform during the Taconian Orogeny (St-Julien and Hubert, 1975). The recent discovery of oil reservoirs in the Humber Zone in western Newfoundland has raised interest in the hydrocarbon potential of the Humber Zone in Quebec. In response, an integrated stratigraphic, sedimentological, maturation, and structural study of this region was initiated at the Quebec Geoscience Centre (Lavoie, 1997; Lynch and Arsenault, 1997). This study is part of that project and its object is to evaluate the porosity history of some stratigraphic units that have the potential for forming reservoirs, and to look for evidence of hydrocarbon migration. Microthermometric studies of fluid inclusions entrapped in authigenic phases were carried out. The homogenization temperatures of fluid inclusions were used to estimate the thermal (and burial) conditions of cementation. The presence of hydrocarbon fluid inclusions is used as evidence of the passage of liquid or gaseous hydrocarbons. The results presented here are preliminary, and our continued research will integrate these data into a stratigraphic-structural model for exploration.

Location and petrography

Twenty-two samples from the Kamouraska Formation (quartzite) and two samples from the Rivière Ouelle Formation (limestone) were collected from the Grande Vallée, Matane, and Montmagny areas (Fig. 1). The Late Cambrian Kamouraska Formation and the Early Ordovician Rivière Ouelle Formation are part of stratigraphic packages 3 and 4 respectively of Lavoie (1997). The stratigraphic divisions of the Humber Zone are summarized in Lavoie (1997) and discussed in Lavoie (1998).

The Kamouraska Formation consists of cyclic sequences of limestone- and shale-bearing conglomeratic orthoquartzite, orthoquartzite, and thinly interbedded shale and siltstone. All the samples from the Kamouraska Formation are orthoquartzite. The quartzite forms very thick beds (3 to 50 m) (Fig. 2a), with very well rounded and sorted quartz particles ranging in size from 0.12 to 0.25 mm (Hubert, 1973). Visual

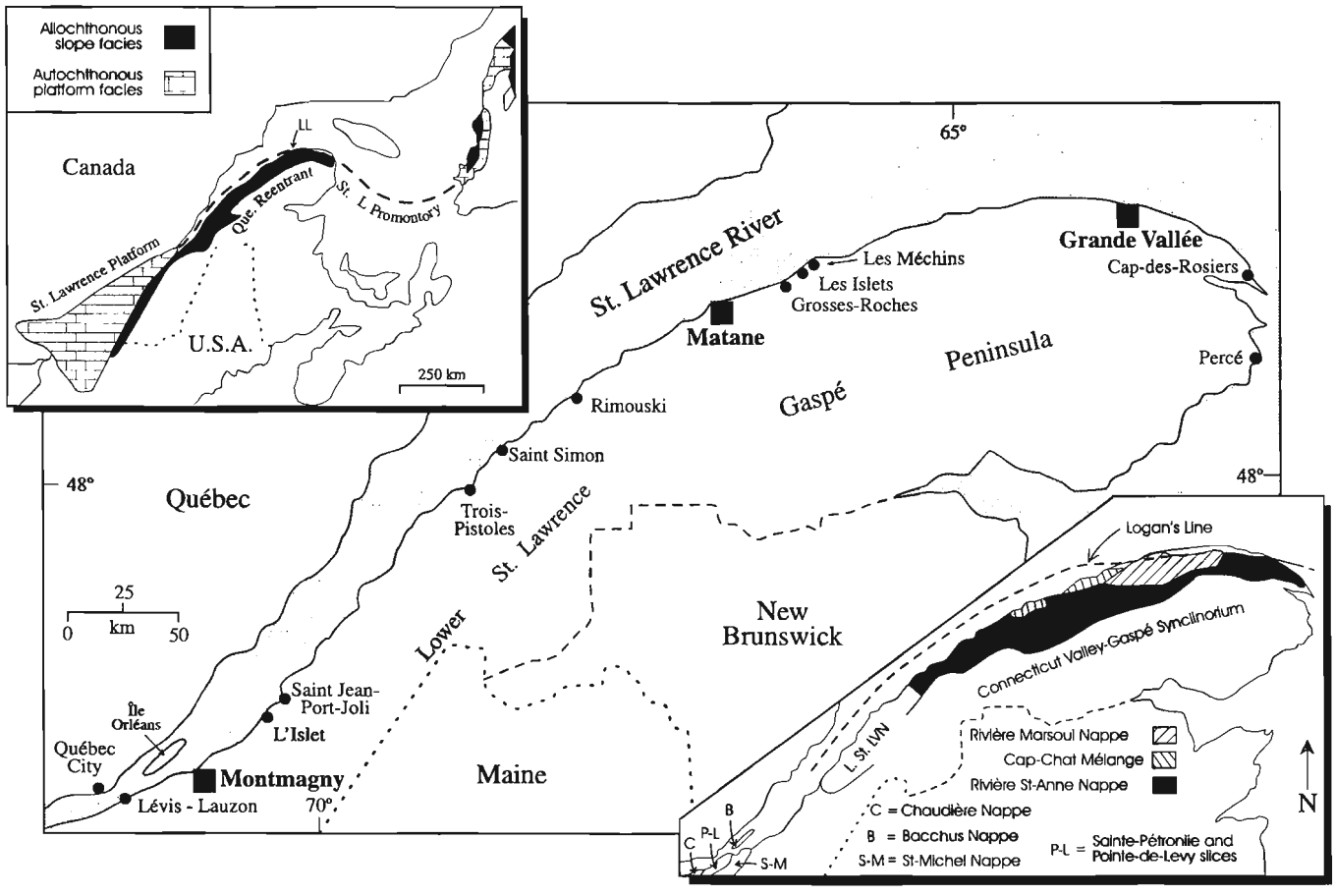

Figure 1. *Location map showing the Grande Vallée, Matane, and Montmagny areas where the study samples were collected. The inset maps show the distribution of Cambro-Ordovician allochthonous slope and autochthonous platform sedimentary rocks in the Quebec Reentrant (after Lavoie, 1997). LL = Logan's Line; LStLVN = Lower St. Lawrence Valley North.*

estimates of the current quartzite porosity range from near zero to 5%. The pores were partly occluded by quartz cement (Fig. 3a, b), which makes up <5% to 15% of the rock. Millimetre-sized quartz-filled veins with or without minor calcite are common (Fig. 3c); some are only partly filled, leaving visible open space. Black to brown matter, which is very weakly fluorescent under blue light, was observed in many of the samples studied; it occurs along grain boundaries, coats residual pores, or cuts detrital quartz grains. Until a chemical analysis is done, this material will be called 'bituminous matter'. Similar observations have been reported by Hubert (1973, p. 152). Locally, faint 'bubbles' are seen in the bituminous matter suggesting the past existence of liquid hydrocarbons. In most cases, the bituminous matter postdates the quartz cements (Fig. 3d), except in the Grande Vallée area where some authigenic quartz apparently postdates the bituminous matter. Figure 4 summarizes the petrographic characteristics of the Kamouraska quartzite.

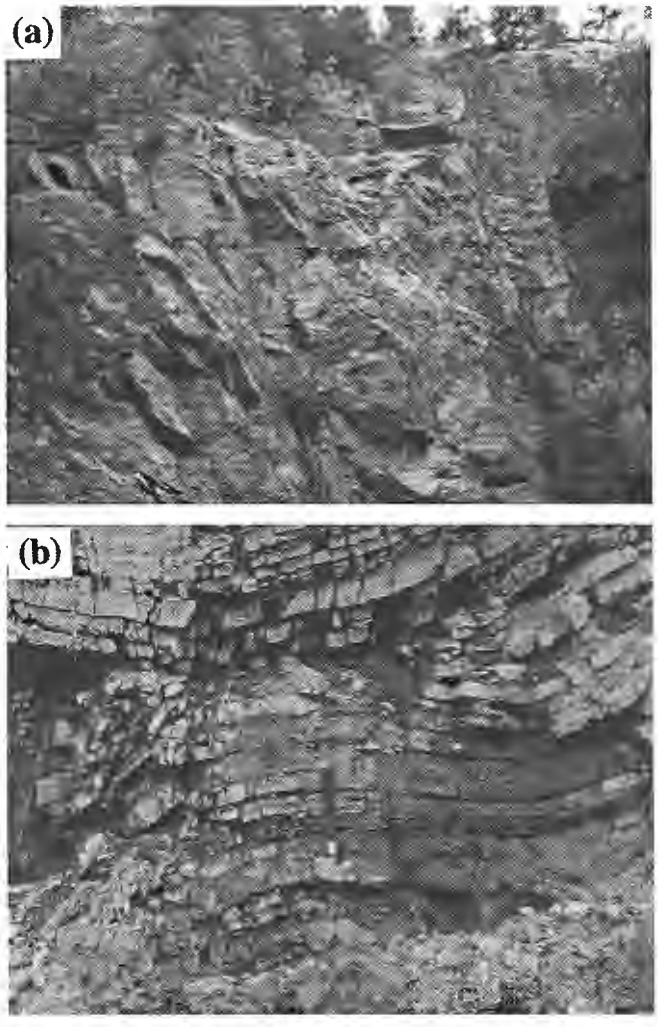

Figure 2. *(**a**) Thick quartzite beds of the Kamouraska Formation in the Grande Vallée area. (**b**) Limestone beds of the Rivière Ouelle Formation in the Grande Vallée area.*

The Rivière Ouelle Formation, which overlies the Kamouraska Formation, comprises mainly shale and thinly interbedded limy shale and siltstone, and with individual beds of orthoquartzite, subarkose, arkose, calcisiltite, oligomictic limestone conglomerate, and shale breccia (Hubert, 1973). Limestone can be fairly thick (Fig. 2b). One sample, from the Matane area, is calcarenite; the other, from the Grande Vallée area, is a calcite vein cutting limestone. The calcarenite is completely cemented by calcite and cut by calcite veins.

Fluid-inclusion microthermometry

Microthermometric measurements were carried out on fluid inclusions from various authigenic phases in the samples. The results are summarized in Table 1. The distribution of homogenization temperatures (T_h) is shown in Figures 5 and 7.

Quartzite of the Kamouraska Formation

Fluid inclusions in pore-filling quartz are generally very small (<3 μm). Fluid inclusions occurring along the contact between detrital and authigenic quartz are usually all liquid at room temperature (Fig. 3a). In samples from the Grande Vallée and Matane areas, some fluid inclusions in the quartz cement are all liquid while others are biphase (liquid+vapor; Fig. 3b). Samples from the Montmagny area, however, only contain all-liquid inclusions. The T_h of biphase fluid inclusions in quartz cement ranges from 58°C to 167°C for samples from the Grande Vallée area and from 54°C to 222°C for samples from the Matane area (Table 1; Fig. 5). Where workable biphase inclusions occur in clusters, the variation of T_h within individual clusters is less than 20°C. The overall range of T_h in a given area probably indicates a long period of cementation. Salinity in the fluid inclusions varies from 1.9 to 8.0 wt. % in the Grande Vallée area, from 2.1 to 4.7 wt. % for the matane area, and from 6.4 to 8.3 wt. % for the Montmagny area. In comparison, the salinity of seawater is about 3.5 wt. %.

Fluid inclusions in fracture-filling quartz and calcite have generally higher (partly overlapping) T_h than those in pore-filling quartz (Fig. 5). The T_h ranges from 130°C to 222°C for samples from the Grande Vallée area, from 71°C to 244°C for samples from the Matane area, and from 104°C to 142°C for samples from the Montmagny area. Salinity is similar to that of pore-filling quartz (Table 1), except in the veins from the Montmagny area, where salinity ranges from 13 to 21 wt. %. Abundant hydrocarbon inclusions occur in some veins from the Montmagny area; they are monophase at room temperature (Fig. 6), and nucleated a bubble at low temperatures. One inclusion homogenized to the vapor phase at -88°C; others homogenized to the liquid phase at temperatures between -82.4° and -32.4°C (Table 1; Fig. 5). They are weakly fluorescent under blue light. The inclusions with T_h lower than the critical temperature of methane (-82.1°C) likely comprise methane, whereas those with T_h higher than -82.1°C are likely mixtures of methane and other light hydrocarbons. Ettner et al. (1996) reported similar inclusions in the Bidjovagge gold-copper deposit in Norway and detected the presence of CH_4, C_2H_6, C_3H_8, and butane using Raman microprobe and gas chromatography.

Limestone of the Rivière Ouelle Formation

Fluid inclusions in pore-filling calcite in calcarenite from the Matane area have T_h ranging from 94°C to 168°C and salinity ranging from 2.7 to 14 wt. %. Fluid inclusions in fracture-filling calcite have T_h ranging from 94°C to 168°C and salinity ranging from 2.7 to 14 wt. % (Table 1; Fig. 7). The sample from the Grande Vallée area shows fluid inclusions in fracture-filling calcite with T_h from 63°C to 132°C and salinity from 0.9 to 1.7 wt. %. Fracture-filling calcite in both samples contains methane inclusions that homogenize to the liquid phase at temperatures between -98°C and -84°C (Table 1; Fig. 7).

Implications for porosity evolution and hydrocarbon migration

The all-liquid inclusions likely indicate homogenization temperatures <50°C (Goldstein and Reynolds, 1994). Therefore, the presence of all-liquid inclusions along the border between

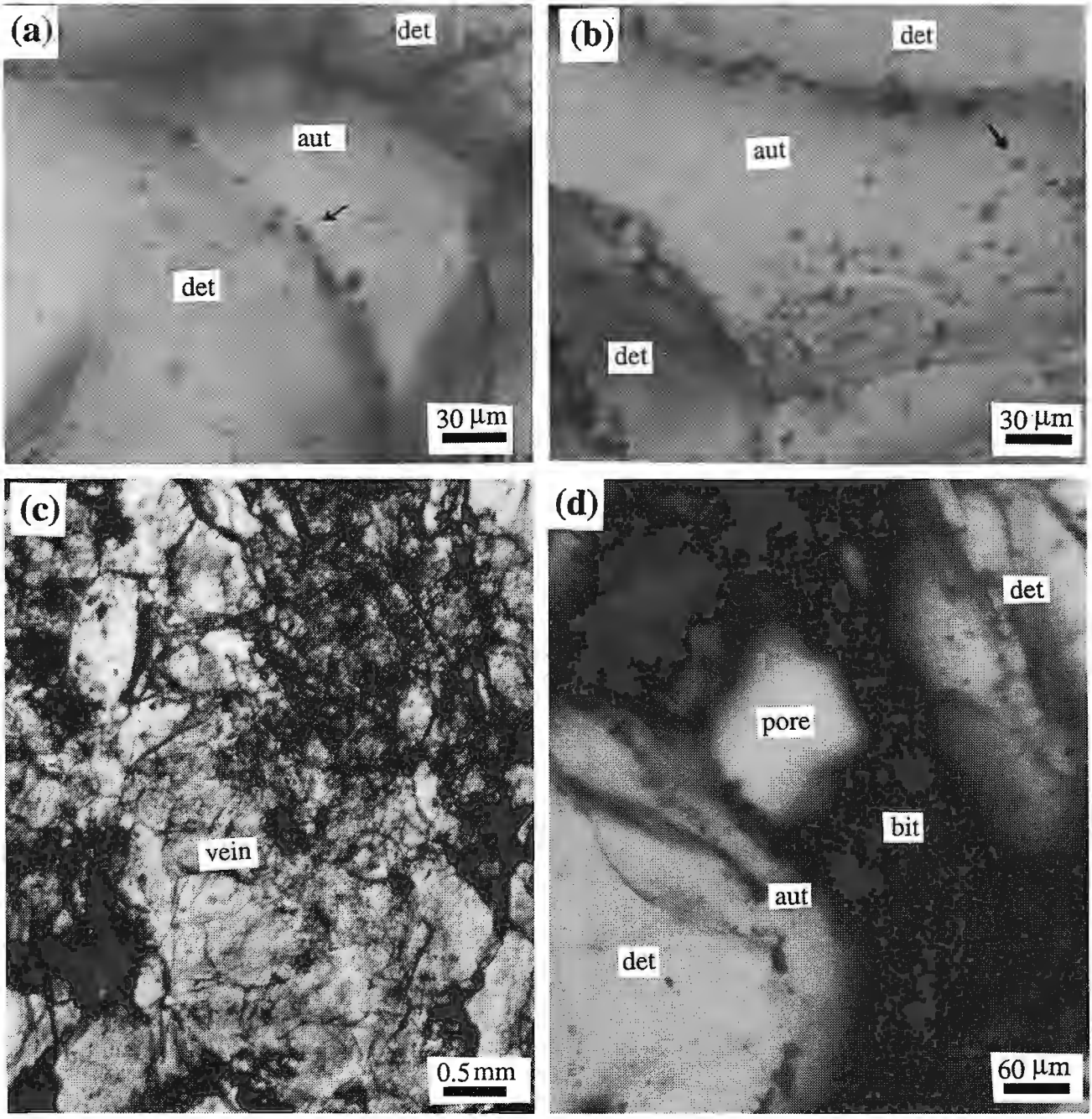

Figure 3. *(**a**) Monophase (liquid) inclusions at the contact between authigenic and detrital quartz (MT-230). (**b**) Biphase (liquid + vapor) inclusions in authigenic quartz (MT-49A). (**c**) A quartz and calcite veinlet cutting quartzite (MY-17C). (**d**) Bituminous matter that postdates authigenic quartz coating an open pore. Det = detrital quartz; aut = authigenic quartz; bit = bituminous matter.*

detrital and authigenic quartz suggests that quartz cementation started at relatively low temperatures. The wide range of T_h for fluid inclusions in quartz cement probably indicates a long history of cementation. However, because of the small size of fluid inclusions and the difficulty in recognizing the 'growth pattern' of the quartz cements, it is currently impossible to determine the proportion of cementation as a function of temperature (or burial depth). Therefore, although the fluid-inclusion data suggest that part of the pores remained open until significant burial, we still do not know the importance of those paleoporosities. The available data is insufficient for us to either confirm or discount the possibility that significant primary porosities in the Kamouraska quartzite could have been preserved until late in the tectonic history of the Humber Zone. For the limestone of the Rivière Ouelle Formation, our limited fluid-inclusion data indicate that significant primary

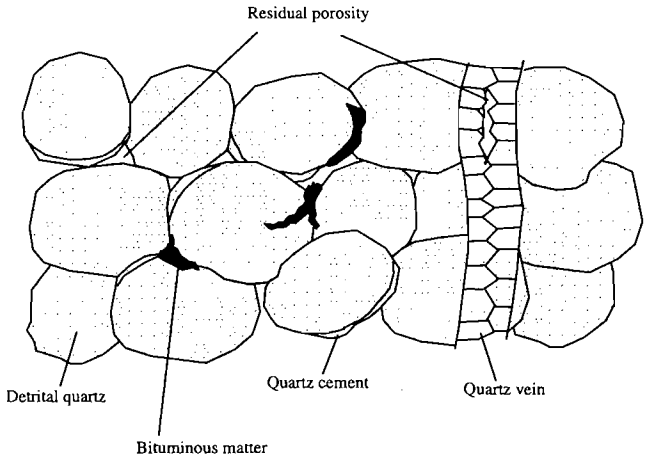

Figure 4. *Relationship between detrital quartz, quartz cement, quartz vein, bituminous matter, and residual pores in quartzite of the Kamouraska Formation.*

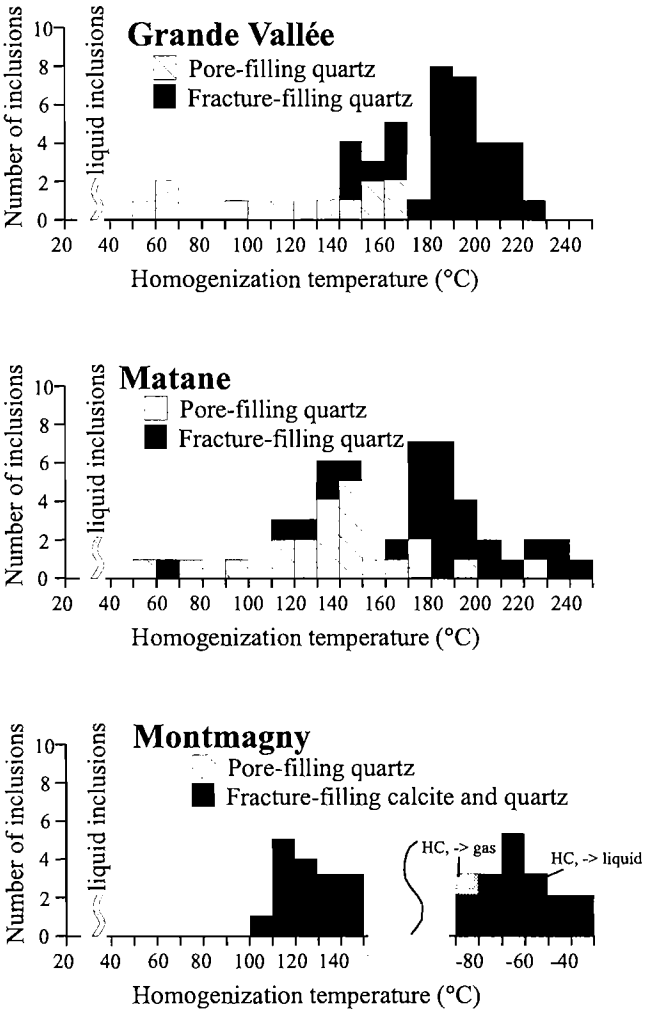

Figure 5. *Histograms of homogenization temperatures of fluid inclusions from pore-filling and fracture-filling quartz and calcite in the quartzite of the Kamouraska Formation.*

Table 1. Summary of fluid-inclusion microthermometric data.

Area (n samples)	Pore-filling cements		Fracture-filling cements	
	T_h (°C)	Salinity (wt.%)	T_h(°C)	Salinity (wt.%)
Quartzite of the Kamouraska Formation				
Grande Vallée (5)	L...58.3 to 167.4 (11)	1.9 to 8.0 (4)	129.8 to 221.9 (34)	2.2 to 7.3 (15)
Matane (6)	L...54.4 to 221.7 (20)	2.1 to 4.7 (8)	71.4 to 243.6 (29)	2.1 to 6.7 (9)
Montmagny (7)	L... ?	6.4 to 8.3 (2)	104.2 to 142.5 (16)	13.2 to 21.1 (8)
			-88.4 (1) (to vapour; methane) -82.4 to -32.4 (15) (to liquid; light HC)	
Limestone of the Rivière Ouelle Formation				
Grande Vallée (1)			62.5 to 132.8 (10)	0.9 to 1.7 (2)
			-97.4 to -84.0 (10) (to liquid; methane)	
Metane (1)	94.1 to 168.1 (12)	2.7 to 14.0 (10)	145.1 to 193.7 (3)	3.2 to 4.8 (3)
			-97.6 to -90.4 (2) (to liquid; methane)	
T_h = homogenization temperature; L = all-liquid inclusion; HC = hydrocarbons				

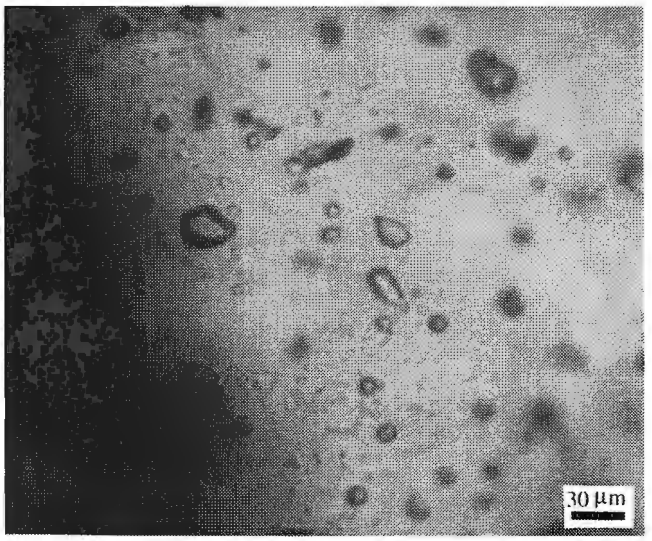

Figure 6. Monophase hydrocarbon fluid inclusions in a calcite crystal from a quartz-calcite vein in quartzite of the Kamouraska Formation (MT-17C). The inclusions nucleated a bubble while cooling and homogenized to the liquid phase at temperatures between -82° and -32°C.

porosities could have been preserved until burial temperatures reached 100°C to 120°C. More studies are needed to evaluate the evolution of porosity in this unit.

Our observation that bituminous matter postdates quartz cements and that hydrocarbon inclusions are contained in quartz-calcite veins suggests a late hydrocarbon migration event. The quartz-calcite veins could have been formed in fractures associated with the Taconian or later tectonic events. We speculate that some potential reservoir rocks such as the Kamouraska Formation quartzite could have been thrust over potential source rocks during the Taconian Orogeny (Lynch and Arsenault, 1997) and that the fractures created during the tectonic events could have served as conduits for hydrocarbon migration. Obviously, an understanding of the timing of hydrocarbon migration is critical to proposing a sound exploration strategy. This is especially true in a region such as the Humber Zone, which has undergone complex tectonic events. Our ongoing research will attempt to establish the relative 'age' of hydrocarbon migration, through field observations of crosscutting relationships from hydrocarbon-inclusion-hosting veins. Future research should include analyzing the isotopic compositions of the hydrocarbon inclusions so that a given hydrocarbon flow may be related to a certain source region.

ACKNOWLEDGMENTS

This work was funded by the Geological Survey of Canada. We thank R. Bertrand and Y. Héroux for help in the fluorescence study. G. Lynch is thanked for reading the manuscript and for helpful suggestions.

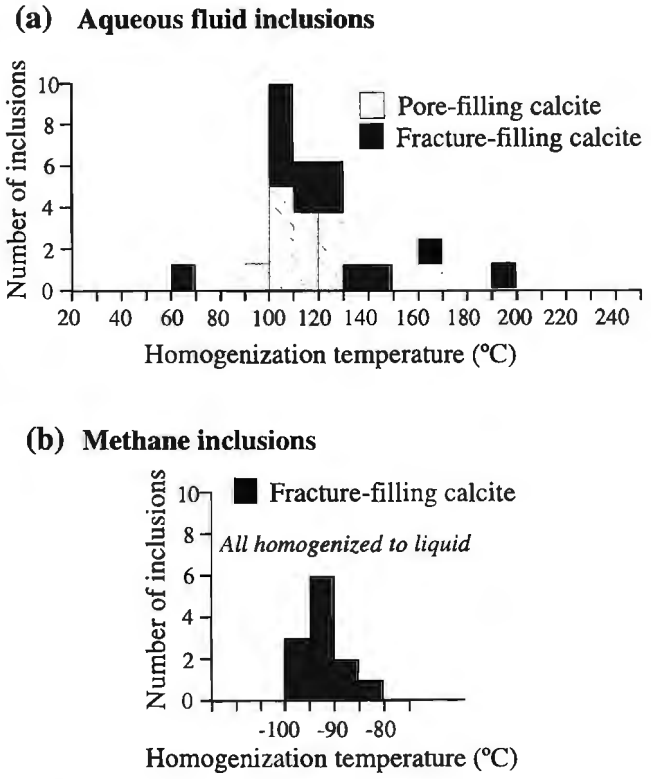

Figure 7. Histograms of homogenization temperatures of fluid inclusions from pore-filling and fracture-filling calcite in limestone of the Rivière Ouelle Formation. (a) Aqueous fluid inclusions. (b) Methane inclusions.

REFERENCES

Ettner, D.C., Lindblom, S., and Karlsen, D.
1996: Identification and implications of light hydrocarbon fluid inclusions from the Proterozoic Bidjovagge gold-copper deposit, Finnmark, Norway; Applied Geochemistry, v. 11, p. 745-755.

Goldstein, R.H. and Reynolds, T.J.
1994: Systematics of fluid inclusions in diagenetic minerals; Society of Economic Geologists and Mineralogists Short Course 31, 199 p.

Hubert, C.
1973: Kamouraska, La Pocatière, and Saint-Jean-Port-Joli area; Quebec Department of Natural Resources, Geological Exploration Service, Geological Report 151, 205 p.

Lavoie, D.
1997: Cambrian-Ordovician slope conglomerates in the Humber Zone, Quebec Reentrant, Quebec; in Current Research 1997-D; Geological Survey of Canada, p. 9-20.

Lavoie, D.
1998: Along strike Upper Cambrian–Lower Ordovician stratigraphic nomenclature and framework along strike in the external domain of the Humber Zone, from Quebec City to Gaspé; in Current Research 1998-D; Geological Survey of Canada, p. XX-XX.

Lynch, G. and Arsenault, O.
1997: Stratigraphy and deformation of the Humber Zone in Gaspésie, Quebec; in Current Research 1997-D; Geological Survey of Canada, p. 1-8.

St-Julien, P. and Hubert, C.
1975: Evolution of the Taconian orogen in the Quebec Appalachians; American Journal of Science, v. 275-A, p. 337-362.

Geological Survey of Canada Project 960012ZH

Electrical characteristics of mineralized and nonmineralized rocks at the Caribou deposit, Bathurst mining camp, New Brunswick[1]

T.J. Katsube, S. Connell, N. Scromeda, W.D. Goodfellow, and M.E. Best[2]
Mineral Resources Division, Ottawa

Katsube, T.J., Connell, S., Scromeda, N., Goodfellow, W.D., and Best, M.E., 1998: Electrical characteristics of mineralized and nonmineralized rocks at the Caribou deposit, Bathurst mining camp, New Brunswick; in Current Research 1998-D; Geological Survey of Canada, p. 25-35.

Abstract: Electrical anisotropic (λ) characteristics of ten mineralized (massive sulphides) and non-mineralized (foliated volcanic tuffs) rock samples from the Caribou deposit (Bathurst mining camp, New Brunswick) have been studied to provide information to assist interpretation of airborne, ground, and borehole EM surveys.

Results indicate that electrical resistivities (ρ_r) of massive sulphides and foliated volcanic tuffs fall within the ranges 0.1-3.0 Ω-m and $1.5x10^2$-$4.6x10^4$ Ω-m, respectively. Little anisotropy is seen in the massive suphides, except for those with calcitic veins cutting across the sample, which increase ρ_r by 6-390 times (λ=6:1 to 390:1) in the direction perpendicular to the vein compared to values obtained where no veins are present. The volcanic tuffs display high and low ρ_r values: 6800-15 000 Ω-m and 150-2700 Ω-m, in the directions perpendicular and parallel to the foliation, resulting in respectively, values of λ ranging from 4:1 to 70:1. Petrological characteristics which can explain the low ρ_r values are thin layers containing high concentrations of chloritic material.

Résumé : Les caractéristiques électriques anisotropiques (λ) de dix échantillons de roches minéralisées (sulfures massifs) et non minéralisées (tufs volcaniques foliés) du gisement de Caribou (camp minier de Bathurst, Nouveau-Brunswick) ont été étudiées afin d'obtenir des informations permettant de faciliter l'interprétation des levés électromagnétiques aéroportés, au sol et de sondage.

Les résultats obtenus indiquent que les résistivités électriques (ρ_r) des sulfures massifs et des tufs volcaniques foliés s'inscrivent dans les fourchettes 0,1-3,0 Ωm et 1,5 x 10^2-4,6 x 10^4 Ωm, respectivement. On observe peu d'anisotropie dans les sulfures massifs, à l'exception de ceux dont les échantillons sont recoupés par des filons calcitiques, où ρ_r s'accroît de 6 à 390 fois (λ=6/1 à 390/1) dans la direction perpendiculaire au filon comparativement aux valeurs obtenues en l'absence de filons. Les tufs volcaniques présentent des valeurs maxima et minima de ρ_r de 6 800-15 000 Ωm et de 150-2 700 Ωm dans les directions perpendiculaire et parallèle à la foliation respectivement, les valeurs de λ variant de 4/1 à 70/1. La présence de minces couches contenant des concentrations élevées de substances chloritiques est une caractéristique pétrologique susceptible d'expliquer les valeurs faibles de ρ_r.

[1] Contribution to the 1994-1999 Bathurst Mining Camp, Canada-New Brunswick Exploration Science and Technology (EXTECH II) Initiative
[2] Bemex Consulting International, 5288 Cordova Bay Road, Victoria, British Columbia V8Y 2L4

INTRODUCTION

The electrical characteristics of mineralized and nonmineralized rock samples from the Caribou massive sulphide deposit (Fig. 1) have been studied in order to determine the electrical connectivity of the sulphide mineralization and its relationship to mineral deposits and tectonic fabrics. The objective of this study is to provide information to assist in the interpretation of airborne, ground, and borehole EM surveys. Following the study on Brunswick No. 12 massive sulphide deposit (Katsube et al., 1997), the Caribou deposit is the second of five chosen for this type of study in the Bathurst mining camp. These deposits were chosen because of variations in their EM responses, in their sulphide mineral grain sizes, and in their tectonic setting.

The electromagnetic responses from massive sulphide ore bodies in the Bathurst mining camp are quite variable. Factors such as textures, grain size (connectivity), mineralogy, fractures, and crosscutting veins all affect the EM response of massive sulphides. Previous work (Katsube et al., 1996a, b, c, 1997; Jones et al., 1996) suggested that electrical anisotropy may also be an important factor which can affect the magnitude of the EM responses. Therefore, this study includes laboratory electrical measurements made in three directions whenever possible. The purpose of this paper is to document the geological characteristics of each sample, to describe the research methodology, and to present the preliminary results.

METHOD OF INVESTIGATION

Samples and sample preparation

Ten core samples (sample numbers MXC-1 to MXC-10) consisting of massive sulphide and volcanic tuff, were obtained from one drillhole (#62-48) intersecting the Caribou deposit. Sample depths and geological units are listed in Table 1. At least two specimens were cut from each sample, one for determination of bulk density, δ_B, and electrical resistivity, ρ_r, and one for measurement of effective porosity, ϕ_E. Several specimens (e.g. a, b, c, and d) were cut from some samples so that different components of the inhomogeneities and anisotropy could be characterized by the ρ_r measurements, as shown in Figure 2. Specimens prepared for anisotropic studies were of rectangular shapes (Table 2) to allow three directional ρ_r measurements (e.g. sample MXC-2a and MXC-2b, in Fig. 2a). The three directions are identified by α, β and γ.

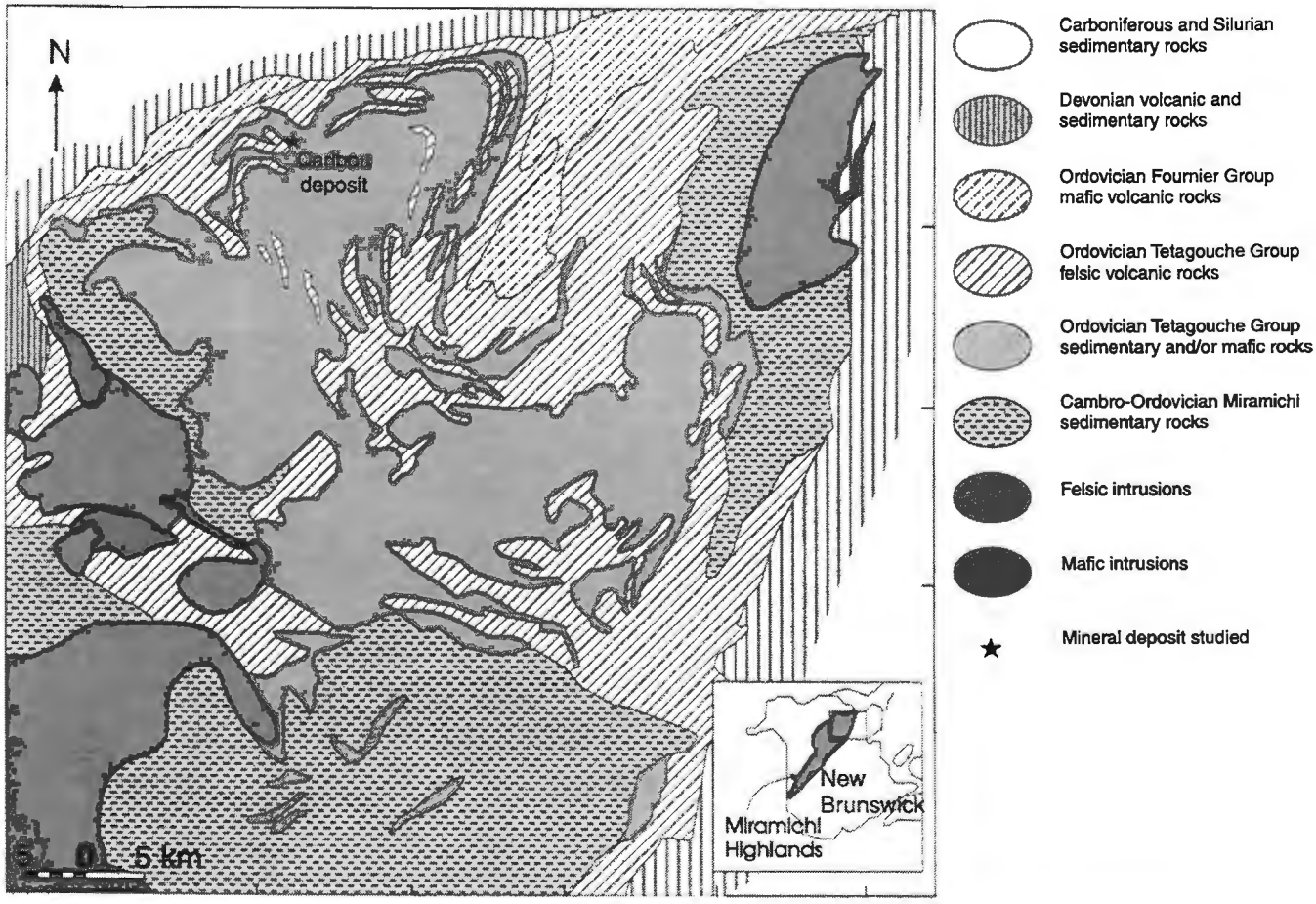

Figure 1. *Map of Bathurst mining camp, New Brunswick (modified from Davies, 1977), showing location of the Caribou deposit.*

Those prepared for ϕ_E measurements were either partial-disc or irregular in shape (Fig. 2). The δ_B and ρ_r measurements were performed on thirteen specimens, representing the ten samples. The measurement of ϕ_E was made on specimens from only five of these samples, containing little or no visible sulphides. The geometric characteristics of the specimens used for ρ_r and δ_B measurements are listed in Tables 2 and 3. Preparations are in progress for petrographic thin section analysis and scanning electron microscope analysis of selected samples/specimens to determine connectivity of the electronic conductive minerals (e.g. pyrite).

Table 1. Field descriptions and depths for samples collected from Caribou deposit drillhole #62-48.

Sample no.	Sample I.D.	Depth (m)	Rock type
MXC-1	62-48-1	7.47	Volcanic tuff
MXC-2	62-48-2	20.19	Volcanic tuff
MXC-3	62-48-3	23.22	Massive sulphide
MXC-4	62-48-4	29.11	Massive sulphide
MXC-5	62-48-5	38.71	Massive sulphide
MXC-6	62-48-6	48.31	Massive sulphide
MXC-7	62-48-7	55.04	Volcanic tuff
MXC-8	62-48-8	61.87	Volcanic tuff
MXC-9	62-48-9	38.94	Massive sulphide
MXC-10	62-48-10	67.67	Volcanic tuff

Bulk density and effective porosity measurements

The caliper method (API, 1960) has been used to determine the bulk density (δ_B) of the samples, by measuring the dimensions and weight of the rectangular specimens. The results of these measurements have also been used in the procedure to determine porosity. Effective porosity (ϕ_E), in principle, represents the pore volume of all interconnected pores. In this study, it is determined from the difference in weight between the oven-dried and water-saturated rock specimen. Another parameter derived on a routine basis is the irreducible water saturation, S_{ir}, which represents the pore space occupied by the bound or adsorbed water on the pore surfaces. Measurements are taken at room temperature (23°C) and atmospheric pressure (Scromeda and Katsube, 1994; Katsube and Scromeda, 1995).

Table 2. Dimensions of specimens cut out from the samples for electrical measurements, and the results of the bulk density (δ_B) determinations.

Sample	a_1 (cm)	a_2 (cm)	ℓ (cm)	W (g)	V (cm^3)	K_G (10^{-2}m)	δ_B (g/mL)
MXC-1aα	1.875	2.304	0.636	7.7355	2.75	6.79	2.82
MXC-1aβ	0.636	2.304	1.875	7.7355	2.75	0.782	2.82
MXC-1b	1.899	2.296	0.544	6.6062	2.37	8.01	2.79
MXC-1cα	0.870	1.518	0.577	2.0657	0.76	2.29	2.71
MXC-1cβ	0.577	1.518	0.870	2.0657	0.76	1.01	2.71
MXC-2aα	1.626	2.220	1.017	10.0679	3.67	3.55	2.74
MXC-2aβ	1.017	2.220	1.626	10.0679	3.67	1.39	2.74
MXC-2bα	1.606	1.993	1.158	10.1185	3.71	2.76	2.73
MXC-2bβ	1.158	1.993	1.606	10.1185	3.71	1.44	2.73
MXC-3aα	1.221	1.444	1.160	9.8313	2.05	1.52	4.81
MXC-3aβ	1.160	1.444	1.221	9.8313	2.05	1.37	4.81
MXC-4a	1.652	1.782	1.161	16.3056	3.42	2.54	4.77
MXC-5aα	1.275	1.421	1.218	10.1829	2.21	1.49	4.61
MXC-5aβ	1.218	1.421	1.275	10.1829	2.21	1.36	4.61
MXC-5aγ	1.218	1.275	1.421	10.1829	2.21	1.09	4.61
MXC-6aα	1.023	1.525	1.004	7.3461	1.57	1.55	4.69
MXC-6aβ	1.004	1.525	1.023	7.3461	1.57	1.50	4.69
MXC-6aγ	1.004	1.023	1.525	7.3461	1.57	0.674	4.69
MXC-7aα	1.705	2.280	0.971	10.7624	3.77	4.00	2.85
MXC-7aβ	0.971	2.280	1.705	10.7624	3.77	1.30	2.85
MXC-8aα	1.779	2.258	1.305	14.3644	5.24	3.08	2.74
MXC-8aβ	1.305	2.258	1.779	14.364	5.24	1.66	2.74
MXC-9aα	1.427	1.496	1.288	12.4347	2.75	1.66	4.52
MXC-9aβ	1.288	1.427	1.496	12.4347	2.75	1.23	4.52
MXC-10aα	1.058	2.282	0.922	6.2046	2.23	2.62	2.79
MXC-10aβ	0.922	2.282	1.058	6.2046	2.23	1.99	2.79

a_1, a_2 : Length of the two sides of the rectangular specimen
ℓ : Thickness of specimen
W : Weight of specimen under room dry conditions
V : Volume of specimen
K_G : Geometric factor
δ_B : Bulk density

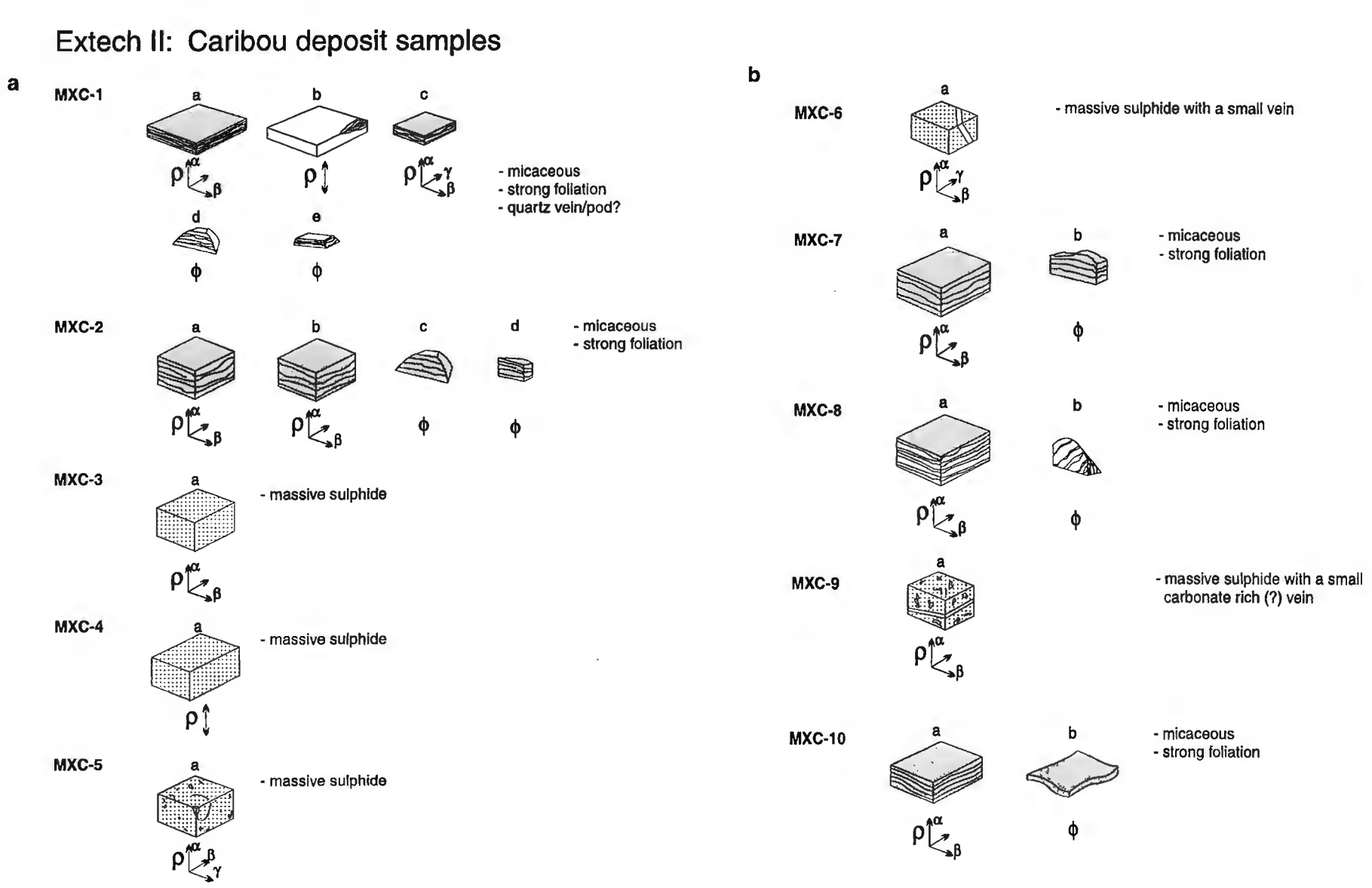

Figure 2. *Block diagrams of specimens cut from the ten samples, and used for electrical resistivity and porosity measurements in this study* ***a)*** *for samples MCX-1 to MXC-5, and* ***b)*** *for samples MXC-6 to MXC-10.*

Table 3. Results of the effective porosity (ϕ_E) measurements.

Sample	δ_B (g/mL)	W_W (g)	W_D (g)	S_{ir} (%)	ϕ_E (%)
MXC-1d	2.71	7.1980	7.1440	33.5	2.05
MXC-1e	2.71	1.7863	1.7710	8.5	2.34
MXC-2c	2.73	10.6387	10.4484	7.9	4.97
MXC-2d	2.73	8.9641	8.7957	6.6	5.23
MXC-7b	2.85	6.0196	5.9908	23.3	1.37
MXC-8b	2.74	7.6085	7.5801	15.5	1.03
MXC-10b	2.79	4.6190	4.6023	27.0	1.01

W_w = wet weight
W_D = dry weight
S_{ir}= irreducible water saturation
δ_B = bulk density (Equation 2)
ϕ_E = effective porosity

Table 4. Results of electrical resistivity (ρ_r) measurements.

Sample	Mes. #1	ρ_r (10^3 Ω-m) Mes. #2	Mean **
MXC-1aα	9.70	9.58	9.64 ± 0.06
MXC-1aβ	0.52	0.59	0.56 ± 0.04
MXC-1b	39.21	52.29	45.75 ± 6.54
MXC-1cα	10.59	8.60	9.60 ± 1.00
MXC-1cβ	0.66	0.71	0.69 ± 0.03
MXC-1cγ	0.78	1.07	0.92 ± 0.15
MXC-2aα	6.53	7.33	6.93 ± 0.40
MXC-2aβ	0.15	0.15	0.15 ± 0.00
MXC-2bα	14.48	15.16	14.82 ± 0.34
MXC-2bβ	0.21	0.22	0.22 ± 0.10
MXC-3aα	0.0003	0.0002	0.0003*
MXC-3aβ	0.0003	0.0002	0.0003*
MXC-4a	0.0002	0.0002	0.0002*
MXC-5aα	0.0006	0.0002	0.0004*
MXC-5aβ	0.0001	0.0001	0.0001*
MXC-5aγ	0.0002	0.0002	0.0002*
MXC-6aα	0.0004	0.0005	0.0005*
MXC-6aβ	0.0004	0.0050	0.003*
MXC-6aγ	0.0005	0.0007	0.0006*
MXC-7aα	6.56	7.11	6.84 ± 0.28
MXC-7aβ	0.83	0.86	0.85 ± 0.02
MXC-8aα	13.75	15.43	14.59 ± 0.84
MXC-8aβ	0.59	0.62	0.61 ± 0.02
MXC-9aα	0.41	0.37	0.39 ± 0.02
MXC-9aβ	0.0002	0.0003	0.0003*
MXC-10aα	7.38	7.13	7.26 ± 0.13
MXC-10aβ	0.19	0.20	0.20 ± 0.01

ρ_r = Bulk electrical resistivity
Mes. (#1) = Measurement after 24 hours of saturation
Mes. (#2) = Measurement after 48 hours of saturation
* = Possible error >± 100%
** = The value after the "±" is the maximum difference between the mean and the individually measured values

The API Recommended Practice for Core-Analysis Procedures (API, 1960) has generally been followed in these measurements. Details of the standard procedures routinely used in our measurements are described in the literature (Katsube and Salisbury, 1991; Katsube et al., 1992; Scromeda and Katsube, 1994; Katsube and Scromeda, 1995).

Bulk electrical resistivity measurements

The bulk electrical resistivity (ρ_r) is determined from the complex electrical resistivity (ρ^*) measurements made by methods described in recent publications (e.g. Katsube et al., 1991, 1992, 1996a, b; Katsube and Salisbury, 1991; Katsube and Scromeda, 1994). The complex electrical resistivity (ρ^*) was measured on specimens saturated with distilled water for 24-48 hours (Katsube and Salisbury, 1991). It (ρ^*) is measured over a frequency range of 1-10^6 Hz, with ρ_r usually representing a bulk electrical resistivity at frequencies of about 10^2-10^3 Hz. It (ρ_r) is a function of the pore structure and pore fluid resistivity, and is understood to exclude any other effects, such as electrode, pore surface, dielectric, or any other polarizations (Katsube and Walsh, 1987; Katsube, 1975).

When electrical resistivity is measured over these frequencies, dielectric polarization, Warburg impedance, and electrode polarization effects are reflected in the measurements (Katsube, 1975; Katsube and Salisbury, 1991). A simple method applied to distinguish different mechanisms for improvement of the measurement accuracy is to use Cole-Cole plots where imaginary-resistivity (ρ_I) is plotted against real-resistivity (ρ_R) (Katsube and Walsh, 1987). Katsube (1975) considered plots consisting of three arcs and suggested that each arc includes the effect of different groups of electrical conduction mechanisms. It was proposed that the left-most arc reflects the effects of the dielectric constant, double layer, pore structure, and pore water chemistry. In accordance with this model, ρ_r is determined from the point where the left arc intersects the horizontal axis, as will be shown later in this paper.

The geometric factor, K_G (with the units 10^{-2} m), required for derivation of ρ^* from the actual electrical measurements, is defined as

$$K_G = A/\ell, \quad (1)$$

where A (cm^2) is the cross-section area and ℓ (cm) is the thickness. This parameter was determined for all specimens prior to the electrical measurements, using the specimen dimensional data in Table 2.

EXPERIMENTAL RESULTS

Bulk density (δ_B) results (Table 2) presented are in the ranges of 4.52-4.81 g/mL for the massive sulphide samples and 2.71-2.85 g/mL for the volcanic tuff. The effective porosities (ϕ_E) are listed in Table 3, the values falling in the range of 1.0-5.2%. These samples are represented by sections containing little or no sulphide minerals. The specimens with δ_B values used to determine ϕ_E are those used in the electrical measurements, and are not for those prepared to measure porosity. This is because the caliper method, used for δ_B determinations, cannot be used on irregular-shaped specimens which were those used to determine ϕ_E. However, the two specimens were taken from locations in the sample as close to each other as possible, and with similar petrography.

Results of the electrical resistivity (ρ_r) measurements are listed in Table 4. Determinations have been made at 24 and 48 hours after water saturation to check the stability of the ρ_r values with time. After these time periods, it is expected that the distilled water has chemically equilibrated with the rock, and represents the in situ conditions. Normally differences within ±20 % of their mean are considered to be within measurement error and represent stable conditions. In the present study, few of the higher resistivity (>10 Ω-m) samples exceed that value. For ρ_r values of 10 Ω-m and below, the error range is considered to increase with decreasing ρ_r, with error ranges

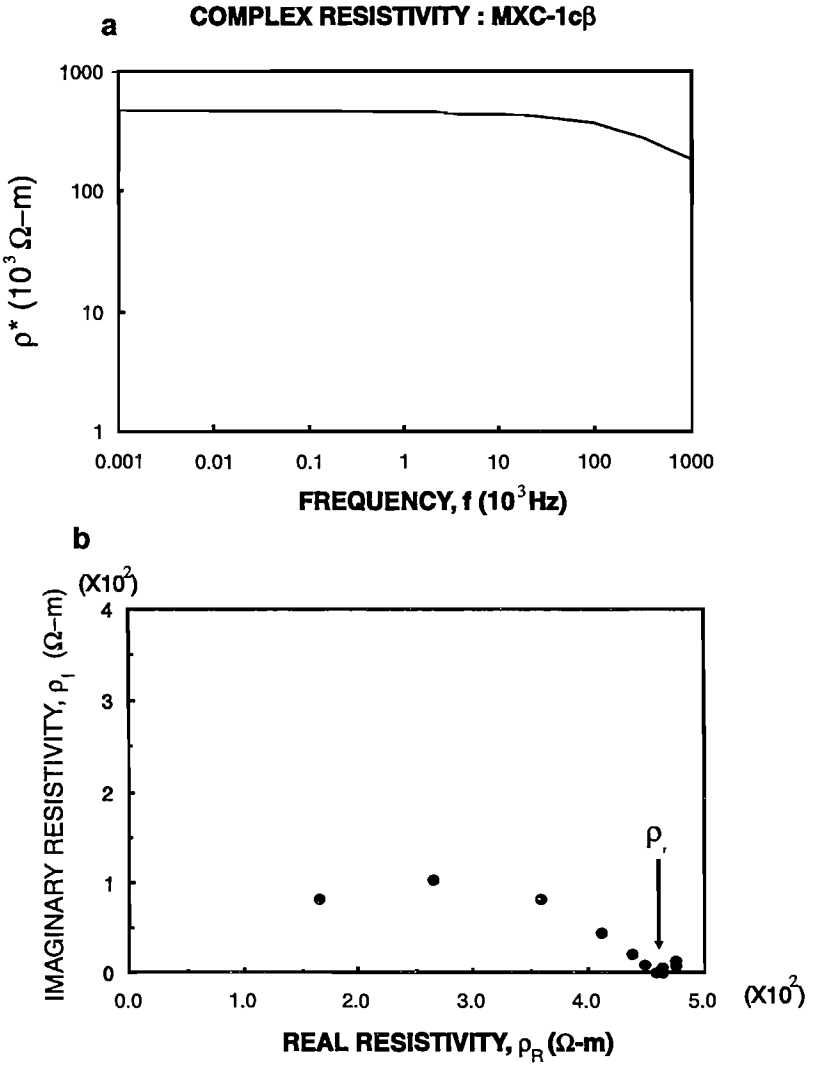

Figure 3.

Typical examples of complex resistivity (ρ^*) plots used to determine bulk electrical resistivity (ρ_r), where ρ_R and ρ_I are the real and imaginary resistivities (Katsube, 1975; Katsube and Walsh, 1987; Katsube and Salisbury, 1991), respectively. ***a)*** *Complex resistivity (ρ^*) as a function of frequency (f), and* ***b)*** *Imaginary resistivity (ρ_I) as a function of real resistivity (ρ_R) for sample/specimen MXC-1cβ (24 hour saturation). This plot displays a normally shaped arc, a pattern usually associated with rocks of intermediate resistivity.*

Table 5. Electrical ainisotropy (λ) characteristics of samples from the Caribou deposit.

Sample no.	Specimen no.	ρ_{rH} (Ω-m) (minimum)	ρ_{rV} (Ω-m) (maximum)	λ
MXC-1	a	560	9640	17:1
	c	680	9600	14:1
MXC-2	a	150	6930	46:1
	b	220	14 820	67:1
MXC-6		0.5	3	6:1
MXC-7	a	850	6840	8:1
MXC-8	a	610	14 590	24:1
MXC-9	a	1*	390	390:1
MXC-10	a	200	7260	36:1

ρ_{rH} = Bulk electrical resistivity values taken in the direction parallel to the foliation or bedding

ρ_{rV} = Bulk electrical resistivity values taken perpendicular to the foliation or bedding

λ = Electrical resistivity anisotropy

* = ρ_r=1.0 Ωm if ρ_r<1.0

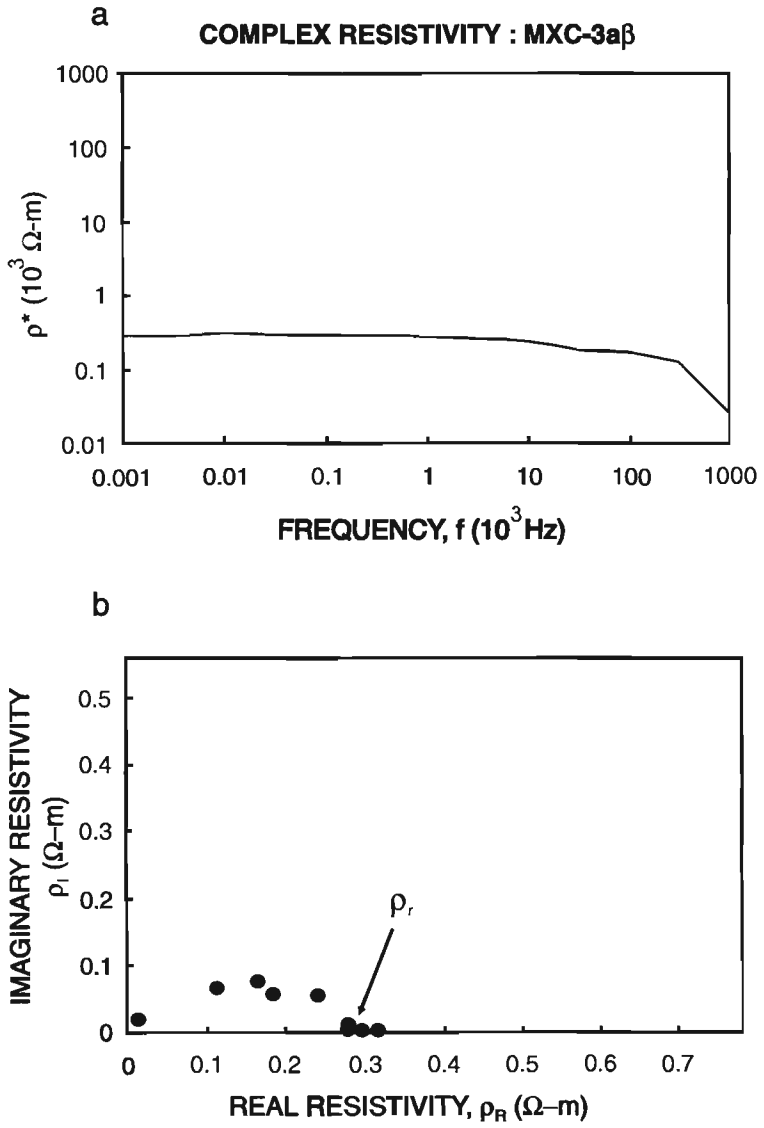

Figure 4.

Typical examples of complex resistivity (ρ^*) plots, for cases in which difficulty is experienced in determining ρ_r, where ρ_R and ρ_I are the real and imaginary resistivities (Katsube, 1975; Katsube and Walsh, 1987; Katsube and Salisbury, 1991), respectively. ***a)*** *Complex resistivity (ρ^*) as a function of frequency (f), and* ***b)*** *imaginary resistivity (ρ_I) as a function of real resistivity (ρ_R) for sample/specimen MXC-3aβ (24 hour saturation). The plot takes the form of a slightly distorted arc. This pattern is commonly seen in rocks of very low resistivity (Katsube et al., 1992).*

estimated to reach ±100% at <1.0 Ω-m (e.g. MXC-6aβ, Table 4). Twenty-seven determinations (including multidirectional measurements) were made for thirteen specimens representing ten samples. Further details of the analytical procedures have been described previously (e.g. Katsube and Scromeda, 1994; Katsube et al., 1996a).

Some examples of complex resistivity plots used to determine low to high ρ_r values are shown in Figures 3 to 6. Figure 3 displays a typical complex resistivity plot for a sample of volcanic tuff (MXC-1cb) with intermediate ρ_r values. Figure 4 displays complex resistivity plots typical of a very electrically conductive sample, a massive sulphide, where difficulties were encountered when determining the ρ_r value due to the distortion in the arc. Figure 5 displays complex resistivity plots for specimen MXC-9aα, another massive sulphide, which shows two rather suppressed arcs. One arc (left-hand side) represents the electrical characteristics of the rock sample and the other (right-hand side) resulted from electrode or other polarizations. Electrode polarization is often seen in intermediate resistivity rocks when electrically conductive minerals (e.g. sulphides) are present. Although this sample is a massive sulphide, the cole-cole plot resembles that of an intermediate resistivity rock because of the higher resistivity of the vein that has interrupted the conductive path. Therefore, the cole-cole plot presented here (Fig. 5) best represents the electrical characteristics of the vein rather than the massive sulphide containing it. Figure 6 displays plots for the same specimen as MXC-9aα (Fig. 5), but this time measurements were made in a different direction, β rather than α. The increased conductivity in the β direction parallel to the vein has, likely, resulted in distorted plots. The plot shown here (Fig. 6) best reflects the electrical characteristics of the sulphide.

The ρ_r values observed in this study are in the range of 0.1-3.0 Ω-m for the massive sulphides and $1.5x10^2$-$4.6x10^4$ Ω-m for the felsic tuff. The lower values for felsic tuff resemble those for late terrestrial (Quaternary to Paleozoic) sedimentary rocks (Keller and Frischknecht, 1966), and the higher values are similar to those for crystalline rocks (Katsube and Hume, 1987, 1989; Katsube and Mareschal, 1993).

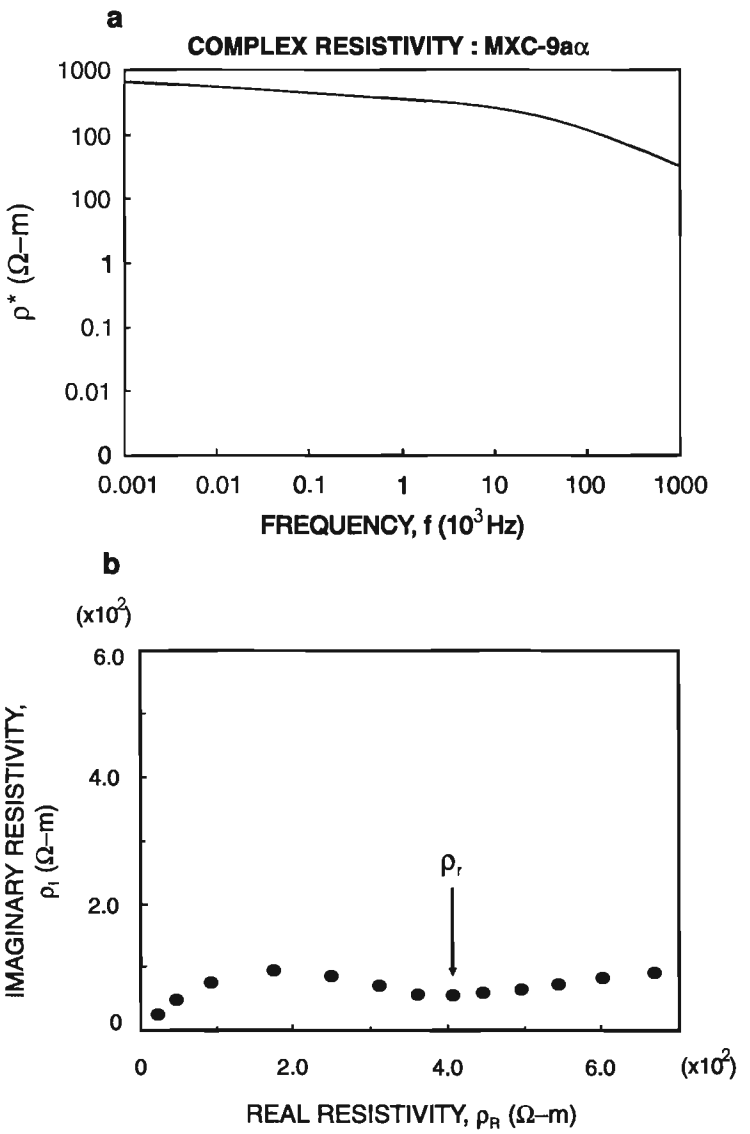

Figure 5.

Typical examples of complex resistivity (ρ^*) plots used to determine bulk electrical resistivity (ρ_r), where ρ_R and ρ_I are the real and imaginary resistivities (Katsube, 1975; Katsube and Walsh, 1987; Katsube and Salisbury, 1991), respectively. ***a)*** *Complex resistivity (ρ^*) as a function of frequency (f), and* ***b)*** *imaginary resistivity (ρ_I) as a function of real resistivity (ρ_R) for sample/specimen MXC-9aα (24 hour saturation), manifested as a plot displaying two rather suppressed arcs, often seen in rocks of intermediate resistivity containing electrically conductive minerals (e.g. sulphides, Katsube et al., 1996a).*

DISCUSSIONS AND CONCLUSIONS

The ten samples used in this study consist mainly of massive sulphides and strongly foliated volcanic tuffs. The massive sulphides display electrical resistivity (ρ_r) values in the range of 0.1-3.0 Ω-m, whereas those for foliated volcanic tuffs are in the range of $1.5x10^2$-$4.6x10^4$ Ω-m, as previously indicated.

The five massive sulphide samples (MXC-3, MXC-4, MXC-5, MXC-6, and MXC-9) have bulk density (δ_B) values in the range of 4.52-4.81 g/mL, suggesting a high metallic sulphide content. This high content is also reflected by the low ρ_r values (0.1-3.0 Ω-m), which indicate good electrical connectivity between the metallic sulphide grains. Little anisotropy is seen in these samples, except for samples/specimens MXC-9 and MXC-6a, because either anisotropy is nonexistent or it is not recognizable due to the low resolution of the measurements at these low ρ_r values. Samples MXC-9 shows a strong anisotropy (λ) of 390:1 (Table 5), due to a calcitic vein cutting across the specimen used for the electrical measurement. This raises the ρ_r value considerably in the α-direction (Fig. 2b). The specimen representing Sample MXC-6a is partially intersected by a calcitic vein, raising the ρ_r values slightly in the β- and γ-directions, producing a λ value of 6:1.

The five volcanic tuff samples (MXC-1, MXC-2, MXC-7, MXC-8, and MXC-10) display δ_B and effective porosities (ϕ_E) in the ranges of 2.71-2.85 g/mL and 1.0-5.2%, respectively, resembling those of tight shales (Katsube and Williamson, 1994). They display high ρ_r values (6800-15 000 Ω-m) in the direction perpendicular to the foliation, and low ρ_r values (150-2700 Ω-m) in the direction parallel to the foliation, resulting in an anisotropy (λ) of approximately 4:1 to 70:1 (e.g. Fig. 7). Trace, fine grained sulphides are visible, but the grains do not appear to be interconnected. Essentially, there is no evidence of metallic sulphide minerals being the cause of these low ρ_r values. The major petrological characteristic consistent with the low ρ_r trend is the presence of thin

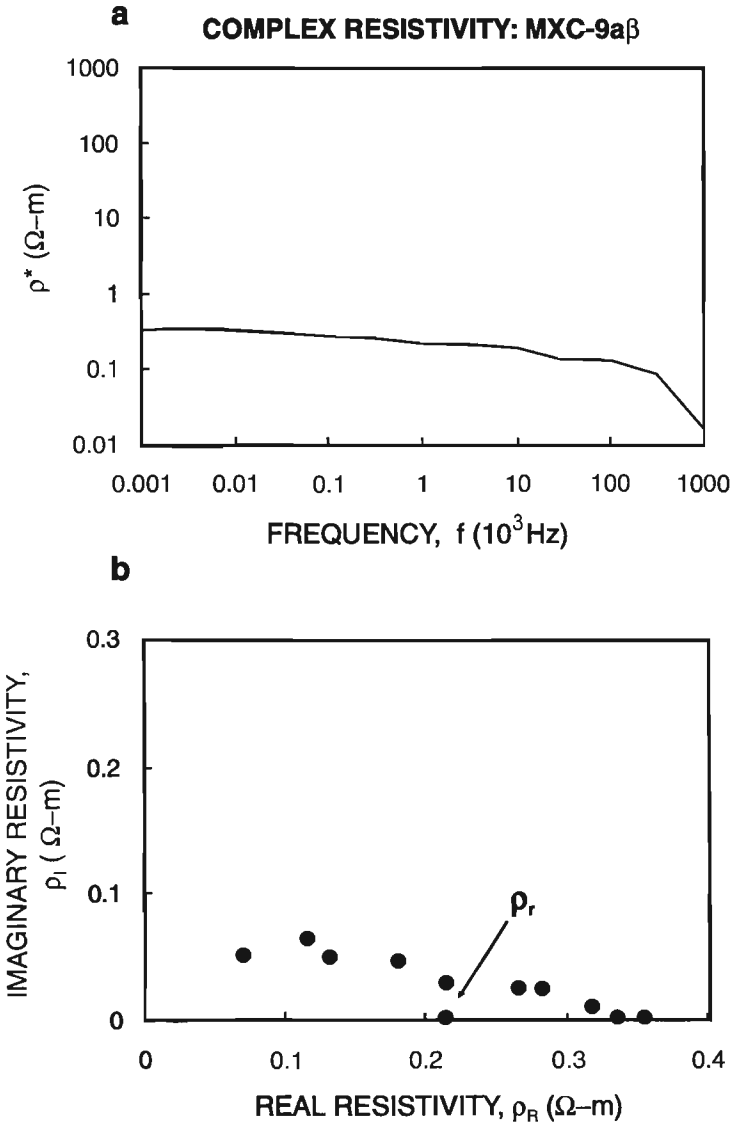

Figure 6.

*Typical examples of complex resistivity (ρ^*) plots, for cases in which difficulty is experienced in determining ρ_r, where ρ_R and ρ_I are the real and imaginary resistivities (Katsube, 1975; Katsube and Walsh, 1987; Katsube and Salisbury, 1991), respectively. **a)** Complex resistivity (ρ^*) as a function of frequency (f), and **b)** imaginary resistivity (ρ_I) as a function of real resistivity (ρ_R) for sample/specimen MXC-9aβ (24 hour saturation), that plots in the form of a slightly distorted arc. This pattern is commonly seen in rocks having very low resistivity (Katsube et al., 1992).*

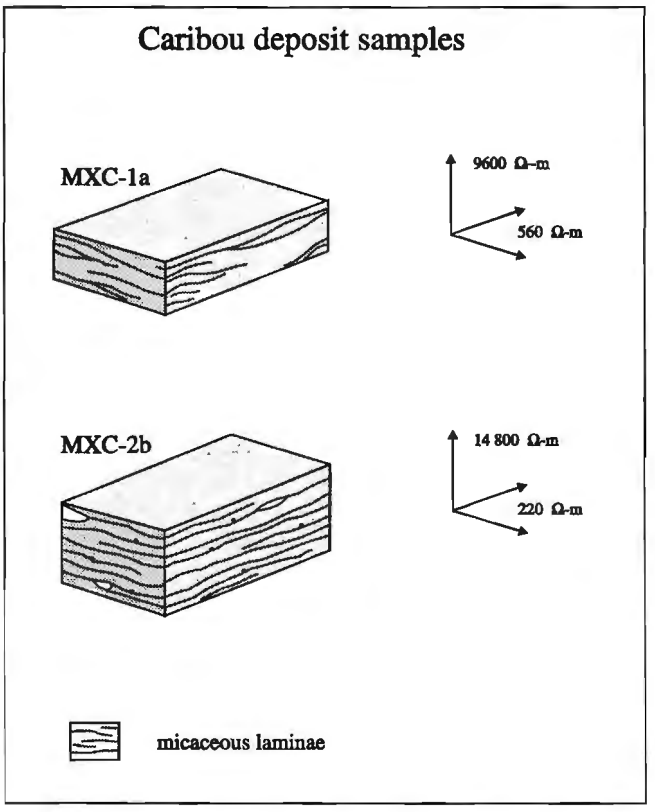

Figure 7. Block diagrams illustrating anisotropic effects present in two of the sample/specimens (specimens MXC-1a and MXC-2b). Both specimens display strong directional effects and are devoid of any visible sulphide mineralization. Electrical resistivities of 200-600 Ω-m are present in a direction parallel to foliation, and 10 000-15 000 Ω-m in the direction perpendicular to foliation.

layers along the foliation containing high chlorite content. It is not currently known, however, if this is the direct cause of the low ρ_r values. One of the specimens (MXC-1b) displays a ρ_r value of 40 000-50 000 Ω-m, the largest in this group of samples. This is most likely, a result of a relatively thick layer of quartz present along the plane of foliation (Fig. 2a).

The existence of the large λ values (1:70 to 1:390) and of the wide range of ρ_r values (<1 to >$4x10^4$ Ω-m) for the massive sulphides and volcanic tuffs implies that there could be areas where the magnitude of the airborne EM signals could vary according to flight direction and applied frequency of the system (Katsube et al., 1996a).

ACKNOWLEDGMENTS

The authors are grateful for the critical review of this paper and for the very useful suggestions by M.D. Thomas (GSC).

REFERENCES

API (American Petroleum Institute)
1960: Recommended practices for core-analysis procedure; API Recommended Practice 40 (RP 40) First Edition, American Petroleum Institute, Washington, D.C., p. 55.

Davies, J.L.
1977: Geological map of northern New Brunswick; New Brunswick Department of Natural Resources, Map NR-3, scale 1:250 000.

Jones, A.G., Katsube, T.J., and Ferguson, I.
1996: Paleoproterozoic tectonic processes revealed through electromagnetic studies of the North American Central Plains (NACP) conductivity anomaly; from continental to hand sample scale; in Society of Exploration Geophysicists Expanded Abstracts with Authors' Biographies, Technical Program, 66th Annual Meeting and International Exhibition (Denver, November 10-15, 1996), Volume I, p. 269-272.

Katsube, T.J.
1975: The electrical polarization mechanism model for moist rocks; in Report of Activities, Part C; Geological Survey of Canada, Paper 75-1C, p. 353-360.

Katsube, T.J. and Hume, J.P.
1987: Electrical properties of granitic rocks in Lac du Bonnet batholith; in Geotechnical Studies at Whiteshell Research Area (RA-3); CANMET, Report MRL 87-52, p. 205-220.
1989: Electrical resistivity of rocks from Chalk River; in Workshop Proceedings on "Geophysical and Related Geoscientific Research at Chalk River, Ontario", Atomic Energy of Canada Limited Report AECL-9085, p. 105-114.

Katsube, T.J. and Mareschal, M.
1993: Petrophysical model of deep electrical conductors; Graphite lining as a source and its disconnection due to uplift; Journal of Geophysical Research, v. 98, no. B5, p. 8019-8030.

Katsube, T.J. and Salisbury, M.
1991: Petrophysical characteristics of surface core samples from the Sudbury structure; in Current Research, Part E; Geological Survey of Canada, Paper 91-1E, p. 265-271.

Katsube, T.J. and Scromeda, N.
1994: Physical properties of Canadian kimberlites; Somerset Island and Saskatchewan; in Current Research 1994B; Geological Survey of Canada, p. 35-42.
1995: Accuracy of low porosity measurements in granite; in Current Research 1995-C; Geological Survey of Canada, Paper 95-1C, p. 265-270.

Katsube, T.J. and Walsh, J.B.
1987: Effective aperture for fluid flow in microcracks; International Journal of Rock Mechanics and Mining Sciences and Geomechanics Abstracts, v. 24, p. 175-183.

Katsube, T.J. and Williamson, M.A.
1994: Effects of diagenesis on shale nano-pore structure and implications for sealing capacity; Clay Minerals, v. 29, p. 451-461.

Katsube, T.J., Best, M., and Jones, A.G.
1996b: Electrical anisotropy of mineralized and non mineralized rocks; in Society of Exploration Geophysicists Expanded Abstracts with Authors Biographies, Technical Program, 66th Annual Meeting and International Exhibition (Denver, November 10-15, 1996), Volume II, p. 1279-1281.

Katsube, T.J., Best, M.E., and Mudford, B.S.
1991: Petrophysical characteristics of shales from the Scotian shelf; Geophysics, v. 56, p. 1681-1689.

Katsube, T.J., Jones, A.G., Scromeda, N., and Schwann, P.
1996c: Electrical characteristics of rock samples from the La Ronge Domain of the Trans-Hudson Orogen, Northern Saskatchewan; in Current Research 1996-E; Geological Survey of Canada, p. 159-169.

Katsube, T.J., Palacky, G.J., Sangster, D.F., Galley, A.G., and Scromeda, N.
1996a: Electrical properties of disseminated sulphide ore samples from Snow Lake; in EXTECH I: Multidisciplinary Approach to Massive Sulphide Research in Rusty Lake-Snow Lake Greenstone Belts, Manitoba, (ed.) G.F. Bonham-Carter, A.G. Galley, and G.E.M. Hall; Geological Survey of Canada, Bulletin 426, p. 319-329.

Katsube, T.J., Scromeda, N., Best, M.E., and Goodfellow, W.D.
1997: Electrical characteristics of mineralized and non-mineralized rocks at the Brunswick No. 12 deposit, Bathurst mining camp, New Brunswick; in Current Research 1997-E; Geological Survey of Canada, p. 97-107.

Katsube, T.J., Scromeda, N., Mareschal, M., and Bailey, R.C.
1992: Electrical resistivity and porosity of crystalline rock samples from the Kapuskasing Structural Zone, Ontario: in Current Research, Part E; Geological Survey of Canada, Paper 92-1E, p. 225-236.

Keller, G.V. and Frischknecht, F.C.
1966: Electrical Methods in Geophysical Prospecting; Pergamon Press, New York, 517 p.

Scromeda, N. and Katsube, T.J.
1994: Effect of temperature on drying procedures used in porosity measurements of tight rocks; in Current Research 1994-E; Geological Survey of Canada, p. 283-289.

APPENDIX

Geological sample descriptions

MXC-1: Volcanic tuff (ID: 62-48-1)

Shows a very strong foliation with shiny cleavage planes. Appears to be quite a bit of mica and/or chlorite. Quartz pods are rounded to subrounded (could be used as shear sense indicators). Overall hardness of approximately 2 (can be scratched with fingernail). Grey-green in colour with darker bands.

MXC-2: Volcanic tuff (ID: 62-48-2)

Shows strong foliation, similar to sample MXC-1. Light green and very soft (silky). Hardness approximately 2. Fine crenulations visible on cleavage plane. Small dark green specks visible on lighter green, softer chloritic groundmass. The rounded pods (white) appear to have been altered, they are much softer than those described in sample MXC-1 (approximately 4-5). Trace of fine grained disseminated sulphides.

MXC-3: Massive sulphide (ID: 62-48-3)

Partial/split core segment Fine grained massive sulphide, apparent faint foliation or some type of banding. Few small pores visible (diameter <1 mm).

MXC-4: Massive sulphide (ID: 62-48-4)

Split core segment with an infilled fracture. Fine grained massive sulphide.

MXC-5: Massive sulphide (ID: 62-48-5)

Medium grained massive sulphide, split core segment with some extensional fractures. A few pore spaces infilled with a very soft mineral (talc?) are visible. There are some darker fragments (remnants of the host rock?) intermixed with the sulphides and the talc(?).

MXC-6: Massive sulphide (ID: 62-48-6)

Fine grained massive sulphide, split core segment similar to sample MXC-5. Some pore space infilled with the soft white mineral (talc?). Stringers of various sulphide minerals present.

MXC-7: Volcanic tuff (ID: 62-48-7)

Strong foliation present, although rather irregular in places. Approximately 5-7% fine- to medium-grained disseminated sulphides concentrated in the white quartzitic bands (hardness approximately 6-7), but not in the greenish (chlorite-rich?) bands (hardness approximately 2).

MXC-8: Volcanic tuff (ID: 62-48-8)

Very strong foliation, with fine chlorite rich layers (green, soft, silky) between thicker and more predominant quartzitic layers. The green layers are weathering out (flaking).

MXC-9: Massive sulphide (ID: 62-48-9)

Split core segment of porous massive sulphide, with a few rusty patches. Talc(?) infills the pores and fractures, similar to sample MXC-5. Few larger, dark subrounded fragments are visible.

MXC-10: Volcanic tuff (ID: 62-48-10)

Very strong foliation present. There appears to have been some swelling/alteration, possibly due to water, as sides of the core segment bulge out in places. Very soft (hardness approximately 2) with some harder (hardness approximately 5) white layers. Some crenulations are apparent. Very similar to sample MXC-2.

Preliminary results of the 1997 Polar Margin Aeromagnetic Program survey of northern Greenland and the Lincoln Sea[1]

J.B. Nelson[2], D. Damaske[3], D. Marcotte[4], D. Hardwick[4], D. Forsyth[5], P. Keating[5], M. Pilkington[5], and A. Okulitch[6]

Nelson, J.B., Damaske, D., Marcotte, D., Hardwick, D., Forsyth, D., Keating, P., Pilkington, M., and Okulitch, A., 1998: Preliminary results of the 1997 Polar Margin Aeromagnetic Program survey of northern Greenland and the Lincoln Sea; in Current Research 1998-D; Geological Survey of Canada, p. 37-42.

Abstract: In 1997, in conjunction with the Polar Margin Aeromagnetic Program, 13 000 line-kilometres of aeromagnetic data were collected at a line spacing of 3 km. Lines were flown at a constant altitude of 300 m over the Lincoln Sea and in draped mode over northern Greenland. New data provide the first magnetic map of the Kap Washington volcanic province on northern Greenland. Anomalies indicate extensions of tectonic elements mapped from existing data and new magnetic signatures of regional structures. These include: 1) a magnetic low following the Harder Fiord fault zone and area to the south, 2) high frequency, north-south anomalies characterizing dyke swarms south of Kap Washington, 3) a margin-parallel zone of high-amplitude, short-wavelength anomalies extending 40 km offshore, 4) large amplitude, long-wavelength highs over the Arctic Ocean north of Greenland and 5) high-amplitude, linear anomalies near the continental shelf break north of Ellesmere Island.

Résumé : En 1997, dans le cadre du Programme aéromagnétique de la marge polaire (PAMP), un total de 13 000 kilomètres linéaires de données aéromagnétiques ont été recueillis, le long de lignes espacées de 3 kilomètres l'une de l'autre. Les levés ont été effectués à une altitude constante de 300 mètres au-dessus de la mer de Lincoln et en moulant le relief au-dessus de la partie nord du Groenland. Les nouvelles données fournissent la première carte magnétique de la province volcanique de Kap Washington (partie nord du Groenland). Les anomalies indiquent la présence d'extensions d'éléments tectoniques déjà identifiés à partir des données existantes et font ressortir la signature magnétique de nouvelles structures régionales. En voici des exemples : 1) un creux magnétique suit la zone de faille de Harder Fiord et la région adjacente vers le sud; 2) des anomalies nord-sud de haute fréquence caractérisent les essaims de dykes au sud de Kap Washington; 3) une zone d'anomalies de courte longueur d'onde et de grande amplitude s'observe parallèlement à la marge et à 40 kilomètres au large de la côte; 4) il y a des crêtes de grande longueur d'onde et de grande amplitude au-dessus de l'océan Arctique, au nord du Groenland; 5) une série d'anomalies linéaires de grande amplitude s'observe près de la rupture de pente de la plate-forme continentale, au nord de l'île d'Ellesmere.

[1] Contribution to Polar Margin Aeromagnetic Program

[2] Esquimalt Defence Research Detachment/Defence Research Establishment Atlantic, Victoria, British Columbia
[3] Bundesanstalt für Geowissenschaften und Rohstoffe, Hannover, Germany
[4] Institute for Aerospace Research, Flight Research Laboratory, Ottawa, Ontario
[5] Continental Geoscience Division, Ottawa
[6] GSC Calgary, Calgary

INTRODUCTION

The Polar Margin Aeromagnetic Program was initiated in 1989 to survey unmapped and tectonically strategic areas of the arctic continental margin and adjacent Arctic Ocean. Previous surveys were conducted over northern Ellesmere Island, northwestern Greenland and the Lincoln Sea from 1989 to 1991 (Nelson et al., 1991), over the northern Sverdrup Basin from 1991 to 1993 and the Beaufort Sea in 1994 (Nelson et al., 1995). Structural and tectonic interpretations are described in Forsyth et al. (1994, 1997). The 1997 survey was designed to resolve the polar margin anomaly pattern as far east as the Kap Washington volcanic province on Greenland and confirm the offshore extension of major tectonic trends from Ellesmere Island seen in the earlier data. Funding for the 1997 Polar Margin Aeromagnetic Program survey was provided by the Natural Resources Canada (GSC Calgary, GSC Atlantic, Continental Geoscience Division, Ottawa), the Department of National Defence, the National Research Council, and the German Bundesanstalt für Geowissenschaften und Rohstoffe.

SURVEY PARAMETERS, INSTRUMENTATION, AND PROCEDURES

The survey was conducted with the Convair 580 aircraft, operated by the Institute for Aerospace Research (IAR) based at the Canadian Forces Station Alert from 29 April to 13 May 1997. Thirteen thousand line kilometres were collected on thirteen flights of five hours duration each and include 60 survey lines and fifteen tie lines. The survey lines were oriented approximately 30° to the coast of Greenland becoming margin-parallel at the continental shelf break north of Ellesmere Island. Lines were flown at a nominal spacing of 3 km with a constant altitude of 300 m over the Lincoln Sea, and in a draped mode over the mountains of Northern Greenland (Fig. 1). Figure 1 also shows reduced flight line and higher resolution coverage of the 1997 survey compared to the 1989-1991 data.

The Convair 580 aircraft was instrumented with four cesium total-field magnetometers and two sets of vector magnetometers. The total field (tf), the longitudinal gradient (gx), and the transverse gradient (gy) of the total field were measured using the two wingtip Cesium magnetometers. One set of Narod vector magnetometers was used to model the aircraft-generated magnetic noise from the outputs of the cesium magnetometers using a 27 term model developed at IAR. Data collected during a series of pitches and rolls on the four cardinal headings at the beginning of the first flight were used to determine the 27 model coefficients. The standard deviation of the residual total field noise after aircraft compensation was less than 0.02 nT. These 27 coefficients were then applied in real time to the measurements taken during the survey. The magnetic data were sampled at 32 Hz and recorded on DAT tape.

The Convair was equipped with a barometric altimeter, a radar altimeter, an inertial navigation system, and two CA-Code GPS receivers. The navigation data used for both flight guidance and flight track recovery consisted of Novatel GPS data sampled at 2 Hz, updated with inertial velocity information to generate a 32 Hz navigation data rate. The barometric and radar altimeter data were recorded at 32 Hz on DAT tape.

A Novatel GPS receiver was also set up at CFS Alert to record the raw satellite information. By combining these data with the aircraft Novatel raw satellite data we were able to perform post-flight differential GPS processing for

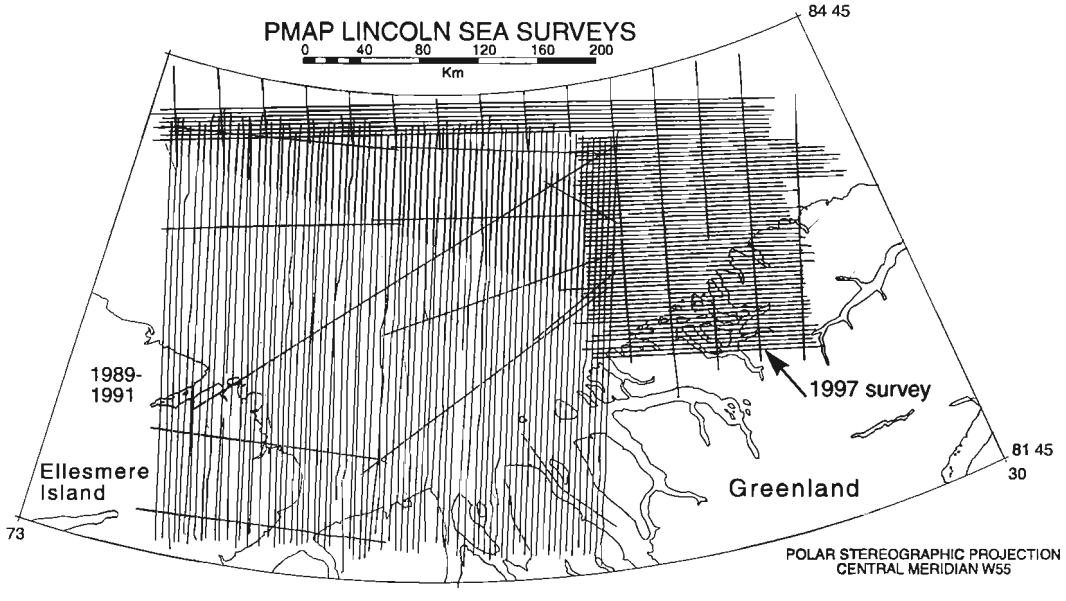

Figure 1. *Polar Margin Aeromagnetic Program (PMAP) flight line locations in the Lincoln Sea area.*

approximately one half of the survey. These data were used for flight track recovery when available, otherwise the as-recorded inertially-updated CA-Code positions were used.

Correcting the survey data for the small diurnal field changes recorded by the GSC magnetometer at CFS Alert produced no improvement and are not included in Figure 2.

DATA PREPROCESSING

The navigation and magnetic data were first subsampled to 8 Hz. To ensure that the total field and gradient noise levels remained very low for the entire survey, a short series of rolls and pitches were flown on each survey line in an area where

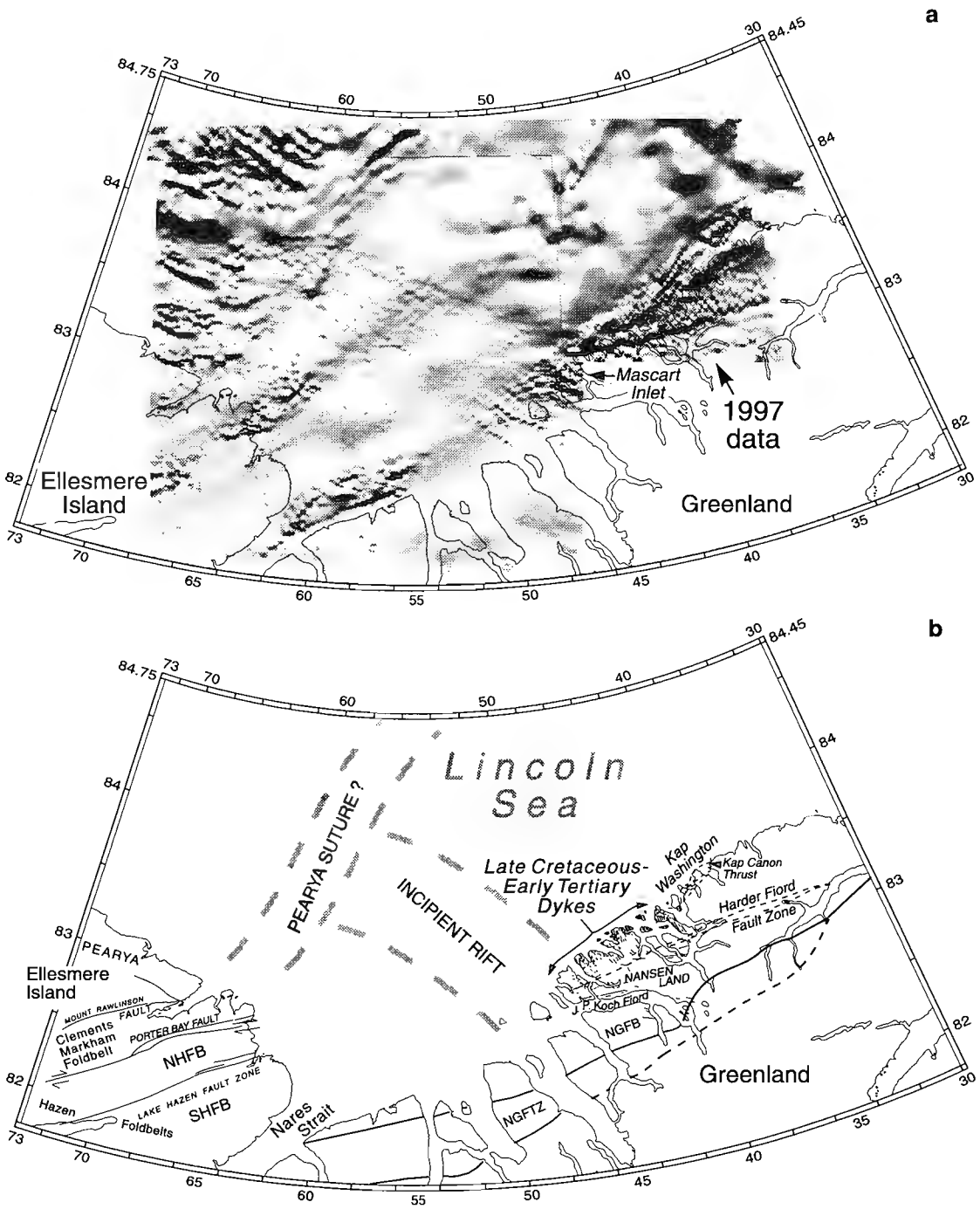

Figure 2. a) *Shaded relief of the total magnetic field highlighted from the north.* ***b)*** *Tectonic elements and major structural features discussed in the text. NGFB – Northern Greenland Fold Belt, NGFTZ – Northern Greenland Fold and Thrust Zone, SHFB – Southern Hazen Fold Belt, NHFB – Northern Hazen Fold Belt.*

the magnetic gradients were small. A second set of 27 "trim compensation coefficients" was generated for each survey and tie line. These coefficients were only applied to the line on which they were calculated. This ensured that noise levels always remained below the following levels:

standard deviation of tf (measured in 0.1-1 Hz band) <0.03nT,

standard deviation of gx (measured in 0-1 Hz band) <0.002 nT/m,

standard deviation of gy (measured in 0-1 Hz band) <0.002 nT/m .

The barometric altimeter and radar altimeter data were compared at constant survey altitude on each line over the Lincoln Sea. The barometric altitude was thus corrected for temporal changes in the barometric pressure.

The magnetometer and navigation data were then smoothed with a 9-point (1.125 second) boxcar average and subsampled to 2 Hz.

LEVELLING AND GRIDDING

Although both the total field and gradient data are available, only observations based on a preliminary levelling of the total field data are presented here. A lateral-gradient enhanced total field has been created and will be incorporated in later analyses. The total field data were levelled with the commercial software package OASIS from Geosoft Inc.

The off-shore portion of the survey was levelled without difficulty, but because the mountainous on-shore portion was not flown with a formal drape program, there were altitude differences at the tie line crossing points, resulting in significant total field differences at these points.

Several different methods were used to reduce the crossing point errors in the on-shore data. They can be summarized as follows:

1. Base station magnetic field removal: there was no improvement in crossing point error statistics with either data point-for-data point subtraction or with subtraction of a mean value of the base station along each line. We concluded that there was excessive spatial decorrelation over the long baseline between the base station at Alert and the survey area.
2. Two methods for correcting the altitude differences at the crossing points were tried. It should be noted that the altitude reference in all cases was barometric, corrected to GPS height or to DGPS, when that was available.
   a) The vertical gradient as given by the IGRF at the tie points, was used to correct the tie line total fields to the survey line altitudes. For the on-shore data, this resulted in a reduction in the crossing-point errors from 44.5 nT to 36.8 nT (RMS).
   b) Calculation of the vertical gradient along each flight line using the one-dimensional (1-D) Hilbert transform was attempted, but applying it for altitude correction did not improve the error statistics.
3. Conventional levelling was applied to the altitude-corrected data from 2a) above.
   a) The DC (mean) value of each tie line was brought to the DC value of its survey line crossing points. This reduced the error from 36.8 to 26.1 nT RMS.
   b) For each survey line, a first order trend was fitted to its crossing point errors and this trend was subtracted from the line. This reduced the error to 12.75 nT RMS.
   c) Steps a) and b) were iterated several times to refine the DC adjustment of the tie lines and the first order fits. The final result was an error of 10.47 nT RMS. This can be compared to the final levelling error of the offshore data, which was 4.8 nT.

Figure 2 shows the levelled, gridded total field over the entire survey area.

GEOLOGICAL INTERPRETATION

The geology of the study area is drawn largely from Soper and Higgins (1991a, b). Within the area covered by the 1997 aeromagnetic data, the geology of North Greenland consists of three Siluro-Devonian tectonic zones of the North Greenland Fold Belt. Intensity of deformation and metamorphism increases to the north; polyphase folds overprinted by amphibolite grade conditions occur at the coast. The fold belt was also affected by intrusion of Late Cretaceous (and younger?) dykes, thermal effects associated with the Cretaceous/Tertiary Kap Washington volcanic suite, northerly verging thrust faulting in the Kap Washington region, and Cretaceous dextral movement on the east-west Harder Fjord Fault Zone (HFFZ; Fig. 2b). This fault zone also exhibits mid-Tertiary extensional faulting, Recent seismic and volcanic activity, and has been speculated to be related to pre-existing deep crustal features.

The North Greenland Fold Belt is the eastern extension of the Hazen Fold Belt of northern Ellesmere Island, on the basis of similar stratigraphy and tectonic history, although the geometry of the resulting structures differs somewhat. Close links between the two regions can only be demonstrated within platformal strata south of the fold belts.

The preliminary aeromagnetic anomaly pattern of Figure 2a shows several intriguing but not yet fully resolved coincidences with known structures, and reveals several new features apparently unrelated to mapped geological elements. The most prominent is the abrupt change from the broad, low amplitude anomalies offshore to northeast-trending, short wavelength, high amplitude anomalies about 20-30 km north of the coastline. The short wavelength anomalies occupy an elongated triangular area truncated along most, but not all, of

its southern edge by the surface trace of the Harder Fjord Fault Zone. Between the Harder Fjord Fault Zone and the offshore, anomaly trends are dominantly north. The southern edge of this anomaly pattern diverges toward the coast from the Harder Fjord Fault Zone in the western half of the study area. The gently curving Harder Fjord Fault Zone extends west-southwest and becomes indistinct near Mascart Inlet (Fig. 2a, northwestern Nansen Land). In comparison, the anomaly that coincides with the Harder Fjord Fault Zone in the east continues due west where it coincides with the southern limit of a dense swarm of northerly trending Cretaceous diabase dykes in northern Nansen Land. An impressive magnetic high lies nearshore within the southwest corner of the 1997 survey area and just west of the dyke swarm. Its origin is unknown. Northerly trending dykes are clearly represented in the anomaly pattern east of Nansen Land between Harder Fjord and Kap Washington. Northeast trending curvilinear elements of the anomaly pattern at Kap Washington coincide with the Kap Cannon Thrust Zone.

In general, the triangular area of high amplitude anomalies coincides with the region of polyphase deformation and metamorphism that has been substantially injected by Cretaceous dykes. Abrupt truncation of the pattern to the north suggests the presence of another major fault zone offshore, one presumably related to transform motion of the Harder Fjord Fault Zone and opening of the Atlantic Ocean, however its extent westward appears interrupted by an incipient rift zone delineated by the 1989-1991 Lincoln Sea surveys. Although extrapolation of northeast trends from regional data towards Nares Strait contributed to controversial early interpretations of the magnitude and nature of faulting in the strait (e.g. Kovacs, 1982; Okulitch et al., 1990), the new higher resolution data indicates a much more complex tectonic history of the area between Nares Strait and the Arctic Ocean.

Similarly, westward extensions of the Harder Fjord Fault Zone are unclear. If both the Harder Fjord Fault Zone and Nares Strait are transforms related to rifting which is manifested by the northerly- and northwesterly-trending dyke swarms coinciding with the anomaly patterns in and near the eastern Lincoln Sea, no westward extensions should be expected.

Farther offshore to the northeast, discrete anomalies are lacking. Instead, the greater offshore area features elements of anomaly patterns that appear to be the southwest ends of features possibly extending from the Amundsen Basin and the Morris Jessup Plateau regions to the northeast but no clear relationship can yet be demonstrated.

CONCLUSIONS

This survey has revealed unexpected and important crustal features, the understanding of which bears significantly on the tectonic and magmatic evolution of this portion of the Arctic margin. The Kap Washington volcanic province and associated northerly trending dyke swarm, appear to be tectonically isolated from the Arctic Ocean to the north and from the greater Greenland continent to the south. No comparable features exist to the west or east, and the relationship to the northwest-trending incipient rift to the west is uncertain. Resolution of the divergence of the western part of the Harder Fjord Fault Zone from the prominent magnetic anomaly that coincides with it in the east will require additional field mapping and geophysical studies. Although some of the dykes have now been reliably dated (90 Ma; D.J. Kontak, pers. comm., 1997) and confirmed to be Late Cretaceous in age, much additional work is needed to date the Kap Washington Group itself, other dyke swarms (e.g. those along the Harder Fjord Fault Zone and the incipient rift) and to clarify the timing of deformation. Quantitative integration of the exposed and geophysically imaged major structures of this region with the plate tectonic evolution of the Arctic Ocean remains a major, but increasingly resolvable, challenge.

FUTURE WORK

Magnetic anomaly data have delineated the extension of several major new tectonic elements from limited exposures on Ellesmere Island and northern Greenland to apparent intersections beneath the Lincoln Sea. The magnetic mapping is delineating new tectonic segments of the Arctic margin and their continuation beneath the adjacent the Arctic Ocean. The magnetic data also provide new crustal properties of dyke swarms on northern Greenland, outline the first order seaward limits of the Kap Washington Volcanic province of northern Greenland, and provide an alternative image of the Harder Fiord Fault Zone. By default, new constraints are being placed on the evolution of the adjacent Arctic Ocean and the nature of the Danish and Canadian landmasses. Future Polar Margin Aeromagnetic Program surveys will extend the coverage further north to investigate the possible extension of a Pearya suture from Ellesmere Island and the enigmatic Lincoln Sea plateau at the southern terminus of the Lomonosov Ridge.

REFERENCES

Forsyth, D.A., Keating, P., Pilkington, M., and Okulitch, A.O.
1997: Lincoln Sea: new magnetic data reveal an incipient rift and place fresh constraints on Greenland-Ellesmere evolution; Abstracts of the 8th Scientific Assembly of International Association of Geomagnetism and Aeronomy with International Committee on the Middle Atmosphere and Solar Terrestrial Physics, Uppsala, Sweden, Session 5.15, p. 502.

Forsyth, D.A., Argyle, M., Okulitch, A.O., and Trettin, H.P.
1994: New seismic, magnetic and gravity constraints on the crustal structure of the Lincoln Sea continent-ocean transition; Canadian Journal of Earth Sciences, v. 31, p. 905-918.

Kovacs, L.C.
1982: Motion along Nares Strait recorded in the Lincoln Sea: Aeromagnetic evidence; in Nares Strait and the Drift of Greenland: a Conflict in Plate Tectonics, (ed.) P.R. Dawes and J.W. Kerr; Meddelelser om Gronland, Geoscience, v. 8, p. 275-290.

Nelson, B., Hardwick, D., Bower, M., Marcotte, D., MacPherson, M., Forsyth, D.A., Macnab, R., and Teskey, D.
1991: Preliminary analysis of data from the Lincoln Sea aeromagnetic Surveys 1989-1990; in Current Research, Part B; Geological Survey of Canada, Paper 91-1B, p. 15-21.

Nelson, B., Marcotte, D., Hardwick, D., Macnab, R., Forsyth, D., Okulitch, A., and Teskey, D.
1995: Tectonic constraints based on Canadian Polar Margin Aeromagnetic Program data; in Proceedings of the XXI General Assembly of the International Union of Geodesy and Geophysics, Session 5:16 Boulder, Colorado, 2-14 July 1995.

Okulitch, A.V.,Dawes, P.R., Higgins, A.K., Soper, N.J., and Christie, R.L.
1990: Towards a Nares Strait solution: structural studies on southeastern Ellesmere Island and Northwestern Greenland; Marine Geology, v. 93, p. 369-384.

Soper, N.J. and Higgins, A.K.
1991a: Deformation (Devonian-Early Carboniferous deformation and metamorphism, North Greenland); in Chapter 11 of Geology of the Innuitian Orogen and Arctic Platform of Canada and Greenland, H.P. Trettin (ed.); Geological Survey of Canada, Geology of Canada, no. 3, p. 283-291 (also Geological Society of America, The Geology of North America, v. E).
1991b: Late Cretaceous-Early Tertiary deformation, North Greenland; Chapter 16 in Geology of the Innuitian Orogen and Arctic Platform of Canada and Greenland, (ed.) H.P. Trettin; Geological Survey of Canada, Geology of Canada, no. 3, p. 461- 465 (also Geological society of America, The Geology of North America, v. E).

Geological Survey of Canada Project 870047

Small air-gun arrays for high-resolution marine geophysical surveying

D.C. Mosher, R. MacDonald, A. Hewitt, and W. Hill
GSC Pacific, Sidney

Mosher, D.C., MacDonald, R., Hewitt, A., and Hill, W., 1998: Small air-gun arrays for high-resolution marine geophysical surveying; in Current Research 1998-D; Geological Survey of Canada, p. 43-50.

Abstract: Careful monitoring of the seismic source signature and implementation of two-gun arrays can greatly enhance the data quality of high-resolution, air-gun, seismic-reflection surveys. The goal of this study was to design and implement an array of small air guns for seismic-reflection surveying that would maximize resolution and eliminate or significantly reduce the bubble pulse, reducing the need for post-processing. It is the first step in an attempt to develop and improve the standard operating procedures for collecting marine high-resolution seismic-reflection data within the Geological Survey of Canada with tools that are already available. Arrays of small coalesced air guns, tuned to optimize frequency and source shape, can eliminate the bubble pulse while maintaining resolution and increasing power. Arrays which employed guns of equal size were most effective at eliminating the bubble pulse. Arrays at a shallow tow depth (0.5 m) were most effective at producing high-resolution, broadband signals.

Résumé : La surveillance attentive de la signature sismique de la source et l'utilisation de réseaux à deux canons peuvent largement améliorer la qualité des données recueillies lors de levés de sismique-réflexion à haute résolution au moyen de canons pneumatiques. L'objectif de la présente étude était de concevoir et de mettre en oeuvre un réseau de petits canons pneumatiques pour les levés de sismique-réflexion maximisant la résolution et éliminant ou diminuant de manière significative la pulsation bulle, ce qui réduirait ainsi la nécessité du post-traitement. Cela constitue la première étape d'une tentative de développment et d'amélioration des procédures normales de fonctionnement pour la collecte de données de sismique-réflexion marine à haute résolution par la Commission géologique du Canada au moyen d'outils déjà disponibles. Des réseaux de petits canons pneumatiques, syntonisés de manière à optimiser la fréquence et la configuration de la source, peuvent éliminer la pulsation bulle tout en conservant la résolution et en accroissant la puissance. La disposition la plus efficace pour l'élimination de cette pulsation est l'emploi de réseaux de canons de même taille. La plus efficace pour la production d'un signal à large bande à haute résolution est l'utilisation de réseaux à faible profondeur de remorquage (0,5 m).

INTRODUCTION

With careful monitoring of the seismic source signature and by using arrays of small air guns, great improvement in high-resolution seismic-reflection records can be had. This improvement in quality reduces the need for post-processing and, at the same time, makes the data easier to post-process. These principles have been applied in deep seismic work for decades, but the high-resolution field has lagged because of the lack of digital data. High-resolution seismic-reflection geophysical surveying traditionally has been recorded in analogue form with little concern about post-processing. In part as a consequence of this fact, little attention has been paid to details of source signatures. With the capability of digital acquisition of high-resolution seismic-reflection data, post-processing is more feasible, but still expensive and labour intensive - especially with the large volumes of data inherent in high-resolution sampling. This paper demonstrates simple techniques to optimize source signature characteristics by showing a few signatures of various air-gun sizes and arrays of air guns. This work follows from previous studies by Quinn et al. (1985) and Poley et al. (1985), but is specific to designing arrays of air guns that can be practically used as routine survey tools.

Air and sleeve guns are pneumatic sources that are an industry standard for marine seismic-reflection surveying. In the high-resolution survey field, small air and sleeve guns provide a scale of resolution between ultra-high resolution piezoelectric and boomer sources (e.g. 3.5 kHz, Huntec, and Seistec) and large sources for deep seismic surveying (e.g. large air guns and explosives). They are particularly useful where penetration is critical, either to image deeper into the sediment section, or to penetrate hard sediments or gas-bearing sediment, for example, and yet maintain resolution. They work by creating a sound source with the sudden release of compressed air into the water column. In addition, they tend to be reliable, easily repaired and maintained, and readily available because of their wide usage. One of the main hindrances, however, is the presence of the bubble pulse, which occurs shortly after the primary pulse and tends to severely affect the ability to interpret the geology in the shallow part of the record; the portion which is of great significance in high-resolution surveying.

Objectives

This study of air-gun signatures was undertaken as a first step in an attempt to develop and improve the standard operating procedures for collecting marine high-resolution seismic-reflection data within the Geological Survey of Canada, with tools that are readily available. This particular study addresses only small air-gun sources and not other sources nor receiving arrays, which are equally important in determining data quality and will be the topic of future study. The intent was to prove the concept and its practical implementation. The goal of this study was to design and implement an array of small air guns that would maximize horizontal and vertical resolution and eliminate or significantly reduce the bubble pulse, reducing the need for post-processing. Specifically, a system was required that would produce a scale of resolution that would integrate with that of the Huntec DTS; a system that is in common use in the Geological Survey of Canada for high-resolution seismic-reflection studies.

Methods

Seismic source signature tests were conducted from the CCGS *Vector* in Saanich Inlet with a variety of sizes of Bolt air guns. Signals were received by a far-field hydrophone, fixed at 15 m below the source. The hydrophone was a single-element EDO 141B cartridge. Data were acquired with a Zonic model 3525 spectral analyzer, sampled at 19.53 μs for a period of 160 ms. Data were written to floppy disk and subsequently converted to ASCII files. Air guns were arranged within an iron frame, suspended horizontally with chain, and kept 0.5 m apart (Fig. 1). Firing time was controlled with a three-channel Bolt firing unit, permitting adjustment of firing time between guns to a tenth of a millisecond. Frequency analyses of the source signals were conducted by the fast-fourier transform (FFT) technique with no windowing of the data.

RESULTS AND DISCUSSION

The marine seismic-reflection trace is created as a result of the convolution of an impulsive sound source with the Earth's reflection coefficient series (impedance contrast profile) (Telford et al., 1976). Convolution in the time domain is multiplication in the frequency domain. Any frequencies missing in the source, therefore, will be absent in the convolution, i.e. multiplication by zero. It is implicit therefore, that the appearance of a seismic-reflection record is as much a function of

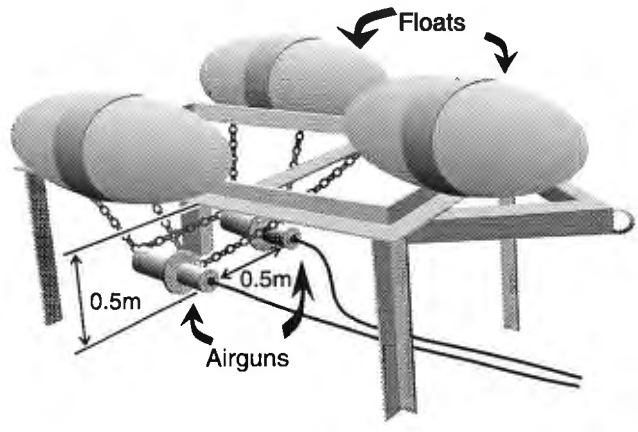

Figure 1. *Schematic of the air-gun array sled and setup. The frame consists of angle iron, the guns are suspended from chains, and the floats keep the unit upright. Tow depth of the guns can be adjusted with the chains. The package is of significant mass to tow well through waves with enough inertia to be unaffected by short period heave.*

Table 1. Gun depth and related frequency notches as a result of interference of the source ghost with the primary pulse. Acoustic velocity in water is assumed to be 1450 m/s. The frequency notch occurs where the source depth equals one-half the wavelength (1/2 λ).

Gun depth (metres)	Notch Frequency (primary)	Notch Frequency (1st Harmonic)	Notch Frequency (2nd Harmonic)	Notch Frequency (3rd Harmonic)
0.5	1450 Hz	2900 Hz	4350 Hz	5800 Hz
0.75	967 Hz	1934 Hz	2901 Hz	3868 Hz
1.0	725 Hz	1450 Hz	2175 Hz	2900 Hz
2.0	362 Hz	725 Hz	1087 Hz	1450 Hz
3.0	242 Hz	483 Hz	725 Hz	967 Hz
4.0	181 Hz	362 Hz	544 Hz	725 Hz

the characteristics of the source as it is of the Earth's reflection coefficient series or geology. This point is critical for the geophysical interpreter to understand.

The ideal impulsive seismic source is a zero-phase delta function; a spike in the time domain that peaks at time zero and is infinitely broad in the frequency domain. In practice this delta function is impossible to obtain, but marine sources generally attempt to approximate it. Pneumatic sources, such as air and sleeve guns typically are non-zero-phase (minimum phase) spikes of some width and include a tail of coherent noise. The width of this spike and the following noise degrade the seismic record in terms of the resolution possible. Some of these source characteristics can be minimized through signal-processing techniques, either in real time or after the fact. It is far better, however, to optimize the source characteristics for the survey, thereby minimizing the need for post-processing.

The air gun produces an acoustic signal by the explosive release of high-pressure air directly into the surrounding water. The basic air gun consists of two high-pressure chambers connected and sealed by a double-ended piston. An electrically activated solenoid fires the gun by opening a valve, which allows high-pressure air to enter between the base of the upper chamber and the piston. The resulting pressure differential drives the piston forward simultaneously releasing high-pressure air from the lower chamber into the surrounding water. The initial explosive venting of this air into the water produces the primary acoustic pulse.

Single air-gun sources are omnidirectional; they are of equal power in all direction and no beam forming is done to preferentially direct the source. The typical signature of pneumatic impulsive sources consists of an initial positive pulse (called the primary pulse) which approaches a delta function, followed by a strong negative going pulse which is somewhat wider than the primary and usually slightly lower in amplitude (Fig. 2). This negative going portion is referred to as the source ghost, and it is the reflection of the source wave off the sea surface which then combines with the downward travelling primary wave. It is negative because the impedance contrast of the water-air interface is negative; hence the phase is reversed. The deeper the gun, the longer the lag time from the peak of the primary to the peak of the source ghost because the longer the travel time to reflect off the sea surface (this is known as phase lag). The source ghost

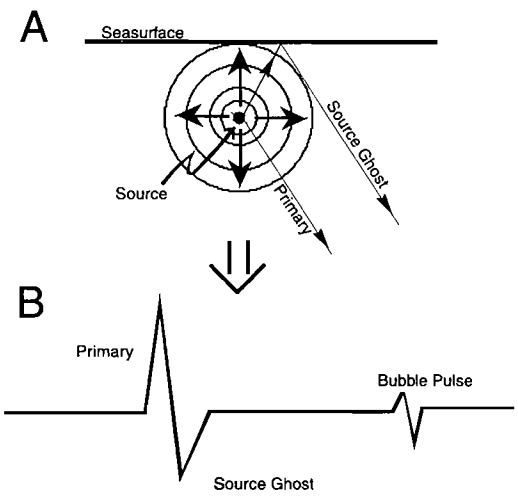

Figure 2. *Schematic showing wave paths of sound source (**A**), convolving to form the characteristic source signature for marine air and sleeve guns (**B**).*

and primary waveforms sum to form the initial portion of the air-gun signature. As a result of this summation, certain frequencies cancel, and major notches or nulls in the amplitude spectra occur. The frequencies which are affected are those where perfect cancellation occurs and are a function of the phase lag between the source primary and the source ghost, which, in turn, is a direct function of source depth. The frequency affected is where the source depth equals a half wavelength (Table 1). Notches will also occur at harmonic frequencies. Source depth thus plays an important role in controlling spectral content of a signature and must be considered when configuring a seismic system for a specific target area.

Figures 3a-e are source signatures for single-gun arrays with associated power spectra for each of the air volumes tested. In each case of a single gun, at 0.5 m depth, the frequency spectrum is broad, spanning 0 to about 1400 Hz. There is no apparent increase in power at the higher frequencies with smaller gun volumes - merely the relative power of high frequency to low frequency is increased. The time-domain signature of each of these single guns shows a strong bubble pulse. The bubble pulse is a 'source' of sound

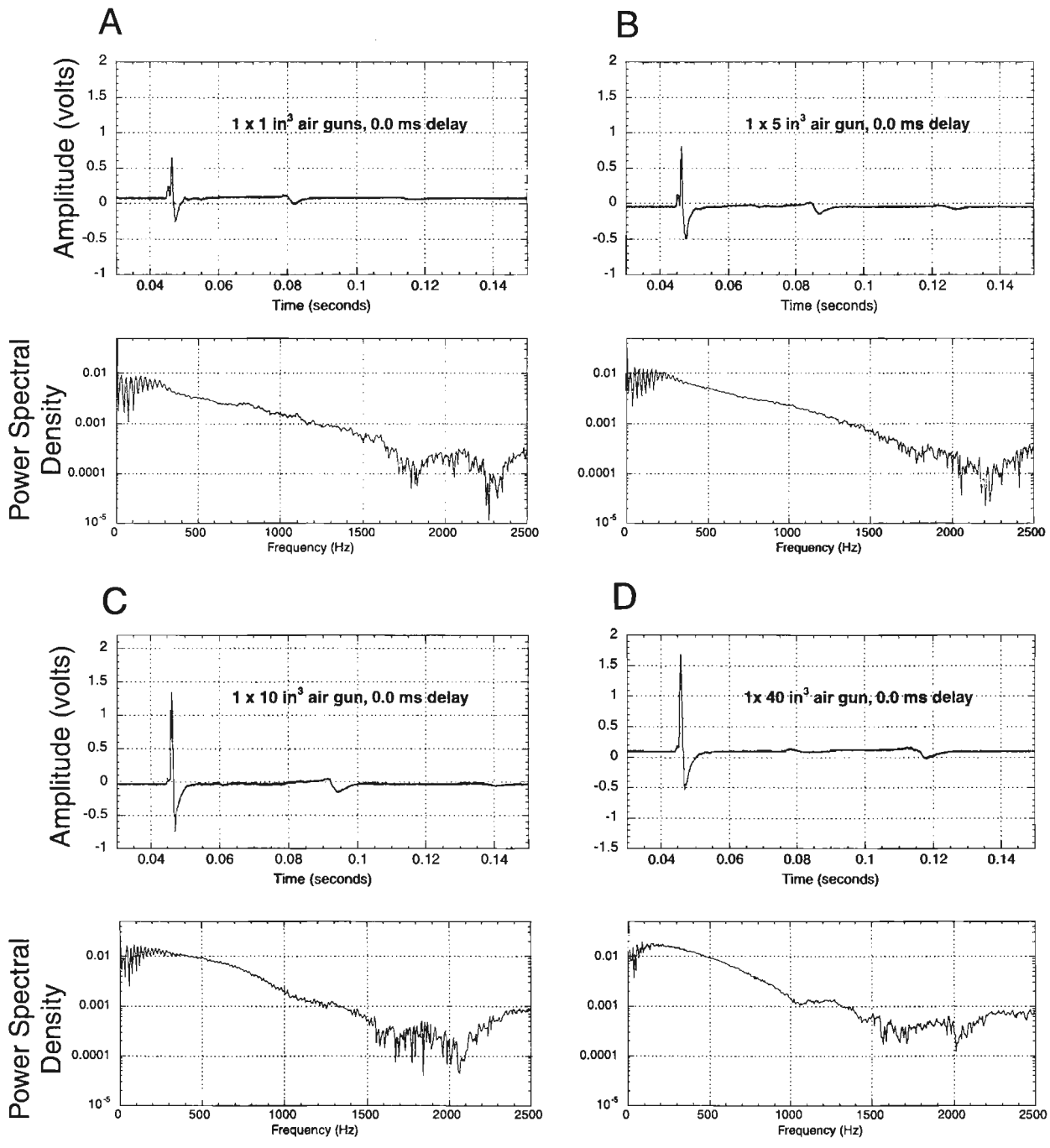

Figure 3. *Seismic source signatures with frequency spectra for single guns at 0.5 m depth:* ***A)*** *1 in³ chamber,* ***B)*** *5 in³ chamber,* ***C)*** *10 in³ chamber,* ***D)*** *40 in³ chamber, and* ***E)*** *40 in³ chamber with wave-shape kit. Note the bubble pulse of each signature for A-D and that the bubble pulse has a longer lag time from the primary pulse with increasing air volume size. Note also the lack of a bubble pulse in E as a result of the wave-shape kit, but that the maximum amplitude of the signal is lower than in D and C.*

generated by the oscillating expansion and collapse of air under hydrostatic pressure after it has been released and during its ascent to the sea surface. The amplitude of the bubble pulse increases with the volume of the air released and the tow depth of the gun. The lag time of the bubble pulse from the initial pulse is a function of its oscillation frequency which is related to the volume of air released. A wave-shape kit in the chamber of the air gun significantly reduces the bubble pulse (e.g. Fig. 3e) by breaking up the bubble upon its release. This wave shape kit also significantly reduces the power and frequency content of the source, however.

The energy contained in the bubble pulse can cause subsidiary notches in the amplitude spectra of a signature, just as the source ghost does. Firing a source close to the water surface has the effect of damping secondary oscillations. This results in a 'spikier' signature and therefore a broader bandwidth spectra. There is, however, lower energy-conversion efficiency, so the total energy contained in the outgoing pulse is reduced. The observation is, therefore, a general increase in power at the lower frequencies and loss of higher frequencies with increasing depth of the source gun (Fig. 4). In addition, the source ghost cancels frequencies of interest at greater tow depths (e.g. from about 1 to 3 m, high frequencies that are of interest in high-resolution surveying can be notched out, see Table 1). The relative amplitude of the

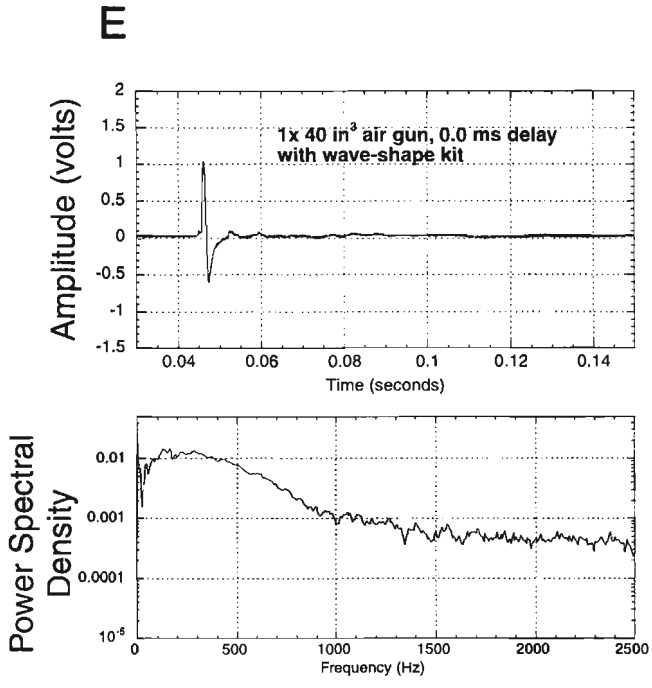

Figure 3E.

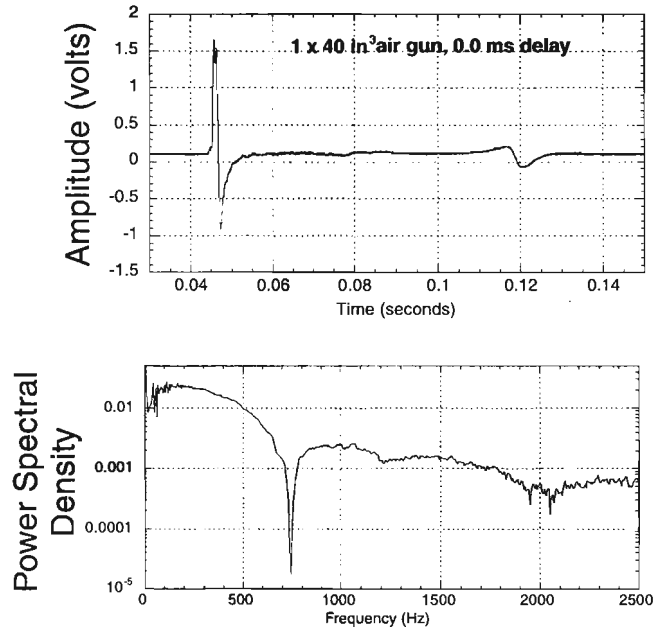

Figure 4. *Seismic source signature and power spectra for a single 40 in³ gun at 1 m depth. Note the higher amplitude of the source ghost pulse (more power) and the larger bubble pulse when compared with the same size gun at 0.5 m depth (Fig. 3D). The notch in the power spectra at 725-750 Hz is a result of destructive interference between the primary and the source ghost signals and is exactly where Table 1 would predict it to be.*

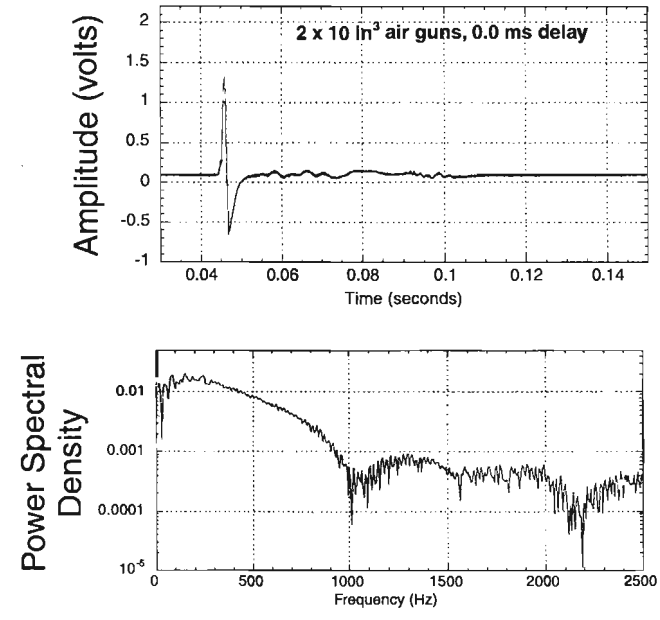

Figure 5. *Seismic source signature for an array of two 10 in³ guns fired synchronously. Note the elimination of the bubble pulse but the poor shape of the source signature and notching in the power spectra at about 1000 Hz. If the fire-time of the guns is not 'tuned' for optimum shape and bandwidth, then destructive interference at critical frequencies results (compare with Fig. 6C).*

bubble pulse to the amplitude of the primary pulse increases with depth of the gun. Interference of the bubble pulse with the primary signal is generally destructive, resulting in degradation of the overall signal (e.g. reduction in power at certain frequencies as shown in Figure 4).

The results shown in Figure 3 indicate that the objectives of a survey must be considered when planning something even as simple as tow depth of the gun. The source should be towed as shallow as possible, if maximum resolution is required. If deeper penetration is needed, then the gun can be towed more deeply, bearing in mind that resolution is being sacrificed. One might consider going to a larger gun size

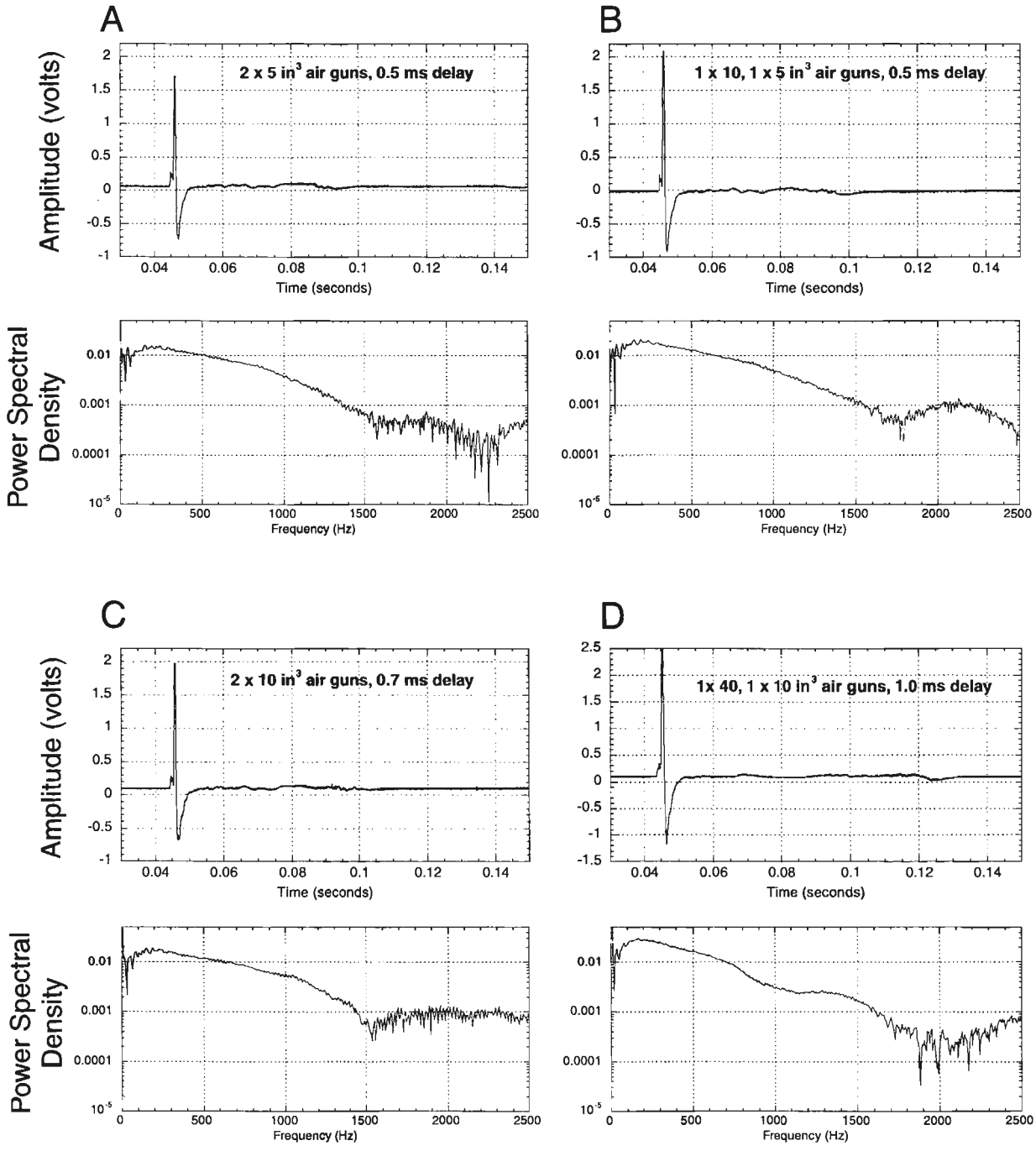

Figure 6. *Seismic source signatures for several two-gun arrays at 0.5 m depth and 0.5 m spacing between guns:* ***A)*** *2 x 5 in³,* ***B)*** *5 and 10 in³,* ***C)*** *2 x 10 in³, and* ***D)*** *40 and 10 in³. Note in each case the elimination of the bubble pulse. Compare C with Figure 3C and Figure 5 and note the bandwidth is maintained, yet power is increased and the bubble pulse is absent.*

rather than deeper tow depth, if that is possible. There are also the practical limitations of towing a gun at shallow depths in choppy or heavy sea states.

Air Gun Arrays

Power can be increased and resolution maintained with a multiple-gun array; timing the relative firing of the guns in a manner to enhance the signal. In addition to increasing signal strength, gun arrays can virtually eliminate the bubble pulse. It is believed that the bubble pulses from the two guns destructively interfere. The source signal can be severely compromised, however, if the firing-time of the two guns is not appropriate (Fig. 5). The waveforms will destructively interfere if they are not tuned for frequency. For the tests shown in this report, only two guns constitute the arrays.

In general, combining guns of similar volume is most effective in increasing signal strength and eliminating the bubble pulse. Several combinations proved successful in these tests; the 2 x 5 in^3 air-gun array (Fig. 6a), the 5 and 10 in^3 air guns (Fig. 6b), 2 x 10 in^3 (Fig. 6c), and the 40 in^3 air gun with the 10 in^3 air gun (Fig. 6d). In each of these cases, the amplitude of the primary pulse is nearly doubled, while the bubble pulse is essentially eliminated. The tow depth, in these cases, was 0.5 m and the separation between guns, which is also critical, was 0.5 m. For the equipment used in these tests, a relative firing delay of 0.5 to 1.0 ms of one gun to the other was used to optimize the signal. This delay will likely vary depending on the characteristics of the electronics, including the firing lines and the solenoids, and the physical separation of the two guns. Any change in the firing delay between guns could severely compromise the source signature, as demonstrated in Figure 5.

Figure 7 is a comparison test from cruise PGC97007, showing an example of a seismic profile collected by firing 2 coalesced 10 in^3 air guns at 0.5 m depth and 0.5 m separation, then just a single 10 in^3 gun in the same towing configuration. These results show, in a qualitative way, the higher power of the two-gun array, with elimination of the bubble pulse, and yet no apparent loss in vertical resolution. By keeping air-gun chamber sizes small, trigger-repetition time does not need to be sacrificed because of the time required to build up air pressure, thus horizontal resolution is maintained. In the case of the data in Figure 7, the air guns were triggered every 4 m, or about every 2 seconds.

CONCLUSIONS

A number of single-gun and two-gun arrays, employing air guns with chambers from 1 to 40 in^3 were tested. In all cases, single-gun signature tests show a significant bubble pulse, although the shallower the gun is towed, the smaller is the relative amplitude to the primary pulse. A wave-shape kit in the chamber of the gun can eliminate or significantly reduce the bubble pulse. In this case, however, the power is significantly reduced and there is a loss of bandwidth.

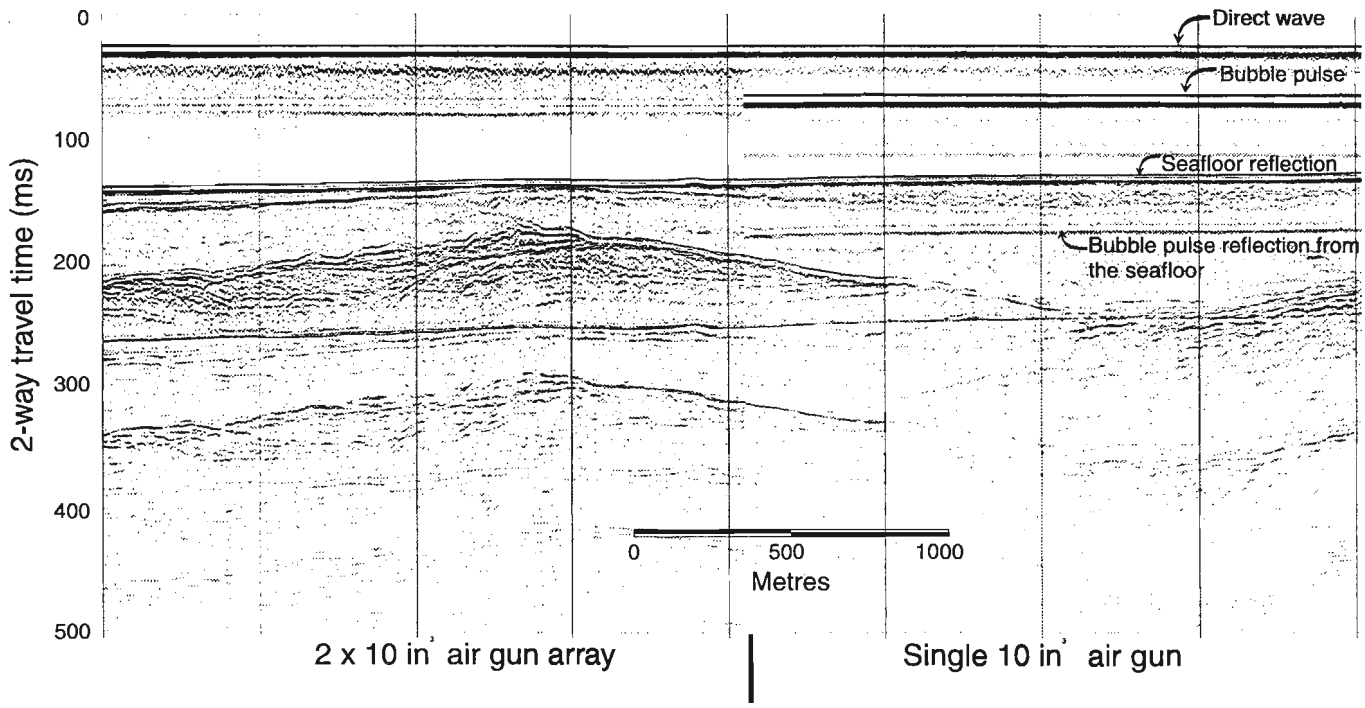

Figure 7. *Seismic profile along a line showing results from the 2 x 10 in^3 air gun array, adjacent to a section with just a single 10 in^3 air gun. Note the higher gains as a result of more energy in the two-gun section, and the strong bubble pulse at 50 ms below the seafloor in the single-gun section.*

Two-gun coalesced arrays of small air guns can effectively eliminate the bubble pulse while maintaining bandwidth (vertical resolution), maintaining shot-repetition frequency (horizontal resolution), and increasing power, thereby greatly enhancing data quality. A variety of combinations using two guns were tested, varying gun size, spacing, depth, and relative fire-time. A number of combinations were successful, bearing in mind that the objectives were to eliminate the bubble pulse while maintaining or enhancing resolution and power. Most effective at eliminating the bubble pulse were arrays which employed guns of equal size, that were spaced at the same interval as their tow depth. Most effective at producing high-resolution, broadband signal were arrays at a shallow tow depth (0.5 m). One of the most effective combinations for improving the source signature was the 2 x 10 in^3 array. Seismic profiling with this two-gun array, with 0.5 m tow depth and 0.5 m separation between guns showed drastic data improvement over a single 10 in^3 gun and still allowed for a two-second firing rate (4 m), to maintain horizontal resolution.

ACKNOWLEDGMENTS

The authors would like to thank the officers and crew of CCGS *Vector* for their cooperation in the sea trials of this experiment. P. Simpkin graciously supplied a hydrophone array. We thank M. Black of the Esquimalt Defence Research Detachment for supplying the Zonic Spectral Analyzer. Terra Surveys supplied the air guns and firing unit.

REFERENCES

Poley, D.F.
1985: Acquisition, processing and interpretation of high resolution seismic data from the Beaufort Sea; Ph.D. Thesis, University of Calgary, Calgary, Alberta, 210 p.

Quinn, F.J., Vigier, L., Poley, D., and Simpkin, P.
1985: Evaluation/calibration of marine sources for high resolution seismic studies; Geological Survey of Canada Open File 1520, 178 p.

Telford, W.M., Geldart, L.P., Sheriff, R.E., and Keys, D.A.
1976: Applied Geophysics; Cambridge University Press, Cambridge, London, 860 pp.

Geological Survey of Canada Project 890052

Shale permeability and its relation to pore-size distribution[1]

T.J. Katsube, D.R. Issler[2], and W.C. Cox[3]
Mineral Resources Division, Ottawa

Katsube, T.J., Issler, D.R., and Cox, W.C., 1998: Shale permeability and its relation to pore-size distribution; in Current Research 1998-D; Geological Survey of Canada, p. 51-57.

Abstract: Shales are characterized by unimodal pore-size distributions. The relationship between shale permeability (k) and the mode (d_m) of these distributions has been investigated, for 22 tight shale samples from Canadian offshore and interior regions, to determine the degree of accuracy and reliability of using d_m to estimate shale permeability. Such an attempt is made, using an indirect method, because tight shales represent some of the lowest permeabilities (10^{-22} m^2 to 10^{-19} m^2) and are extremely difficult to measure.

Results indicate that, although a considerable scatter exists for k plotted against d_m, a relationship of significance exists. Estimates of k using d_m are within one order of magnitude of the measured values for 90% of the data, and within a factor of 3 for 65% of the data, using the equation:

$$k = 10^{-21}\exp(0.13d_m - 0.68)\ m^2$$

Improved estimates of k may result from a better understanding of the role of other pore-structure parameters.

Résumé : Les shales se caractérisent par des distributions unimodales de la taille des pores. La relation entre la perméabilité (k) du shale et le mode (d_m) de ces distributions a été analysée pour 22 échantillons de shale compact provenant de zones extracôtières et intérieures canadiennes afin de déterminer la précision et la fiabilité de la méthode consistant à utiliser d_m pour estimer la perméabilité du shale. On a eu recours à une telle méthode indirecte parce que les shales compacts présentent des perméabilités parmi les plus basses (10^{-22}–10^{-19} m^2) qui sont extrêmement difficiles à mesurer.

Les résultats indiquent, malgré une dispersion considérable de k selon d_m, qu'il existe une relation significative. Les estimations de k au moyen de d_m se chiffrent à moins d'un ordre de magnitude des valeurs mesurées pour 90 pour cent des données, et à moins d'un facteur 3 pour 65 pour cent des données, selon l'équation suivante :

$$k = 10^{-21}\exp(0{,}13d_m - 0{,}68)\ m^2$$

Une meilleure compréhension du rôle des autres paramètres pore-structure permettra d'obtenir des estimations plus précises de k.

[1] Research completed under the Industrial Partners Program (IPP) of the Geological Survey of Canada in collaboration with PanCanadian Petroleum Limited.
[2] GSC Calgary, Calgary
[3] PanCanadian Petroleum Ltd., 150-9th Avenue S.W., Calgary, Alberta T2P 2S5

INTRODUCTION

Shales play an important role in the migration and accumulation of petroleum and metallic mineral-rich fluids in sedimentary basins, so it is important to have a good understanding of their petrophysical evolution throughout the basin history. Such an understanding will assist in the development of efficient exploration strategies. Shales play this role because they can act as seals or barriers to fluid flow. These seal and barrier qualities are due to their extremely low permeability and small pore-sizes (Katsube and Williamson, 1994), which is a result of their fine grained texture. However, tight shale permeabilities represent some of the lowest permeabilities for rocks (Brace, 1980; Neuzil, 1994), and are extremely difficult to measure. For this reason, many attempts are being made to estimate shale permeabilities by indirect methods. The use of the mode of the shale pore-size distribution is one of these methods. The purpose of this paper is to show the degree of accuracy and reliability of such a method in predicting shale permeabilities, and to suggest possible ways of improving these estimates. Previous studies (Katsube and Williamson, 1994) have indicated that permeability (k) decreases with burial depth (h) from 10^{-14} m^2 to 10^{-11} m^2 at the ocean floor surface (Katsube et al., 1991b) to 10^{-22} m^2 to 10^{-19} m^2 at depths of 2.5-4 km.

Shales are generally characterized by unimodal pore-size distributions (Fig. 1; Katsube and Williamson, 1994), regardless of their porosity or the depths from which they were obtained. This is in contrast with other rocks, such as igneous rocks (e.g. granites), where bimodal and trimodal distributions are common (Agterberg et al., 1984; Katsube and Hume, 1987). Pore-size mode (d_m) is one of the parameters that can be used to characterize these unimodal pore-size distributions. There is an abundance of data showing shale pore-size distributions shifting to smaller sizes as depth of burial increases (e.g. Fig. 2, Katsube et al., 1995), implying a decrease in pore-size modes. Similarly, there are abundant data showing decreasing effective porosity (ϕ_E) and permeability with increasing burial depth (e.g. Fig. 3; Katsube and Williamson, 1995). Based on these facts, it is reasonable to propose that k is related to d_m by some function:

$$k = f(d_m). \quad (1)$$

The relationship between permeability and the pore structure parameters is usually expressed as (Wyllie and Spangler, 1952; Walsh and Brace, 1984)

$$k = n d_{Fk}^3/(b_2\tau), \quad (2)$$

where n is the flow-path density (Katsube and Williamson, 1994), d_{Fk} is the average pore-size for fluid flow (Katsube et al., 1991a), τ is the tortuosity, and b_2 is a coefficient equal to 12 for sheetlike pores and to 8 for tubular pores (Walsh and Brace, 1984). Although equation (2) indicates that k is a function of more than one parameter, it also indicates that pore-size is the most significant one, since k is proportional to the cube of d_{Fk}. If d_m is considered to be equal or similar to d_{Fk}, it is reasonable to assume that equation (1) represents a suitable approximation for permeability.

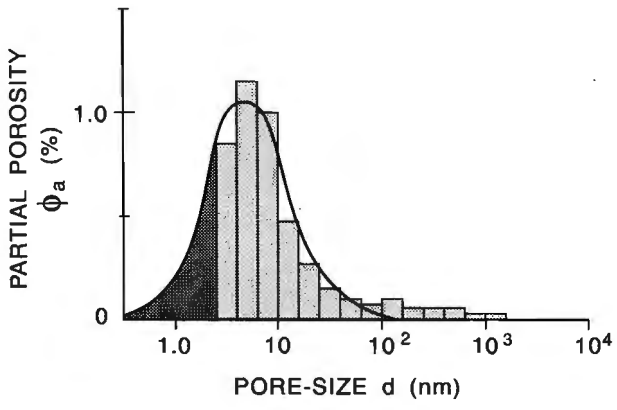

Figure 1. *The pore-size distribution model (Katsube, 1992) used to characterize shales (Katsube and Williamson, 1994). The parameter, ϕ_a, is partial porosity, and d is the general expression for pore-sizes. The smooth curve is the best-fit Gaussian curve and the dark shaded region is the estimated porosity for pore-sizes less than 3 nm (below measurement limit).*

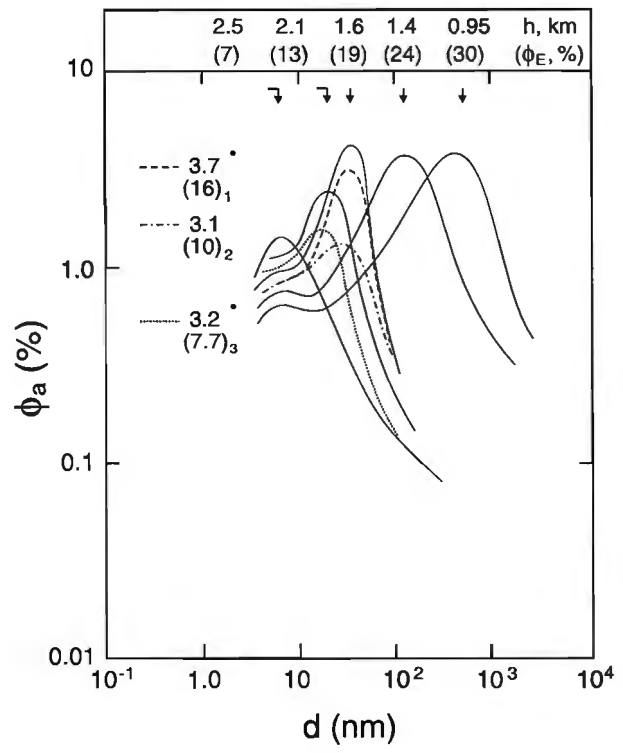

Figure 2. *Variation in pore-size distribution with depth (Katsube et al., 1995). Sample depths (km) are shown above with corresponding effective porosity values (parentheses). Subscripts adjacent to parentheses refer to different compaction zones in the Beaufort-Mackenzie Basin (Issler, 1992). Arrows point to the mode for each pore-size distribution. Solid lines: normally compacted zone (zone 3), broken lines: under compacted zones (zones 1 and 2), bold line: overpressured zone (zone 3, depth3.2 km).*

In a previous study (Katsube, 1993), it was shown that pore-size, porosity (ϕ_E) and tortuosity (τ) are the main factors that determine permeability. In addition, it was indicated that for each pore-size range, only those with porosities above a certain level (critical porosity, ϕ_{cr}) contributed to the permeability, a concept that is consistent with percolation theory (Madden, 1983). When considering these facts, it is also necessary to propose a more complex k-d_m relationship, such as the following:

$$k = f(d_m, \phi_E, \tau, \phi_{cr}). \quad (3)$$

Therefore, the main purpose of this paper is to indicate the degree of accuracy and reliability of using an empirical equation, such as equation (1), to predict permeabilities.

METHOD OF INVESTIGATION

Source of permeability data

Although there are shale permeability data available in the literature (e.g. Brace, 1980; Neuzil, 1994), those accompanying pore-size distribution data on identical samples are difficult to find. Some of this type of data, however, is available in recent publications referenced within Katsube and Williamson (1994, 1995). These data and the references are compiled in Table 2. For example, the permeability and pore-size distribution data for shale samples from depths of 4.7-5.6 km in the Venture gas field, offshore Nova Scotia, can be found in Katsube (1992) and Katsube and Coyner (1994). Sample VSF-D is sea floor sediment (offshore Nova Scotia) which was compacted into thin discs, under pressures of 10-60 MPa, and then analyzed for permeability and pore-size distribution (Katsube et al., 1996a). Only the results for the disc compacted at the pressure of 10 MPa is listed in Table 2. Whereas k decreased with increased pressure, the pore-size mode remained constant for the entire pressure range. The six samples, B-5 to ML-2, are from the Beaufort-Mackenzie Basin (Issler and Katsube, 1994; Katsube et al., 1996b). The data for the five samples (Tables 1a, 1b) at the bottom of Table 2 are new and are from an uplifted and eroded zone in the Western Canada Sedimentary Basin. All original literature data used to determine the permeability values in Table 2 are presented in terms of permeability (k) as a function of effective pressures (P_e), as displayed in Tables 1a and 1b.

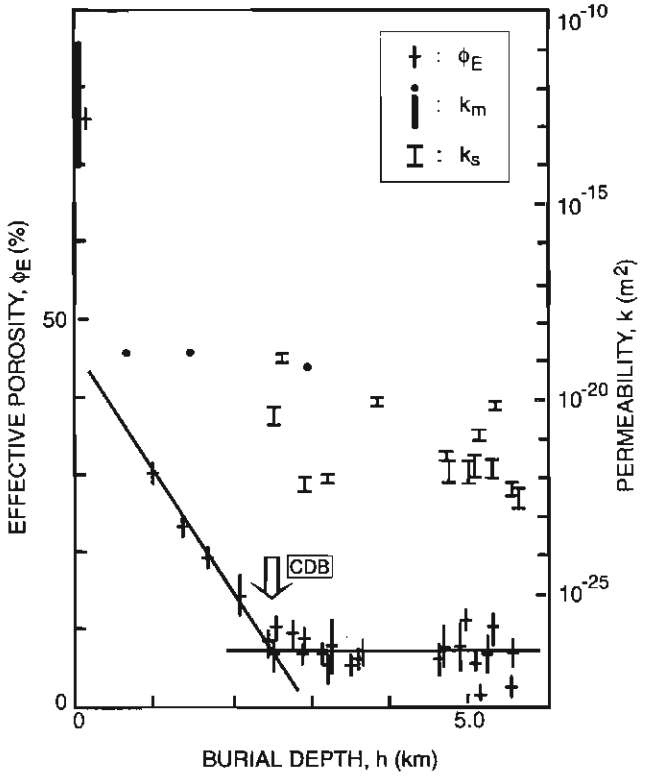

Figure 3. *Porosity and permeability-depth curves for shale, mud, and compacted mud samples from the Venture gas field (offshore Nova Scotia), Beaufort-Mackenzie Basin (Northwest Territories), and the Northeast Pacific (Katsube et al., 1991b). (ϕ_E = effective porosity (Katsube and Williamson 1994; Issler and Katsube, 1994), k_m = mud and compacted mud permeability, k_s = shale permeability (Katsube and Coyner, 1994; Katsube and Williamson, 1994; Katsube et al., 1995), CDB (arrow) = critical depth of burial.*

Depth corrections for the Western Canada Sedimentary Basin

The Venture gas field and Beaufort-Mackenzie Basin shale samples are from depths presently at or close to maximum burial. Therefore, the petrophysical characteristics of these samples were probably most affected by current burial conditions and, in principle, it is relatively straightforward to correct measured permeabilities back to the in situ state, given a sufficient knowledge of subsurface pressures. In contrast, the Western Canada Sedimentary Basin samples are from a region where a significant amount of the sedimentary section has been removed by erosion (about 1-2 km; Hacquebard, 1977). Therefore, present burial depths do not reflect the past conditions which controlled the development of their petrophysical properties. Although, it is possible to correct laboratory measurements back to present in situ conditions, it is more meaningful to approximate maximum paleoburial conditions for the purpose of correlating different petrophysical properties.

Various methods have been used by different workers to reconstruct maximum paleoburial depths for the Western Canada Sedimentary Basin (D.R. Issler, pers. comm, 1997). We use the moisture data for near surface coals (Steiner et al., 1972) and a relation between coal moisture and burial depth (Hacquebard, 1977; Nurkowski, 1984) to reconstruct maximum paleoburial depths for our Western Canada Sedimentary Basin shale samples. Details of the reconstruction procedure are as yet unpublished (D.R. Issler, unpub. data, 1997). These depth corrections significantly improve the relationships for geochemical and petrophysical parameters as a function of depth (D.R. Issler, unpub. data, 1997) which, in tern, gives us confidence that these reconstructions are valid. Both present burial depths and reconstructed maximum paleoburial depths are listed in Table 2 for the Western Canada Sedimentary Basin shale samples.

Table 1a. Permeability data for shale samples from the Western Canada Sedimentary Basin, Alberta.

Sample (Fm.)	h (km)	P (MPa) P_c	P_p	P_e	k (10^{-21} m^2)
ACD-03	0.561	15.0	10.0	5.0	23.1 ± 0.4
		20.0	10.0	10.0	15.2 ± 0.2
		25.0	10.0	15.0	7.97 ± 0.12
		30.0	10.0	20.0	4.55 ± 0.19
		35.0	10.0	25.0	3.69 ± 0.04
		40.0	10.0	30.0	2.96 ± 0.12
		45.0	10.0	35.0	2.20 ± 0.04
		50.0	10.0	40.0	1.77 ± 0.09
ACD-13	0.607	12.5	10.0	2.5	15.9 ±
		15.0	10.0	5.0	11.7 ±
		17.5	10.0	7.5	7.9 ±
		20.0	10.0	10.0	6.97 ±
		25.0	10.0	15.0	3.98 ±
		30.0	10.0	20.0	2.78 ±
		35.0	10.0	25.0	2.12 ±
		40.0	10.0	30.0	1.44 ±
		45.0	10.0	35.0	1.26 ±
		50.0	10.0	40.0	0.935 ±
		55.0	10.0	45.0	0.852 ±
		60.0	10.0	50.0	0.758 ±
BEI-01	0.582	15.0	10.0	5.0	9.71 ± 0.11
		20.0	10.0	10.0	5.15 ± 0.10
		25.0	10.0	15.0	2.52 ± 0.08
		30.0	10.0	20.0	1.78 ± 0.22
		35.0	10.0	25.0	0.99 ± 0.11
		40.0	10.0	30.0	0.87 ± 0.14
		45.0	10.0	35.0	0.747 ± 0.066
		50.0	10.0	40.0	0.52 ± 0.15
		55.0	10.0	45.0	0.318 ± 0.020
		60.0	10.0	50.0	0.236 ± 0.007

Fm. = Formation
h = Depth from which the sample was obtained
P = Pressure
P_c = Confining pressure
P_p = Pore pressure
P_e = Effective pressure
k = Permeability

Table 1b. Permeability data for shale samples from the permeability data for shale samples from the Western Canada Sedimentary Basin, Alberta.

Sample (Fm.)	h (km)	P (MPa) P_c	P_p	P_e	k (10^{-21} m^2)
CRB-02	0.575	15.0	10.0	5.0	17.1 ± 0.9
		20.0	10.0	10.0	8.85 ± 1.56
		25.0	10.0	15.0	2.41 ± 0.31
		30.0	10.0	20.0	1.15 ± 0.15
		35.0	10.0	25.0	0.689 ± 0.076
		40.0	10.0	30.0	0.485 ± 0.058
		45.0	10.0	35.0	0.420 ± 0.043
		50.0	10.0	40.0	0.397 ± 0.044
		55.0	10.0	45.0	0.329 ± 0.027
		60.0	10.0	50.0	0.261 ± 0.018
BSR-12	1.26	12.5	10.0	2.5	9.25 ± 0.09
		15.0	10.0	5.0	6.23 ± 0.66
		17.5	10.0	7.5	5.58 ± 0.50
		20.0	10.0	10.0	4.34 ± 0.25
		25.0	10.0	15.0	3.71 ± 0.12
		30.0	10.0	20.0	2.21 ± 0.19
		35.0	10.0	25.0	1.18 ± 0.10
		40.0	10.0	30.0	0.94 ± 0.04
		45.0	10.0	35.0	0.85 ± 0.09
		50.0	10.0	40.0	0.68 ± 0.03
		55.0	10.0	45.0	0.60 ± 0.05

Fm. = Formation
h = Depth from which the sample was obtained
P = Pressure
P_c = Confining pressure
P_p = Pore pressure
P_e = Effective pressure
k = Permeability

Determination of in situ permeability (k) values

Since the literature permeability data are presented as a function of effective pressure, we must first determine the in situ effective pressure (P_e) for each of the samples. This is achieved by using the equation,

$$P_e = P_L - P_f, \quad (4)$$

where P_L is the lithostatic pressure and P_f is the pore fluid pressure. Values of P_L, P_f and P_e are listed in Table 2 for each sample set. The P_L and P_f data for the Venture gas field samples are interpolated using the data of Ervine and Bell (1987) and Bell (1990) where P_L was calculated using density logs and P_f was estimated from pressure test and mud weight data. An implicit assumption for all samples is that pore pressures measured in reservoir rocks can be used to estimate pore pressures in shales. The in situ pressure values for the Beaufort-Mackenzie Basin samples (Table 2) are from Katsube et al. (1996b).

For the Western Canada Sedimentary Basin, P_e values are calculated for the estimated maximum paleoburial depths (Table 2; D.R. Issler, unpub. data, 1997). The P_L values were calculated using the regional erosion-corrected compaction curve derived from porosity data obtained by mercury porosimetry (D.R. Issler, unpub. data, 1997), a mean grain density of 2675 kg/m^3 (Issler and Katsube, 1994) and a fluid density of 1030 kg/m^3 (sea water). The P_f was assumed to be hydrostatic for normally-compacted sediments and overpressured for undercompacted sediments. These P_e values were used to estimate the in situ permeability values listed in Table 2, by interpolation using the literature and measured permeability-pressure data in Table 1a and 1b.

ANALYTICAL RESULTS

The estimated in situ permeabilities (k), from Table 2, are plotted against the pore-size mode (d_m) values in Figure 4. In the cases where ranges for k values are listed (e.g. V-2 and V-6), only the maximum value were used for the plot. The

Table 2. Permeability (k) and mode of the pore-size distribution (d_m) data for shale samples from Canadian sedimentary basins.

Sample	h[1] (km)	d_m[2] (nm)	P_L[3] (MPa)	P_f[4] (MPa)	P_e[5] (MPa)	k_h[6] ($10^{-21}m^2$)	References[7] k	References[7] d_m
Venture gas field (Scotian Shelf)								
V-1	4.7	5	106	72	34	0.9	[1]	[5]
V-2	4.7	20	106	72	34	<5.4	[1]	[5]
V-3	4.92	7.9	114	84	30	6.2	[1]	[5]
V-4	4.96	3.2	115	86	29	6.6	[1]	[5]
V-5	5.12	3.2	119	91	28	9.2	[1]	[5]
V-6	5.13	7.9	119	91	28	<0.29	[1]	[5]
V-7	5.27	7.9	123	100	23	2.04	[1]	[5]
V-8	5.27	12.6	123	100	23	23.9	[1]	[5]
V-9	5.55	7.9	130	111	19	1.28, 1.32	[1]	[5]
V-10	5.57	5	131	112	19	3.21	[1]	[5]
VSF-D*	0	50.1	15.3[a]	5.3[a]	10[a]	125[a]	[2]	[2]
Beaufort-Mackenzie Basin								
B-5	3.76	31.6	83	65	18	23	[1]	[6]
B-9	2.44	50.1	53	25	28	148	[1]	[6]
AR-5	4.38	12.6	99	75	23	0.82	[3]	[7]
TG-6	2.46	7.9	55	26	29	5	[3]	[7]
TA-1	2.88	3.2	65	29	36	<0.24	[3]	[7]
ML-2	3.22	20	75	50	25	0.19	[3]	[7]
Western Canada Sedimentary Basin								
ACD-03	0.56 2.21[a]	7.9	51	22	29	3.1	[4]	[4]
ACD-13	0.61 2.26[a]	5	52	23	29	1.6	[4]	[4]
BEI-01	0.58 2.31[a]	5	53	23	30	0.87	[4]	[4]
CRB-02	0.57 10.78[a]	12.6	40	18	22	0.97	[4]	[4]
BSR-12	1.26 3.06[a]	7.9	72	36	36	0.82	[4]	[4]

*Results from lab compression experiments on unconsolidated seafloor sediment
[1]Depth of sample; a - reconstructed maximum paleoburial depth
[2]Mode of pore-size distribution
[3]Calculated lithostatic pressure
[4]Estimated in situ pore pressure
[5]Estimated in situ effective pressure
[6]Estimated in situ permeability from permeability laboratory measurements
[7]Sources for permeability and pore-size data:
[1] - Katsube and Coyner (1994)
[2] - Katsube et al. (1996a)
[3] - Katsube et al. (1996b)
[4] - new data
[5] - Katsube (1992)
[6] - Katsube and Best (1992)
[7] - Katsube and Issler (1993)

regression lines are calculated using all data points. The reduced major axis (RMA; Davis, 1986) is represented by a solid line and the two normal regression lines (NRL) by broken lines. These regression lines are expressed by the following equations:

RMA: $k = 10^{-21}\exp(0.132d_m - 0.676)\ m^2$,

$r = 0.68$,

NRL: $k = 10^{-21}\exp(0.090d_m - 0.113)\ m^2$,

$k = 10^{-21}\exp(0.194d_m - 1.50)\ m^2$,

where r is the correlation factor.

Four of the five data points showing the largest deviation from the RMA are highlighted in Figure 4 by "A", "B", "C", and "D". Their most distinguishing petrophysical characteristics are their calculated surface area (A), as determined from mercury porosimetry. The definitions and methods of determining A are described in Katsube et al., (1997). Data points "A", "B", and "C" (samples V-8, V-4, and V-3) represent diagenetically mature shales with relatively large A values (9.5-14 m^2/g). This suggests that they have undergone significant dissolution (Katsube and Williamson, in press), such that the large permeability value may be a result of better than expected pore-interconnectivity.

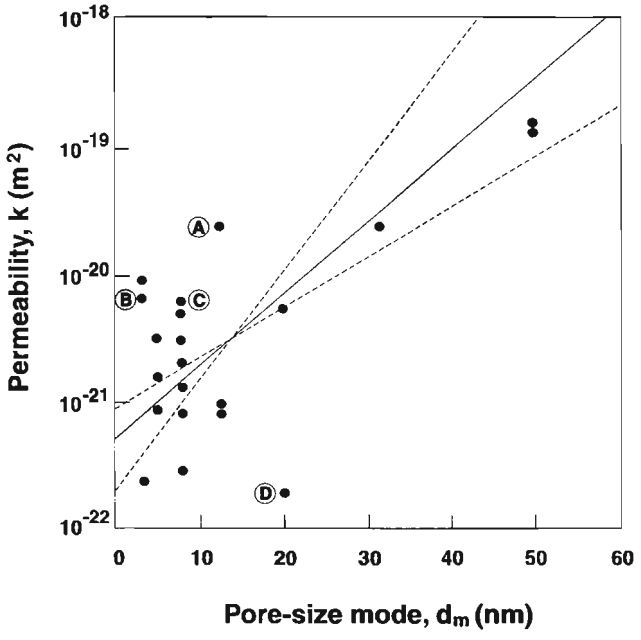

Figure 4. *The functional relationship between permeability (k) and mode of the pore-size distribution (d_m) for shale samples from the Venture gas field (offshore Nova Scotia, Katsube and Coyner, 1994), the Beaufort-Mackenzie Basin (Northwest Territories, Katsube et al., 1996b), and the Western Canada Sedimentary Basin. The solid regression line is the reduced major axis (RMA: Davis, 1986) and the broken lines are the normal regression lines (NRL). Symbols "A", "B", "C", and "D" represent four of the five data points showing the largest deviation from the RMA. They represent samples with either unusually large or small surface area (A) values.*

Data point "D" (sample ML-2) represents a diagenetically immature shale with a surface area much smaller (A <6 m^2/g) than expected for such a shale. This suggests that the sample could be influenced by some form of cementation (Katsube and Williamson, in press), which may affect the connectivity of the connecting pores, such as increased tortuosity, resulting in reduced permeability. No distinguishable petrophysical characteristics have been observed, to date, for the fifth deviating data point (V-5), located just above "B" in Figure 4.

DISCUSSIONS AND CONCLUSIONS

Whereas the relationship between shale permeability (k) and pore-size mode (d_m) data collected in this study displays considerable scatter, as shown in Figure 4, it suggests that a relatively good relationship does exist between the two parameters. The permeability (k) increases by more than 3 orders of magnitude for a pore-size mode (d_m) increase from 3 to 50 nm. Despite the somewhat poor correlation coefficient of 0.68, Figure 4 indicates that k can be estimated within a factor of one order of magnitude for 90% of the data, and within a factor of about 3 for about 65% of the data, using the reduced major axis (RMA):

$$k = 10^{-21}\exp(0.13d_m - 0.68)\ m^2.$$

Considering the fact that k generally varies over a range of more than 10 orders of magnitude (Brace, 1980), with granites commonly displaying k values of 10^{-19} m^2 to 10^{-17} m^2 for mean pore-sizes of 100-300 nm (Katsube and Hume, 1987), this k-d_m relationship presented for shales is not poor. It has practical applications, within limits, as previously indicated.

These results suggest that, while the value of d_m can be used to provide an approximate estimate of k, knowledge of how other parameters, such as surface area (A), affect k is necessary to improve the accuracy of these k estimates. They are, most likely, related to some of the parameters in equation 3, such as effective porosity and tortuosity.

ACKNOWLEDGMENTS

Part of the data used in this study was obtained as a result of a joint study between PanCanadian Petroleum Limited and the Geological Survey of Canada. The authors express their appreciation to Sebastian Bell (GSC Calgary, Calgary) for his assistance in obtaining subsurface pressure data for the Venture study wells. The authors thank L.D. Dyke (GSC, Ottawa) for critically reviewing this paper, and for his constructive comments.

REFERENCES

Agterberg, F.P., Katsube, T.J., and Lew, S.N.
1984: Statistical analysis of granite pore size distribution data, Lac du Bonnet batholith, Eastern Manitoba; in Current Research, Part A, Geological Survey of Canada, Paper 84-1A, p. 29-37.

Bell, J.S.
1990: Lecture: The stress regime of the Scotian Shelf offshore eastern Canada to 6 kilometers depth and implications for rock mechanics and hydrocarbon migration; in Rock at Great Depth, (ed.) V. Maury and D. Fourmaintraux; A.A. Balkema, Rotterdam, p. 1243-1265.

Brace, W.F.
1980: Permeability of crystalline and argillaceous rocks; International Journal of Rock Mechanics, Mineral Science & Geomechanical Abstracts, v. 17, p. 241-251.

Davis, J.C.
1986: Statistics and Data Analysis in Geology; John Wiley & Sons, p. 200-204.

Ervine, W.B. and Bell, J.S.
1987: Subsurface *in situ* stress magnitudes from oil-well drilling records; an example from the Venture area, offshore eastern Canada; Canadian Journal of Earth Sciences, v. 24, p. 1748-1759.

Hacquebard, P.A.
1977: Rank of coal as an index of organic metamorphism for oil and gas in Alberta; in The Origin and Migration of Petroleum in the Western Canada Sedimentary Basin - A Geochemical and Thermal Maturation Study, (ed.) G. Deroo, T.G. Powell, B. Tissot, and R.G. McCrossan; Geological Survey of Canada, Bulletin 262, p. 11-22.

Issler, D.R.
1992: A new approach to shale compaction and stratigraphic restoration, Beaufort-Mackenzie Basin and Mackenzie Corridor, Northern Canada; American Association of Petroleum Geologists Bulletin, v. 76, p. 1170-1189.

Issler, D.R. and Katsube, T.J.
1994: Effective porosity of shale samples from the Beaufort-Mackenzie Basin; in Current Research 1994-B; Geological Survey of Canada, p. 19-26.

Katsube, T.J.
1992: Statistical analysis of pore-size distribution data of tight shales from the Scotian Shelf; in Current Research, Part E; Geological Survey of Canada, Paper 92-1E, p. 365-372.
1993: Nano pore transport mechanism of tight shales from the Scotian Shelf; in Current Research, Part D; Geological Survey of Canada, Paper 93-1D, p. 121-127.

Katsube, T.J. and Best, M.E.
1992: Pore structure of shales from the Beaufort-Mackenzie Basin, Northwest Territories: in Current Research, Part E; Geological Survey of Canada, Paper 92-1E, p. 157-162.

Katsube, T.J. and Coyner, K.
1994: Determination of permeability(k)-compaction relationship from interpretation of k-stress data for shales from Eastern and Northern Canada; in Current Research 1994-D; Geological Survey of Canada, Paper 94-1D, p. 169-177.

Katsube, T.J. and Hume, J.P.
1987: Pore structure characteristics of granitic rock samples from Whiteshell Research Area; in Geotechnical Studies at Whiteshell Research Area (RA-3); CANMET, Report MRL 87-52, p. 111-158.

Katsube, T.J. and Issler, D.R.
1993: Pore-size distribution of shales from the Beaufort-Mackenzie Basin, northern Canada; in Current Research, Part E; Geological Survey of Canada, Paper 93-1E, p. 123-132.

Katsube, T.J. and Williamson, M.A.
1994: Effects of diagenesis on shale nano-pore structure and implications for sealing capacity; Clay Minerals, v. 29, p. 451-461.
1995: Critical depth of burial of subsiding shales and its effect on abnormal pressure development; in Proceedings of the Oil and Gas Forum' 95 ("Energy from Sediments"), Geological Survey of Canada, Open File 3058, p. 283-286.
in press: Shale petrophysical characteristics: permeability history of subsiding shales; in Proceedings of "GSA Annual Meeting – New Orleans", Louisiana, November 6-9, 1995.

Katsube, T.J., Best, M.E., and Mudford, B.S.
1991a: Petrophysical characteristics of shales from the Scotian shelf; Geophysics, v. 56, p. 1681-1688.

Katsube, T.J., Bloch, J., and Issler, D.R.
1995: Shale pore structure evolution under variable sedimentation rates in the Beaufort-MacKenzie Basin; in Proceedings of the Oil and Gas Forum' 95 ("Energy from Sediments"), Geological Survey of Canada, Open File 3058, p. 211-215.

Katsube, T.J., Boitnott, G.N., Lindsay, P.J., and Williamson, M.
1996a: Pore structure evolution of compacting muds from the sea floor offshore Nova Scotia; in Current Research 1996-D; Geological Survey of Canada, p. 17-26.

Katsube, T.J., Dorsch, J., and Connell, S.
1997: Pore surface area characteristics of the Nolichucky shale within the Oak Ridge Reservation (Tennessee, U.S.A.): Implication for fluid expulsion efficiency; in Current Research 1997-E; Geological Survey of Canada, p. 117-124.

Katsube, T.J., Issler, D.R., and Coyner, K.
1996b: Petrophysical characteristics of shales from the Beaufort-Mackenzie Basin, Northern Canada; permeability, formation factor and porosity versus pressure; in Current Research 1996-B; Geological Survey of Canada, p. 45-50.
1996b: Petrophysical characteristics of shales from the Beaufort-Mackenzie Basin, Northern Canada; permeability, formation factor and porosity versus pressure; in Current Research 1996-B; Geological Survey of Canada, p. 45-50.

Katsube, T.J., Wires, K., Cameron, B.I., and Franklin, J.M.
1991b: Porosity and permeability of ocean floor sediments from the Middle Valley Zone in the northeast Pacific; Borehole PAR90-1; in Current Research, Part E; Geological Survey of Canada, Paper 91-1E, p. 91-97.

Madden, T.R.
1983: Microcrack connectivity in rocks: a renormalization group approach to the critical phenomena of conduction and failure in crystalline rocks; Journal of Geophysical Research, v. 88, p. 585-592.

Neuzil, C.E.
1994: How permeable are clays and shales?; Water Resources Research, v. 30, p. 145-150.

Nurkowski, J.R.
1984: Coal quality, coal rank variation and its relation to reconstructed overburden, Upper Cretaceous and Tertiary plains coals, Alberta, Canada; American Association of Petroleum Geologists Bulletin, v. 68, p. 285-295.

Steiner, J., Williams, G.D., and Dickie, G.J.
1972: Coal deposits of the Alberta Plains; in Proceedings, First Geological Conference on Western Canadian Coal (ed.) G.B. Mellon, J.W. Kramers, and E.J. Seagel; Edmonton, Research Council of Alberta, Information Series no. 60, p. 85-108.

Walsh, J.B. and Brace, W.F.
1984: The effect of pressure on porosity and the transport properties of rocks; Journal of Geophysical Research, v. 89, p. 9425-9431.

Wyllie, M.R. and Spangler, M.B.
1952: Application of electrical resistivity measurements to problems of fluid flow in porous media; Bulletin of the American Association of Petroleum Geologists, v. 36, p. 359-403.

Geological Survey of Canada Project 870057

Extraction chimique des éléments du groupe du platine et de l'or et détermination de leurs teneurs par spectrométrie de masse à émission de plasma

K. Gueddari, M.R. LaFlèche et J. Amossé[1]
Centre géoscientifique de Québec, Sainte-Foy

Gueddari, K., LaFlèche et Amossé, J., 1998: Extraction chimique des éléments du groupe du platine et de l'or et détermination de leurs teneurs par spectrométrie de masse à émission de plasma; dans Recherches en cours 1998-D; Commission géologique du Canada, p. 59-64.

Résumé : Nous avons mis au point une méthode d'analyse chimique des éléments du groupe du platine (ÉGP) et de l'or dans les roches basiques et ultrabasiques. Cette méthode implique d'abord une fusion des échantillons au peroxyde de sodium. Après réduction au chlorure stanneux, nous coprécipitons et concentrons les ÉGP et l'or en présence de sélénium et de tellure. Les taux d'extraction sont proches de 100 %. L'analyse est effectuée par SM-ÉP, ce qui permet d'améliorer les limites de détection. Plusieurs points concernant les modalités du dosage par SM-ÉP sont discutés. Des essais de fiabilité sur des échantillons de référence montrent que les teneurs obtenues sont semblables à celles proposées. La méthode présentée est adaptée à l'analyse des échantillons pauvres ou riches en ÉGP et en or, et sert actuellement à déterminer les teneurs en ces éléments dans des roches basiques et ultrabasiques.

Abstract: We have developed a chemical analysis method for platinum group elements and gold. We start by fusing rock samples with sodium peroxide. After reduction with stannous chloride, PGE and Au are extracted by coprecipitation using selenium and tellurium as carriers. Yields approach 100%. The analysis is carried out by ICP-MS to improve detection limits. Instrumental operating conditions, mass interference, internal standards, and calibration are discussed. The results obtained for international standards are generally in good agreement with the proposed values. The method presented here can be used for samples that are either poor or rich in PGE and Au and is currently been used for PGE and Au determinations in mafic and ultramafic rocks.

[1] Institut Dolomieu de géologie, 15, rue Maurice-Gignoux, 38031 Grenoble, France

INTRODUCTION

Dans un très grand nombre de roches (ultrabasiques et basiques non minéralisées), les teneurs en éléments du groupe du platine (ÉGP : Os, Ir, Ru, Rh, Pt, Pd) et en or (Au) sont très faibles, de l'ordre du ng/g (ppb) voire du pg/g (ppt), et de plusieurs fois inférieures à celles en certains éléments de la matrice. Cela impose une technique d'analyse des ÉGP et de Au qui soit fiable et sélective pour leur mise en solution et leur concentration.

Les techniques classiquement utilisées, les fusions au plomb et notamment au sulfure de nickel, restent des méthodes lourdes, polluantes et relativement peu précises. Les procédures relatives à la méthode de fusion au sulfure de nickel sont largement documentées (par exemple Parry et al., 1987; Jackson et al., 1990; Jarvis et al., 1992; références citées dans ces textes). D'une manière générale, cette technique présente l'avantage de pallier aux problèmes d'hétérogénéité de la roche, mais une grande quantité de réactifs est nécessaire. Ces réactifs peuvent être la source de nombreuses interférences de masse lors de l'analyse par SM-ÉP (spectrométrie de masse à émission de plasma; en anglais, ICP-MS, inductively coupled plasma-mass spectrometry) s'il n'y a pas séparation et préconcentration avant l'analyse. De plus, ils peuvent renfermer des traces d'ÉGP et de Au et, ainsi, induire une contamination des échantillons.

PRINCIPE DE LA MÉTHODE

Toute méthode d'analyse des ÉGP et de Au doit, en premier lieu, permettre de solubiliser l'ensemble des constituants de l'échantillon, notamment les phases réfractaires susceptibles de concentrer ces éléments (par ex. les alliages et la chromite). La fusion au peroxyde de sodium (Na_2O_2) dans des creusets de zirconium est une méthode d'attaque plausible pour remédier à ce problème. De plus, pour pallier aux effets de l'hétérogénéité des échantillons, il est possible d'attaquer un plus gros échantillon (dizaines de grammes). Il faut ensuite prélever une aliquote de 3 g ou moins, après fusion et homogénéisation de la solution mère. Cette façon de faire présente aussi l'avantage de consommer moins de réactifs.

Après filtration et élimination de la silice, l'étape d'extraction correspond à une coprécipitation des ÉGP et de Au en présence d'oxydes de sélénium (SeO_2) et de tellure (TeO_2) utilisés comme entraîneurs. La réduction des ÉGP et de Au, assurée par une solution de chlorure stanneux ($SnCl_2$), permet la formation de complexes $[ÉGP\ Sn_4Cl_4]^{4+}$ (Meyer et Ayres, 1955; Amossé et al., 1986). Par la suite, une ébullition amène la décomposition des complexes formés et favorise la précipitation de Ru, Rh, Pt, Pd et Au sous forme de séléniures et de tellurures insolubles. Il semble cependant que Ir ne se décompose pas en raison de la plus grande stabilité des complexes formés, ce qui se traduit par un taux d'extraction faible (environ 30 %). Ainsi, l'utilisation d'une solution d'iodure de potassium (KI) permet d'obtenir des complexes facilement dissociables (par substitution des ions «iode» aux ions «chlore» du complexe stanneux). Quant à Os, sa volatilité précoce sous forme de tétroxyde d'osmium (OsO_4) à des températures relativement basses rend son dosage délicat et exige un protocole d'analyse différent et une méthode d'attaque spéciale en milieu réducteur (Shirey et Walker, 1995).

MÉTHODOLOGIE EXPÉRIMENTALE

Protocole d'analyse

Le schéma ci-dessous illustre les différentes étapes et les principales opérations de la méthode d'extraction et de dosage des ÉGP et de Au présentée dans ce travail :

Fusion → Mise en solution → Évaporation → Filtration de la silice ↘

Attaque du précipité ← Filtration ← Ajout de $SnCl_2$ ← Ajout de Se-Te (et de KI)

↘

Évaporation → Reprise à l'eau régale → SM-ÉP

Réactifs et matériel

* Creusets de Zr, *B-J Scientific Products, Inc.*
* Peroxyde de sodium (Na_2O_2), granules : 140 mesh, 97 %, *Aldrish Chemical Compagny, Inc.*
* Carbonate de sodium et potassium ($KNaCO_3$), *U.S.P., A & C American Chemicals Ltd.*
* Hydroxyde de potassium (KOH), *Laboratoire MAT Inc.*
* Acide chlorhydrique (HCl, 37 %), Aristar®, *BDH Inc.*
* Papier filtre (filtration de SiO_2), dimension des pores 3 µm, Whatman®
* Oxyde de sélénium (SeO_2), 99,9 %, *Aldrish Chemical Compagny, Inc.*
* Oxyde de tellure (TeO_2), 99,995 %, *Aldrish Chemical Compagny, Inc.*
* Iodure de potassium (KI), AnalaR®, *BDH Inc.*
* Étain (Sn), granules, 99,5 %, *Aldrish Chemical Compagny, Inc.*
* Papier filtre (récupération), dimension des pores 0,22 µm, type GS, *Millipore*
* Acide nitrique (HNO_3, 60-71 %), *Seastar Chemicals Inc.*

Mode opératoire

* La fusion de l'échantillon finement broyé est réalisée dans un creuset de zirconium sur une prise de (n) g correspondant à un poids de 3 à 10 g. Il est à noter que si l'échantillon présente une hétérogénéité marquée, l'attaque doit être faite sur une plus grande prise d'échantillon (dizaines de grammes). Pour une prise de (n) g, on ajoute (4 x n) g de Na_2O_2, (0,75 x n) g de $KNaCO_3$. L'ensemble est placé dans un creuset de

zirconium, bien mélangé et, ensuite, porté à fusion sur un bec Mecker. Pendant le chauffage, on ajoute des pastilles de KOH (environ (0,5 x n) g) pour déclencher la fusion.

* La fusion doit aboutir à un liquide homogène dépourvu de grains réfractaires. Après refroidissement, la masse solide se détache facilement du creuset si ce dernier est plongé dans un bécher contenant de l'eau distillée chaude. Après avoir retiré le creuset, la mise en solution totale se fait par ajout d'un volume de HCl 12 M. Cette solution est complètement évaporée sur un bain de sable maintenu à une température d'environ 130 °C afin de précipiter la silice.

* Une fois sec, le résidu est redissous dans un mélange d'eau distillée (environ 150 ml pour 3 g d'échantillon) et de HCl 12 M (environ 20 ml pour 3 g d'échantillon), puis chauffé. La silice non dissoute est récupérée et éliminée après filtration de la solution à travers un papier filtre aux pores d'une dimension de 3 µm.

* Si la quantité d'échantillon attaquée est importante, une aliquote d'un volume défini équivalent à 3 g peut être prélevée de la solution filtrée (cette quantité peut varier selon les teneurs en ÉGP et en Au des roches). À cette aliquote sont ajoutés 10 ml d'une solution contenant des oxydes de Se et de Te (Se : 1 g/l, Te : 0,5 g/l) ainsi que 10 ml d'une solution de KI à 500 g/l. La solution finale est ramenée à HCl 4 M.

* On chauffe et, au début de l'ébullition, on ajoute une solution de $SnCl_2$ (20 %) jusqu'à disparition de la couleur initiale de la solution mère et apparition d'un précipité noir. On laisse bouillir pendant 10 minutes à feu doux.

* Après un court refroidissement, la solution est filtrée à travers un papier filtre Millipore d'acétate de cellulose aux pores d'une dimension de 0,22 µm. Le précipité noir déposé sur le filtre est transféré dans un petit bécher, puis dissous à chaud dans quelques gouttes de HCl 12 M et de HNO_3 16 M. Après remise en solution, le filtre est rincé à l'eau distillée et retiré; on laisse ensuite évaporer la solution contenue dans le bécher à une température d'environ 70 °C.

* Le résidu obtenu est remis en solution par l'ajout de quelques gouttes de HCl 12 M et de HNO_3 16 M et jaugé à 5 ml avant analyse par SM-ÉP.

INSTRUMENTATION ET CONDITIONS D'ANALYSE

La détermination des teneurs en ÉGP et en Au a été effectuée par SM-ÉP (modèle Fisons Instruments, VG-PlasmaQuad Turbo 2+). Cet appareil, comparé au spectrophotomètre d'absorption atomique électrothermique, par exemple, a l'avantage d'être rapide et sensible, en plus de permettre d'analyser plusieurs éléments à la fois. Les conditions d'analyse par SM-ÉP sont présentées dans le tableau 1.

Tableau 1. Conditions opératoires et paramètres d'acquisition du SM-ÉP.

Puissance du générateur : 1 350 W
Puissance réfléchie : < 2 W
Gaz : argon
Débit d'alimentation : 13 l/min
Débit auxiliaire : 1 l/min
Débit d'injection : 0,94 l/min
Chambre de nébulisation : MK2 Quartz
Type de nébuliseur : Meinhardt
Temps de stabilisation («uptake») : 90 s
Nombre d'acquisitions : 3
Temps d'acquisition : 21 s/acquisition
Temps de lavage : 90 s
Type de détecteur : Galileo modèle 4 870V
Mode de détection : comptage d'impulsions («pulse counting»)
Mode d'acquisition : saut de pic («peak jumping»)
Nombre de points par pic : 3
Temps de lecture/uma («dwell-time») : 10 240 µs
Temps de balayage («time/sweep») : 0,98 s

Interférences

Un des principaux problèmes de l'analyse des ÉGP et de Au par SM-ÉP est celui des interférences (Longerich et al., 1990; Jarvis et al., 1992). Toutefois, la méthode décrite ci-dessus est sélective et permet de diminuer la charge (matrice) de la solution et d'éliminer les éléments pouvant interférer avec les ÉGP et Au. Les quelques interférences isobariques entre deux éléments ayant des isotopes de même masse (par exemple ^{104}Pd et ^{104}Ru) peuvent être résolues par le choix d'autres isotopes. La quantité de Zr qui reste dans la solution (provenant des creusets) peut provoquer des interférences de ZrO avec les isotopes suivants : ^{106}Pd, ^{108}Pd et ^{110}Pd. L'analyse de Pd a donc été faite sur l'isotope ^{105}Pd. Par ailleurs, CuAr ($^{65}Cu^{40}Ar^+$ et $^{63}Cu^{40}Ar^+$) peut interférer avec ^{105} Pd et ^{103}Rh, ce dernier étant un élément mono-isotopique (Longerich et al., 1990). Toutefois, les très faibles teneurs en Cu dans la solution analysée écartent la possibilité d'interférences de ce type. En raison de l'absence d'interférences sur les isotopes ^{103}Rh, ^{101}Ru, ^{102}Ru, ^{105}Pd, ^{191}Ir, ^{193}Ir, ^{194}Pt, ^{195}Pt, ^{196}Pt et ^{197}Au, ces derniers ont servi à calculer les teneurs en ÉGP et en Au dans les échantillons de roches.

Standardisation interne et calibration externe

La standardisation interne repose sur l'ajout, dans la solution analysée, d'une quantité connue d'un ou de plusieurs éléments de concentration parfaitement connue. Elle améliore la qualité des résultats en contrôlant la sensibilité et les fluctuations de l'instrument.

Jackson et al. (1990) proposent d'utiliser comme standards internes ^{111}Cd pour les ÉGP légers (Ru, Rh, Pd) et Tl pour les ÉGP lourds (Os, Ir, Pt) et Au. Dans notre cas, nous avons utilisé deux isotopes à une concentration de 100 ppb

chacun : d'une part, ^{187}Re, qui est plus proche des masses des ÉGP lourds et de Au et, d'autre part, ^{93}Nb, pour les ÉGP légers. Il faut noter que ^{93}Nb doit être ajouté aux solutions juste avant leur analyse en raison de son instabilité. L'utilisation de ^{111}Cd (Jackson et al., 1990) n'est pas toujours souhaitée ici, car la présence d'une quantité importante de ^{112}Sn dans les solutions analysées peut perturber le pic du ^{111}Cd.

La calibration externe consiste en l'utilisation de solutions étalons contenant les éléments à doser et les standards internes à des teneurs connues, lesquelles sont choisies en fonction de la fourchette des teneurs en ÉGP et Au des matériaux étudiés. Dans le cas des roches basiques et ultrabasiques que nous avons analysées, cinq solutions étalons ont été préparées pour la calibration externe (0 ppb, 2 ppb, 5 ppb, 10 ppb et 20 ppb ou 0 ppb, 2 ppb, 20 ppb, 50 ppb et 100 ppb), selon les teneurs en ÉGP et Au de ces roches. Il est fondamental que le coefficient de régression soit égal ou très proche de l'unité.

Par ailleurs, il faut souligner que, dans les solutions analysées, ^{93}Nb risque d'interférer avec Se (utilisé comme entraîneur) à la suite de la formation de $^{77}Se^{16}O^{+}$. Il est donc important d'ajouter dans les solutions étalons la même quantité d'oxyde de Se que celle que contiennent les solutions à analyser.

DISCUSSION : APPLICATION À CERTAINES ROCHES

La méthode d'analyse décrite ici permet des taux d'extraction exceptionnels (Amossé et al., 1986; Gueddari, 1996). Ces taux ont été mesurés sur des solutions d'une roche basique très pauvre en ÉGP et en Au. Le principe consiste à ajouter, après filtration de la silice, des concentrations connues d'ÉGP et de Au et, ensuite, faire une extraction et une analyse selon les procédures décrites ci-dessus. Les taux calculés sont proches de 100 % pour les ÉGP et supérieurs ou égaux à 80 % pour Au. Il faut noter qu'en présence de KI, le taux d'extraction de Au est variable et faible, alors qu'en l'absence de KI, l'iridium n'est extrait qu'à environ 30 % (voir ci-dessous).

Un des problèmes majeurs du dosage des ÉGP et de Au réside dans la présence de contaminants dans les réactifs utilisés pour la mise en solution des échantillons et la préconcentration. Cela est le cas, par exemple, de HCl et de Na_2O_2 qui peuvent contenir quelques parties par milliard de Pt. Après réalisation d'essais sur les blancs et vérification de plusieurs réactifs, notre choix s'est porté sur les produits présentés dans la section «Méthodologie expérimentale» et pour lesquels les blancs ont donné de très faibles teneurs en ÉGP et en Au (Ir < 0,01 ng; Ru 0,04 ng; Rh 0,026 ng; Pt 0,33 ng; Pd 0,26 ng; Au 0,15 ng). Par ailleurs, l'adsorption de particules sur les parois des creusets et du matériel utilisé peut être la source de contamination. Il est donc nécessaire de procéder à un nettoyage systématique après le traitement de chaque échantillon et de passer régulièrement la verrerie à l'eau régale.

La méthode a été testée sur trois échantillons de référence, WPR-1 (péridotite altérée), WGB-1 (gabbro) et DTS-1 (dunite), lesquels ont fait l'objet d'une ou plusieurs extractions. Ces échantillons ont été choisis car ils couvrent une large fourchette des teneurs en ÉGP et en Au. Les résultats obtenus sont présentés dans le tableau 2.

Les résultats du tableau 2 montrent que les teneurs obtenues sont très proches des valeurs certifiées données pour les échantillons de référence. Il faut souligner que, contrairement aux teneurs en Au, celles en Ir présentées dans le tableau 2 ont été déterminées à partir de solutions avec ajout de KI. La

Tableau 2. Teneurs en ÉGP et en Au (en ppb) de trois échantillons de référence comparées à celles obtenues dans le cadre du présent travail.

Échantillon de référence	Ir	Ru	Rh	Pt	Pd	Au
DTS-1						
Valeurs proposées*	0,67	2,5 (?)	-	5,7	3 (?)	-
Présent travail (a)	1	5,3	2,6	10	5,6	-
WPR-1						
Valeurs certifiées**	13,5 1,8	22 4	13,4 0,9	285 12	235 9	42 3
Présent travail (b)	14,2 *(1)*	19,9 1,6	12,5 1,2	271 6	236 15	27 3
WGB-1						
Valeurs recommandées***	0,33 0,17	0,3	0,32 0,21	6,1 1,6	13,9 2,1	2,9 1,1
Présent travail (c)	0,36 0,08	0,6 0,14	0,53 0,3	6,2 2	10 1,4	2 *(1)*

* : Valeurs proposées et non certifiées (Potts et al., 1993). (a) Une seule détermination sans KI, écart-type relatif <2 %.
** : Valeurs certifiées (CANMET). (b) Quatre déterminations dont trois sans KI et une avec KI.
*** : Ir, Ru et Rh : valeurs provisoires; Pt, Pd et Au : valeurs certifiées (CANMET). (c) Trois déterminations dont deux avec KI et une sans KI.
(1) : Une détermination, Ir : avec KI, Au : sans KI.
En présence de KI, nous avons observé une meilleure extraction de Ir par opposition à celle de Au et vice versa. L'extraction de Pd est légèrement meilleure sans KI contrairement à celle de Ru. Pour Pt Et Rh, les différentes déterminations donnent des teneurs très proches.

présence de ce dernier favorise l'extraction de Ir et semble inhiber celle de Au. Par conséquent, Ir et Au ne peuvent pas être extraits simultanément par la même procédure d'analyse. Il faut pratiquer deux extractions séparées pour un même échantillon : l'une permettant le dosage de Ir (avec KI) et l'autre, celui de Au (sans KI). L'extraction des autres ÉGP (Ru, Rh, Pt et Pd) peut se faire avec ou sans KI. Par ailleurs, par opposition à la teneur en Au de l'échantillon WGB-1, celle de l'échantillon WPR-1 demeure inférieure à la fourchette des valeurs certifiées (tableau 2). Il est probable que cet élément soit réparti d'une manière très hétérogène dans cet échantillon (effet pépite : «nugget effect»). Des essais préliminaires d'analyse sur des petites prises d'échantillons (< 3 g) montrent que Pt et Pd peuvent présenter un effet pépite, engendrant ainsi des résultats contrastés. Pour des échantillons dont l'hétérogénéité est marquée, il faut attaquer plusieurs dizaines de grammes de matériel. La suite de l'analyse s'effectue ensuite sur une aliquote de 3 g prélevée après homogénéisation de la solution.

La méthode d'analyse chimique exposée ici est actuellement utilisée pour la détermination des teneurs en ÉGP et en Au d'échantillons de plusieurs types de roches. Elle a déjà servi à l'étude géochimique de ces éléments dans les xénolites de péridotite remontés par les basaltes alcalins et dans les roches mantelliques des massifs ultrabasiques de Ronda (Espagne) et de Beni Bousera (Maroc) (Gueddari et al., 1996). Les résultats obtenus pour les roches de ces massifs et les interprétations géochimiques qui en découlent sont très comparables à ce qui est présenté dans une publication récente sur le dosage des ÉGP et de Au par activation neutronique instrumentale, après préconcentration au sulfure de nickel (Garuti et al., 1997). Par ailleurs, dans le présent article, nous nous contenterons de faire état de quelques données

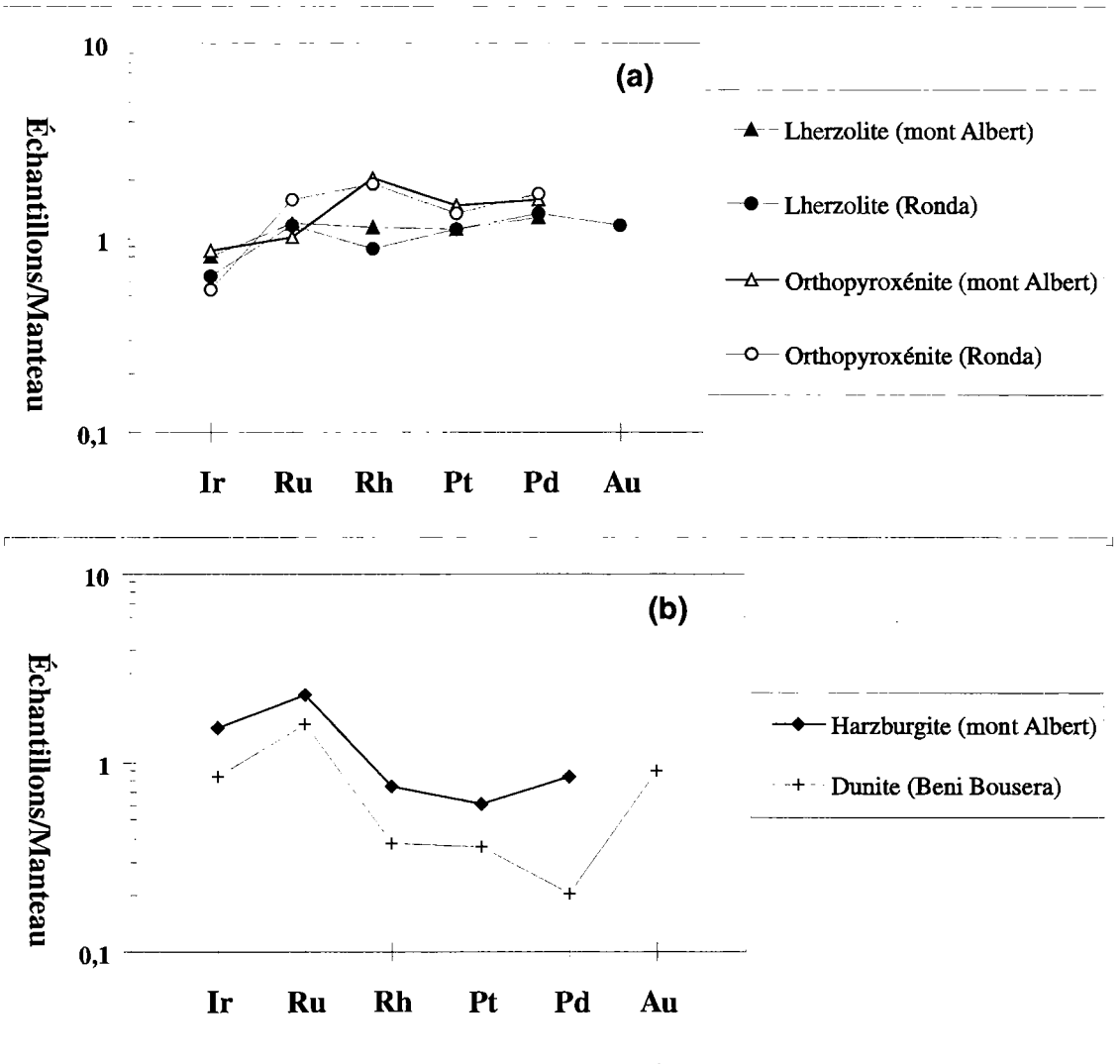

Figure 1. *Spectres des teneurs en ÉGP (et Au) normalisées aux valeurs du manteau primitif (Barnes et al., 1988) qui sont associés à quatre échantillons de péridotite et deux échantillons d'orthopyroxénite provenant de massifs ultrabasiques.*

sur des roches mantelliques (péridotites, orthopyroxénites) illustrées sous la forme de spectres des teneurs en ÉGP et en Au normalisées aux valeurs du manteau primitif (Barnes et al., 1988) (figure 1). Ces spectres montrent des fractionnements fréquemment observés dans les roches mantelliques (Gueddari, 1996); dans le cas des péridotites, par exemple, cette observation suggère que la fusion partielle a joué un rôle important dans le comportement des ÉGP (Gueddari et al., 1996). Ce processus serait à l'origine de la diminution des teneurs en Pt et Pd observée dans les péridotites appauvries (harzburgites et dunites) par rapport aux péridotites fertiles (lherzolites).

CONCLUSION

La technique d'extraction des ÉGP et de Au basée sur la coprécipitation de ces éléments en présence de Se et Te après réduction au $SnCl_2$ est une méthode quantitative fiable et précise permettant de forts taux d'extraction. L'utilisation de KI comme catalyseur améliore nettement l'extraction de Ir avec un taux avoisinant 100 %, mais semble inhiber celle de Au. Même si Ir et Au ne peuvent pas être extraits simultanément, l'extraction des autres ÉGP (Ru, Rh, Pt, Pd) peut se faire en présence ou en l'absence de KI.

Cette méthode présente l'avantage, d'une part, de travailler sur une quantité variable d'échantillon (selon le degré d'homogénéité) et, d'autre part, d'éliminer les éléments susceptibles d'interférer avec les ÉGP et Au. L'utilisation de la SM-ÉP rend la méthode plus précise et rapide, en plus d'améliorer les limites de détection. L'ensemble de ces caractéristiques permet une application en routine et rend la technique décrite ici parfaitement adaptée à des échantillons de roches de diverses compositions pétrographique et chimique, renfermant des ÉGP et Au à des teneurs variables (sulfures, chromite, roches basiques et ultrabasiques, etc.).

REMERCIEMENTS

Nous tenons à remercier J.H. Bédard de la CGC pour ses critiques et ses commentaires sur le manuscrit ainsi que M.A. Dion pour son aide technique quant à l'utilisation de la SM-ÉP. Ce travail a été réalisé grâce à une contribution financière du FCAR (volet equipe, 96-ER-2270).

RÉFÉRENCES

Amossé, J., Fischer, W., Allibert, M. et Piboule, M.
1986: Méthode de dosage d'ultra-traces de platine, palladium, rhodium et or dans les roches silicatées par spectrophotométrie d'absorption atomique électrothermique; Analysis, vol. 14, n° 1, p. 26-31.

Barnes, S.J., Boyd, R., Korneliussen, A., Nilsson, L.P., Often, M., Pedersen, R.B., and Robin, B.
1988: The use of mantle normalization and metal ratio in discriminating between the effects of partial melting, crystal fractionation and sulphide segregation on platinum-group elements, gold, nickel and copper : examples from Norway; in "Geoplatinum 87", (ed.) H.M. Prichard, P.J. Potts, J.F.W. Bowles, and S.J. Cribb; Elsevier, London, p. 113-143.

Garuti, G., Oddone, M., and Torres-Ruiz, J.
1997: Platinum-group elements distribution in subcontinental mantle : evidence from the Ivrea zone (Italy) and the Betic-Rifean range (Spain and Morocco); Canadian Journal of Earth Sciences, v. 34, p. 444-463.

Gueddari, K.
1996: Approche géochimique et physico-chimique de la différenciation des éléments du groupe du platine (PGE) et de l'or dans le manteau supérieur bético-rifain et dans les xénolites de péridotites sous-continentales; Thèse de l'Université Joseph Fourier, Univ. Grenoble I (France), 320 p.

Gueddari, K., Piboule, M., and Amossé, J.
1996: Differentiation of platinum-group elements (PGE) and of gold during partial melting of peridotites in the lherzolitic massifs of the Betico-Rifean range (Ronda and Beni Bousera); Chemical Geology, v. 134, p. 81-97.

Jackson, S.E., Fryer, B.J., Gosse, W., Healey, D.C., Longerich, H.P., and Strong, D.F.
1990: Determination of the precious metals in geological materials by inductively coupled plasma-mass spectrometry (ICP-MS) with nickel sulfide fire-assay collection and tellurium coprecipitation; Chemical Geology, v. 83, p. 119-132.

Jarvis, K.E., Gray, A.L., and Houk, R.S.
1992: Inductively coupled plasma-mass spectrometry; Handbook, Blackie, published in the USA by Chapman and Hall, New York, 380 p.

Longerich, H.P., Jenner, G.A., Fryer, B.J., and Jackson, S.E.
1990: ICP-MS analysis of geological samples: a critical evaluation based on case studies; Chemical Geology, v. 83, p. 105-118.

Meyer, A.S. and Ayres, H.G.
1955: The interaction of platinum (II) and tin (II) chlorides; Journal of American Chemical Society., v. 77, p. 2671-2675.

Parry, S.J., Sinclair, I.W., and Asif, M.
1987: Evaluation of the nickel sulphide bead method of fire-assay for the platinum-group elements using neutron activation analysis; in : "Geoplatinum 87", (ed.) H.M. Prichard, P.J. Potts, J.F.W. Bowles, and S.J. Cribb; Elsevier, London, p. 21-27.

Potts, P.J., Tindle, A.G., and Webb, P.C.
1993: Geochemical reference material compositions; Whittles Publishing, U.K., 313 p.

Shirey, S.B. and Walker, R.J.
1995: Carius tube digestion for low-blank rhenium-osmium analysis; Analytical Chemistry, v. 67, p. 2136-2141.

Evaluation of a Russian-designed borehole resistivity probe based on a capacitive principle

Q. Bristow and C.J. Mwenifumbo
Mineral Resources Division, Ottawa

Bristow, Q. and Mwenifumbo, C.J., 1998: Evaluation of a Russian-designed borehole resistivity probe based on a capacitive principle; in Current Research 1998-D; Geological Survey of Canada, p. 65-73.

Abstract: A new type of resistivity probe, based on the principle of electrical capacitance, has been designed by Russian scientist V.M. Timofeev of the All-Russia Institute of Hydrology and Engineering Geology, Moscow. A prototype version was built under a collaborative project funded jointly by the Geological Survey of Canada and IFG Corporation, a Canadian manufacturer of borehole geophysical instrumentation. The Geological Survey of Canada carried out field tests at its borehole test facilities in Ottawa and at the New Calumet massive sulphide deposit, Quebec. The capacitive resistivity data were compared to the galvanic resistivity and inductive conductivity data. Preliminary results indicate that the capacitive technique is sensitive in the resistivity range 100-10 000 Ω·m and compares well with galvanic and inductively measured resistivities. Field tests were also carried out for several transmitter-receiver spacings and in plastic-cased fluid-filled boreholes. Capacitive resistivity logs acquired in plastic-cased boreholes are almost identical to those acquired in uncased boreholes and therefore, promise to be valuable logs for use in environmental applications where boreholes drilled in unconsolidated sediments often have plastic casing.

Résumé : Un nouveau type de sonde de résistivité fondée sur le principe de la capacité électrique a été conçu par V.M. Timofeev, de l'Institut panrusse d'hydrologie et de géologie technique, à Moscou. Un prototype a été construit dans le cadre d'un projet en collaboration financé conjointement par la Commission géologique du Canada et la IFG Corporation, fabricant canadien d'instruments géophysiques de forage. La Commission a réalisé des essais de terrain à ses installations d'essai de forages à Ottawa et au gisement de sulfures massifs de Nouveau Calumet, au Québec. Les données de résistivité capacitive ont été comparées à celles de résistivité galvanique et de conductivité inductive. Les résultats préliminaires indiquent que la technique capacitive est sensible dans l'intervalle de 100-10 000 Ω·m et se compare favorablement aux résistivités mesurées par voie galvanique et inductive. Des essais de terrain ont été réalisés. Les diagraphies de résistivité capacitive obtenues dans des trous de sondage à tubage en plastique sont presque identiques à celles obtenues dans des trous de sondage sans tubage; elles promettent donc d'être utiles aux applications environnementales, pour lesquelles les trous de sondage forés en sédiments non consolidés sont souvent entourés d'un tubage en plastique.

INTRODUCTION

A key parameter in the application of borehole geophysics to mineral exploration and environmental problems is bulk resistivity. The traditional and well known technique for acquiring bulk resistivity logs involves the use of probes having galvanic electrodes to measure potentials generated by a current source. This technique was pioneered by Conrad Schlumberger (Schlumberger, 1930) and others, primarily for use in the petroleum industry. It continues to be one of the most important tools in that field. This method can only be used, however, in situations where reliable electrical contact can be established between the electrodes and the formation. It cannot be used in boreholes that have plastic or other non-conductive casing, the type most often used in holes drilled for environmental studies. The best alternative to date has been the use of probes based on the inductive technique. This principle is unfortunately subject to significant interference from strong magnetic-susceptibility signals and magnetic hysteresis effects that are generated in minerals such as magnetite, ilmenite, and pyrrhotite. The susceptibility interference can be almost entirely eliminated by meticulous care with the design and layout of the electronic circuitry. The magnetic hysteresis response, however, is electrically indistinguishable from conductivity and therefore represents a serious shortcoming of the inductive technique. A further limitation is the rapid fall-off in sensitivity with increasing resistivity. A realistic upper resistivity limit for most inductive resistivity probes currently available is about 1000 Ω·m.

The development of an alternative technique, based on detecting the effects of bulk resistivity variations using an electrical circuit involving capacitance rather than inductance or resistance, has been underway at a Moscow research institute for several years, spearheaded by V.M. Timofeev. He has already successfully demonstrated a system based on this principle for measurements of resistivity from the surface, (Timofeev et al., 1994). In 1994, V.M. Timofeev visited the Geological Survey of Canada and explained his technique in detail to the authors and others. An agreement was reached whereby he would develop and build a prototype version of a sensor suitable for borehole use, for which a suitable housing to his specifications would be built by IFG Corporation. He would return with the unit on a second visit, during which it would be tested using the Geological Survey of Canada instrumentation system at test holes at Bells Corners near Ottawa, for which suites of detailed geophysical reference logs are available.

This project culminated in the first tests of the capacitive borehole-resistivity probe in the autumn of 1995, with V.M. Timofeev present. The results of these tests showed excellent agreement with logs recorded using the standard galvanic resistivity logging technique. As a result of these tests, a contract was drawn up between IFG Corporation and V.M. Timofeev to produce a commercial probe in Canada that would be sold worldwide by IFG Corporation. A more comprehensive set of field tests were then organized, the results of which are the subject of this paper.

A COMPARISON OF THE PHYSICAL PRINCIPLES OF THE INDUCTIVE AND CAPACITIVE TECHNIQUES

There are three fundamental electrical properties that essentially govern the entire science of electricity, and these are resistance, inductance, and capacitance. These properties are, of course, available in the form of lumped components (resistors, inductors, and capacitors) for use in all manner of applications. A pure resistance has the property that the current flowing through it is proportional to the potential applied across it. There are also no time differences between the applied voltage waveform and the resulting current waveform. A pure inductance has zero resistance, but presents an impedance to a time-varying applied voltage. In the simplest case of a sinusoidal voltage, the corresponding current sinusoid lags the voltage by a quarter of a time period. This is described as a phase lag of 90°. A pure capacitance presents an infinite resistance to a non-varying applied voltage, but presents a finite impedance to a time-varying applied voltage. The corresponding current leads the applied voltage waveform by a phase angle of 90°.

The simplest implementation of a lumped inductance is a coil, and that of a lumped capacitance is a pair of parallel plates closely spaced. A sinusoidally varying current through a coil generates a magnetic field as shown in Figure 1. If this field intersects conductive material, eddy currents are generated and the 90° phase angle between applied voltage and current decreases. The detection and measurement of this decrease is the basis of all inductive conductivity probes. In

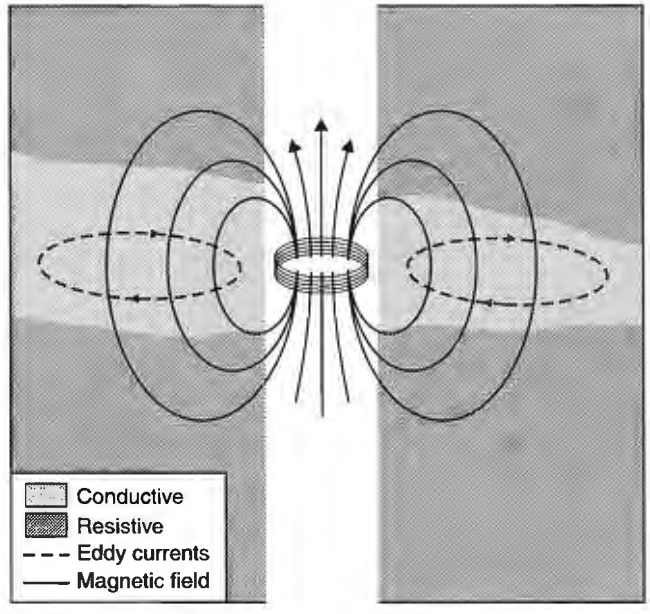

Figure 1. *The coil of an inductive resistivity probe generates a magnetic field that intersects the formation and causes eddy currents in conductive material.*

an analogous manner, a sinusoidal potential applied to the plates of a capacitor generates a corresponding sinusoidal electric field in the material between the plates. If that material is conductive, then there will be a drop in the potential across the plates of the capacitor by an amount which is a function of the bulk resistivity.

The capacitive borehole-resistivity probe exploits this effect by making the formation strata intersected by the borehole the material 'between' the plates of a capacitor in the probe. The 'plates' are constructed in the form of two coaxial metal cylinders separated by a distance sufficient to allow the electric field generated between them to permeate as large a volume of the formation as is practical. This electric field is sensed by a second capacitor constructed in the same way and coaxial with the 'transmitter' (the one generating the electric field). Changes in the potential between the coaxial plates of the transmitter capacitor due to conductive material will cause a reduction of the electric field generated throughout the effective volume of investigation. This in turn will result in a reduction of the potential between the 'receiver' capacitor plates, which is sensed as the signal and processed. The arrangement is shown in Figure 2. It is clear from this that the separation of the two capacitors will have a drastic effect on the volume of investigation. The smaller the spacing, the smaller the volume will be, and the better the resolution of thin layers will be. It will now be apparent that the same geometrical considerations apply to the design and use of this probe as apply to the two-coil inductive conductivity probe.

The property that affects the capacitance measured between two plates is the dielectric constant of the material between them in which the electric field is generated. The proprietary probe sensing circuitry is designed to reject (as much as possible) signals due to variations in the absolute capacitance caused by changes in the dielectric constant of the formation, and to respond only to the changes caused by variations in the bulk resistivity. This potential interference is analogous to the changes in magnetic susceptibility, which can cause errors in the inductive conductivity measurement technique.

PROBE CALIBRATION

The prototype probe used in all the tests presented in this paper was 45 mm in diameter and had provision for three different spacings between the transmitting and sensing capacitors: 67, 83, and 100 cm. They are referred to as 'short', 'medium', and 'long' in the discussions relating to the field data. The calibration of the probe is relatively straightforward. The probe is suspended horizontally above the ground

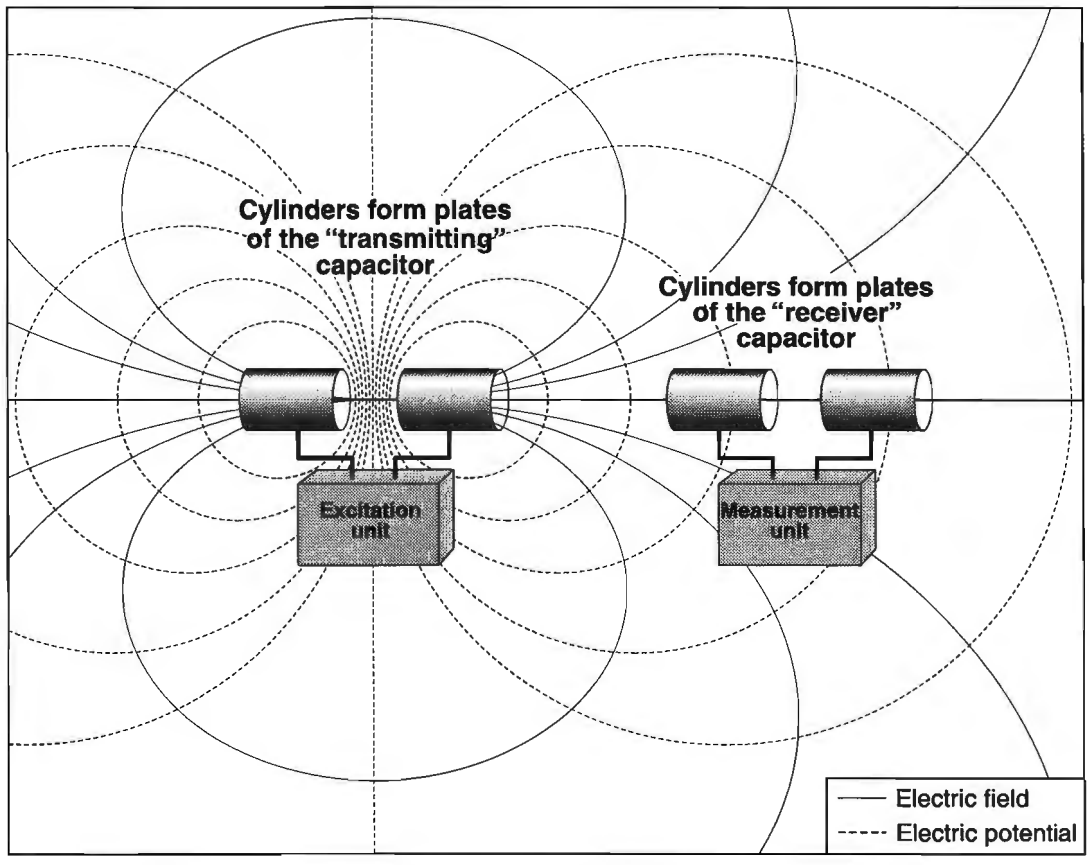

Figure 2. The capacitive probe consists of two pairs of coaxial metal cylinders. Each pair forms a capacitor. The electric field and potential lines shown generated by the 'transmitting' capacitor are drawn as if the plates were point sources of charge for clarity.

in order to register a background reading in the air. This background reading in the air constitutes a calibration value that is incorporated as a constant into a simple formula that is used to convert the instrument readings into resistivities. Experiments were made in the field to determine the height above the ground the probe must be in order to register a true background reading. The probe was suspended horizontally at heights of 20, 50, 100, and 200 cm above the ground on supports made from non-conductive material. Readings were taken with the probe on the ground and at each level. The results of these tests are presented in Figure 3 and indicate that the probe must be at least 100 cm above the ground for the short and medium transmitter-sensor separation and at least 200 cm for the long separation, in order to register a true background value. This occurs when the contribution of the electric field sensed at the receiver is essentially only in the air and not modified in any way by the ground.

RESULTS AND DISCUSSION

Field tests of the probe were made at a number of sites representing several geologic environments and resistivity ranges. These sites included a) the Bells Corners Borehole Geophysical Test site and the Lebreton test hole in Ottawa, representing the sedimentary environment in which resistivity variations are primarily a function of lithology and porosity; and b) the New Calumet massive sulphide deposit on Calumet Island, Quebec, representing a massive sulphide geologic environment within crystalline metamorphic rocks. In all cases, the galvanic measurements were made using a standard 40 cm normal electrode array, and the capacitive measurements were made with the long spacing, unless stated otherwise.

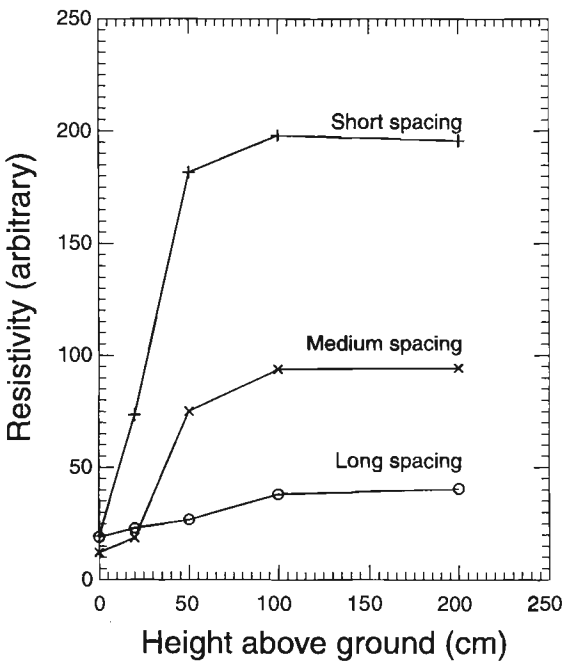

Figure 3. *Determination of background values of the capacitive resistivity probe for three transmitter-receiver spacings.*

Bells Corners borehole geophysical test site

Six vertical NQ (75 mm diameter) boreholes have been drilled by the Geological Survey of Canada to depths ranging from 120 to 300 m at Bells Corners, approximately 10 km west of Ottawa. These holes were drilled to provide facilities for testing and evaluating borehole logging instrumentation and for developing new borehole geophysical techniques. The holes penetrate up to 65 m of Palaeozoic dolomites and sandstones. This sedimentary sequence unconformably overlies Precambrian granites and gneisses. Above the Precambrian rocks occurs an altered/weathered, saprolite zone with abundant chlorite and clay minerals. Numerous fractures and minor faults have been identified within the Precambrian basement rocks. The different rock types and various degrees of fracturing and alteration that are present at the Bells Corners Test Site provide an ideal location for testing the response characteristics of electrical methods in a geologic environment without conductive sulphide minerals. Several geophysical logs have been acquired in these test holes. Figure 4 shows the logging results from the capacitive probe compared to the galvanic resistivity log. These data were acquired in hole BC81-2. There is close agreement between the galvanic and capacitive resistivity logs. Both logs clearly define the two altered/weathered zones between 65 and 77 m that are fairly conductive. The unaltered granite between these two zones exhibits fairly high resistivities. Also, the thin conductive shale unit at approximately 37 m is clearly resolved on both the galvanic and capacitive resistivity logs. Several repeat runs of the capacitive resistivity log were recorded in BC81-2 and show excellent repeatability.

Lebreton Test Hole

The Lebreton borehole, LB-01, is a vertical NQ hole located outside the Geological Survey of Canada Borehole Geophysics Laboratory in Ottawa. LB-01 represents an almost complete suite of the sedimentary stratigraphic sequence in the Ottawa area. The hole intersects shales, limestones, dolomites, sandstones, and the Precambrian basement rocks that consist of dolomites, gneisses, and granites. LB-01 is another ideal borehole for evaluating the electrical characteristics of various sedimentary rock types. Several geophysical logs, including the neutron and galvanic resistivity logs, have been acquired in LB-01. These logs are compared to the capacitive resistivity logs in terms of their response characteristics to variations in lithology and bed-boundary resolution.

Figure 5 shows the geology, galvanic resistivity, capacitive resistivity, and the neutron logs recorded in LB-01. The capacitive resistivity log compares well with the galvanic resistivity log and clearly defines the different rock types intersected. The highest resistivities are observed within the banded limestone and calc-arenites in the upper 150 m of the hole, and within the basement dolomite/gneiss rocks at the bottom of the borehole. The lowest resistivities are observed

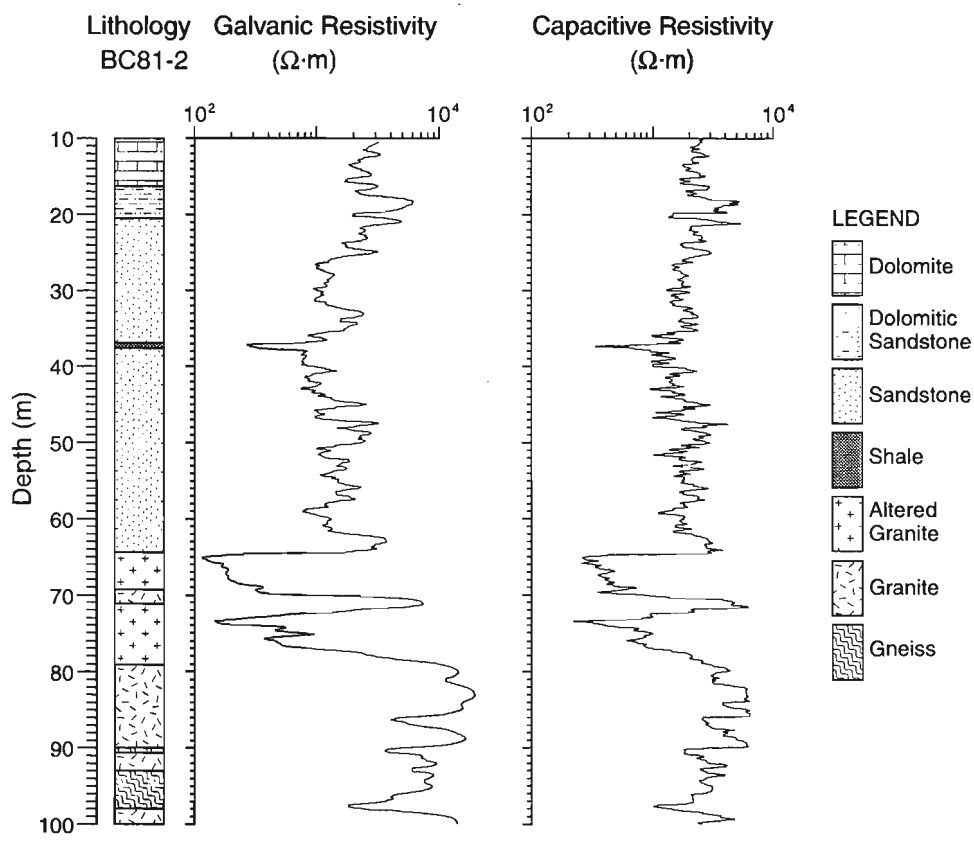

Figure 4. *Capacitive resistivity log compared to the galvanic resistivity log acquired with a 40 cm normal array at the Bells Corners Geophysical Test site in hole BC81-2.*

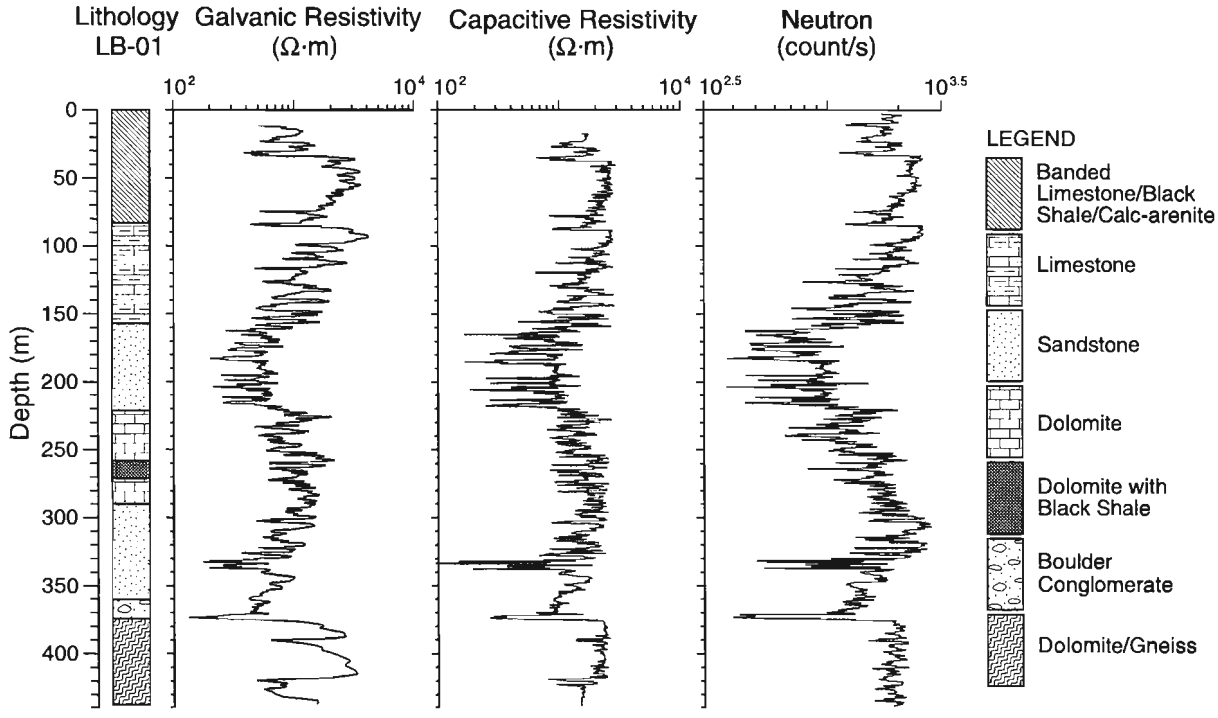

Figure 5. *Geological log, galvanic resistivity, capacitive resistivity, and the neutron logs recorded in the Lebreton hole LB-01.*

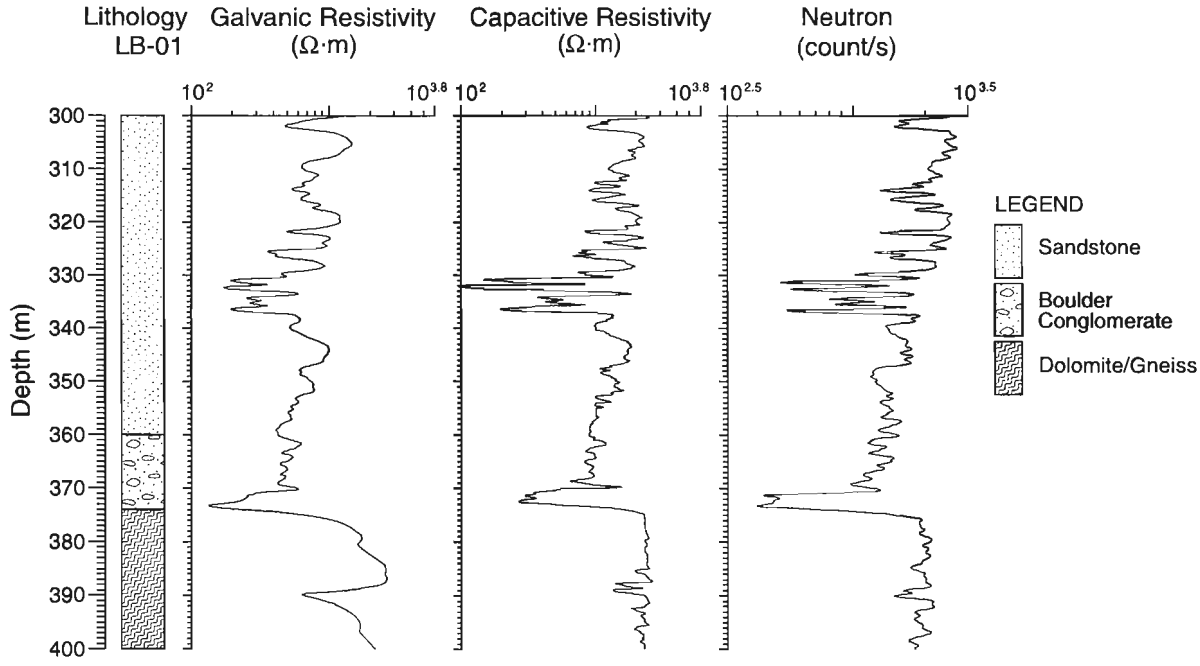

Figure 6. *An expanded section (300-400 m) of the logs presented in Figure 5, showing the detailed response characteristics and spatial resolution of the capacitive resistivity log compared to that of the galvanic resistivity and neutron logs.*

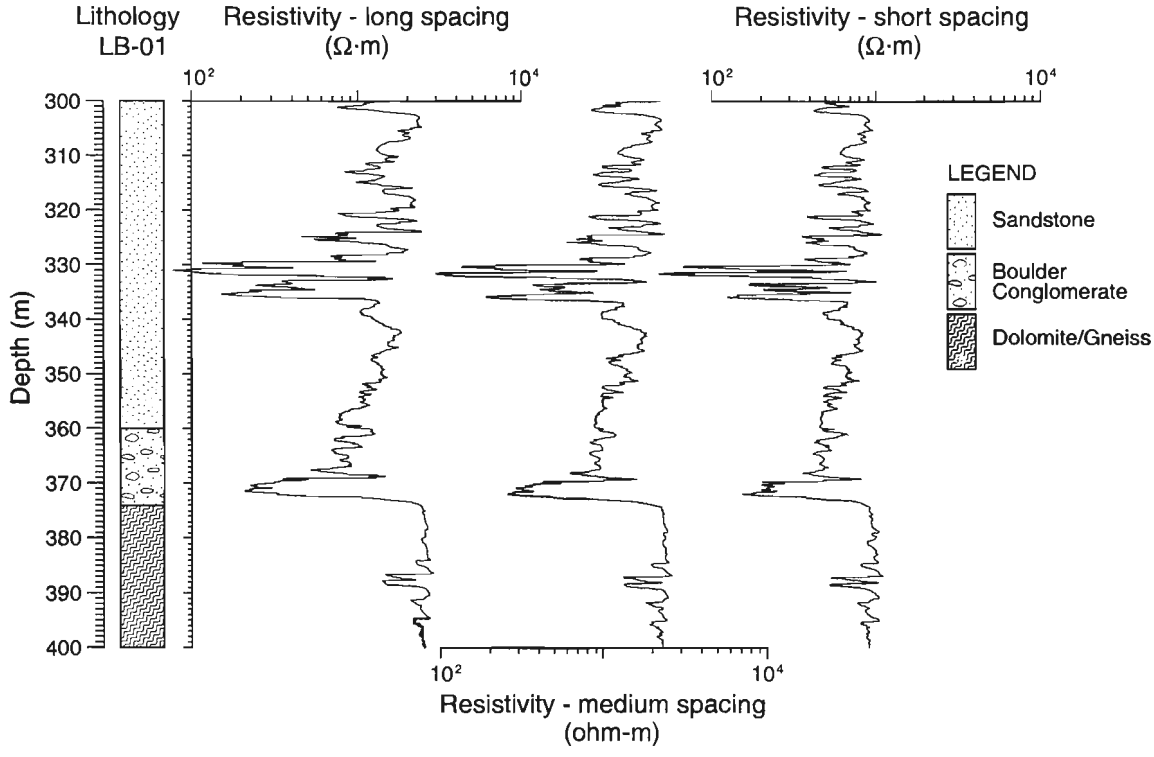

Figure 7. *An expanded section (300-400 m) of capacitive resistivity logs recorded with the short, medium, and long spacing at the Lebreton hole LB-01.*

within the sandstone between 150 and 220 m. Resistivities within the sandstone unit between 300-370 m vary, mainly because of variations in porosity. It is interesting to note that there is an excellent correlation between the capacitive resistivity and neutron porosity log. This might be expected to the extent that porosity is the major factor controlling the conductivity of the formations. A porous formation is likely to be saturated with fluid containing inorganic salts and is therefore likely to be conductive. Figure 6 is an expanded section of the logs from 300-400 m. The response characteristics and spatial resolution of the capacitive resistivity log compares well to that of the neutron log. The conductive zone at the bottom of the boulder conglomerate (370-374 m) is better resolved on the neutron and the capacitive resistivity logs than on the galvanic resistivity log.

Several tests were carried out in LB-01 to investigate differences in the log responses when the transmitter-receiver spacing was varied. Figure 7 shows an expanded section from 300-400 m of the three capacitive resistivity logs recorded with the short, medium, and long spacing. The three logs compare fairly well. Note that there is an improvement in the bed-boundary resolution with a shorter spacing (see section from 350-380 m within the sandstone, and between 370-372 m at the bottom of the Boulder conglomerates).

New Calumet Massive Sulphide Deposit

The deposit is located on Grand Calumet Island, approximately 75 km north of Hull, Quebec. There is still some exploration activity at the mine site, although the mine is currently closed. The rocks at the New Calumet deposit are predominantly high-grade metamorphic rocks consisting of hornblende and biotite gneiss, amphibolite, and marble. Mineralization consists mainly of sphalerite, galena, and pyrrhotite that occur within carbonated amphibolite and calc-silicate/marble host rock. This crystalline metamorphic rock environment is fairly resistive in the absence of conductive minerals and/or fractures that tend to increase the formation porosity and hence decrease their resistivities. There is a large dynamic range in the resistivity variations at the New Calumet deposit, from the highly conductive massive sulphides to the highly resistive metamorphic rocks. Figure 8 shows the general geology and the galvanic and capacitive resistivity logs. The two resistivity logs compare fairly well. There are a few locations where there are some differences in the response characteristics between the resistivity logs that can not be satisfactorily explained (e.g. the relatively high resistivity zone at approximately 76 m on the galvanic log is not as prominent on the capacitive log). The resistivity logs appear to be truncated within the massive sulphide zones. The lowest resistivity that can be measured with the capacitive probe is approximately 100 Ω·m whereas the galvanic resistivities can be measured to approximately 0.1 Ω·m with the present 40 cm normal-array resistivity logging system.

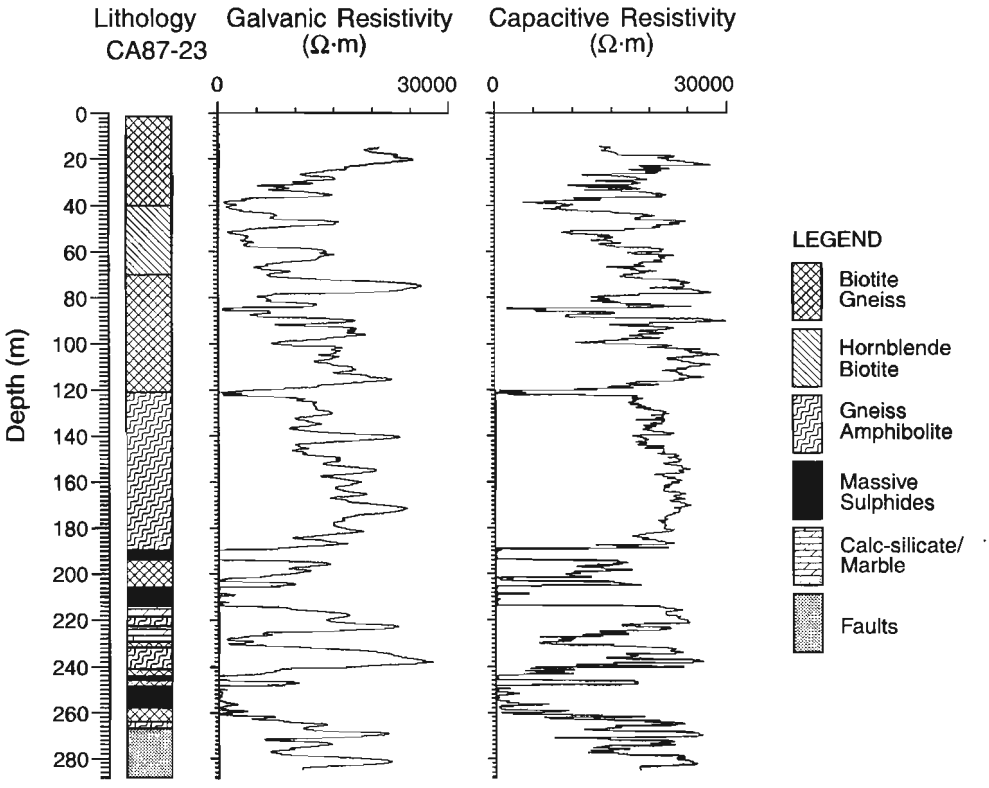

Figure 8. *Geological log, galvanic and capacitive resistivity logs recorded in hole CA87-23 at the New Calumet massive sulphide deposit, Quebec. The resistivities at this deposit vary from <0.1 Ω·m to >30 000 Ω·m.*

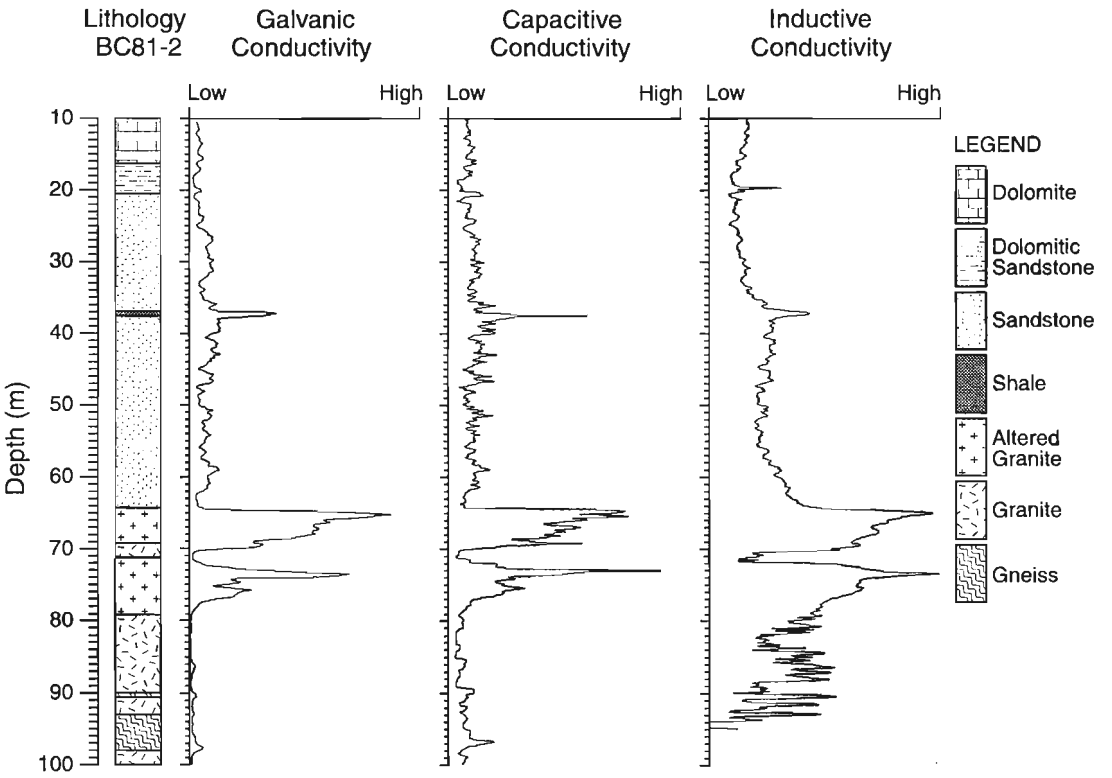

Figure 9. *Comparison between electrical logs acquired galvanically (40 cm normal-array resistivity), capacitively, and inductively (Geonics EM39) at the Bells Corners Borehole Geophysics Test Site. The reciprocal of the galvanic and capacitive resistivity logs is presented and all three logs have been normalized for ease of comparison.*

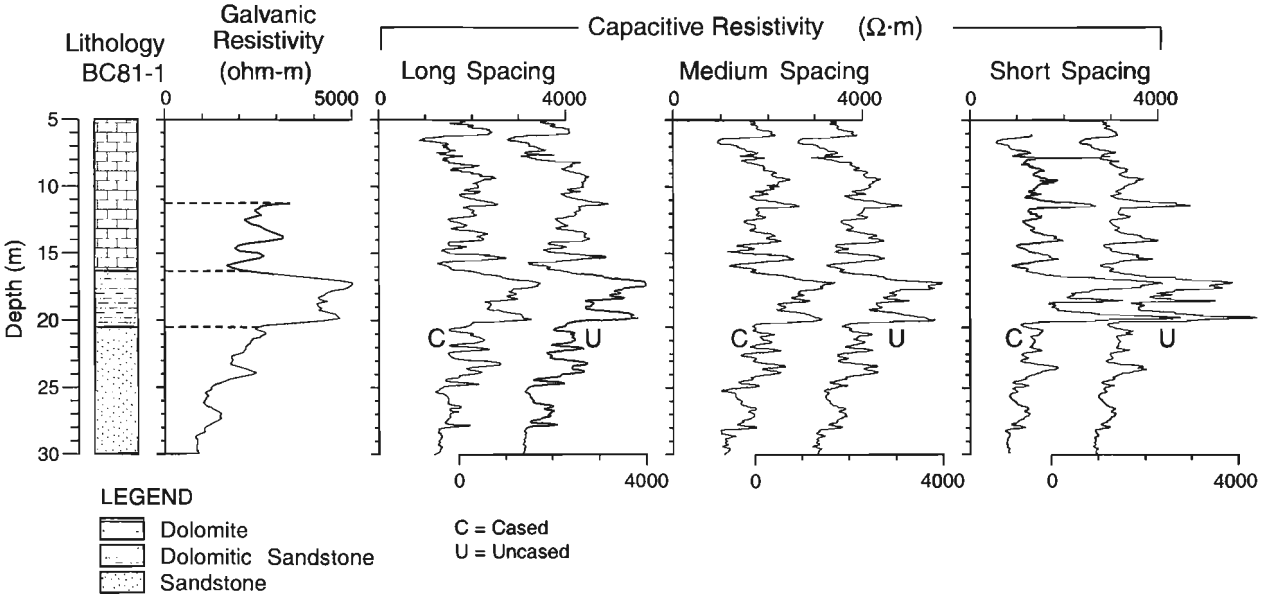

Figure 10. *Capacitive resistivity logs recorded in the upper 30 m of hole BC81-1 at the Bells Corners Test Site. The logs were acquired in a fluid-filled uncased and plastic-cased hole BC81-1 with the short, medium, and long transmitter-receiver spacings.*

COMPARISON OF GALVANIC, CAPACITIVE, AND INDUCTIVE CONDUCTIVITY PROBES

Figure 9 shows a comparison between electrical logs acquired galvanically, capacitively, and inductively at the Bells Corners Borehole Geophysics Test Site. The inductive log was acquired with the Geonics EM39 probe (Taylor et al., 1989). The reciprocal of the galvanic and capacitive resistivity is presented and all the three logs have been normalized. The maximum conductivity within the altered granite is approximately 20 mS/m (recorded with the inductive probe). All three logs clearly define the two conductive, altered, granite zones between 65 and 78 m and the conductive shale at 38 m. There are two things to note on the inductive conductivity log: 1) the high-frequency, high-amplitude conductivity variations near the bottom of the borehole (>80 m) are an artifact of the high magnetic susceptibility variations within the Precambrian granite and gneiss; 2) the conductivity starts to increase from about 55 m towards the conductive altered/weathered granite unit on the inductive log. This response is not observed on either the capacitive or the galvanic resistivity logs.

MEASUREMENTS IN AN UNCASED VERSUS A PLASTIC CASED HOLE

Figure 10 shows the galvanic and capacitive resistivity logs recorded in BC81-1 at the Bells Corners Test Site. The logs were first acquired in a fluid-filled uncased hole. Plastic casing was then installed into the borehole and the logs rerun. The logs were recorded with each of the short, medium, and long transmitter-receiver spacings and repeat runs were acquired in each case. The logs are virtually identical and compare fairly well with the galvanic resistivity data. There is an improvement in the resolution of units with a shorter spacing (see the dolomitic sandstone unit between 16 and 20.5 m).

These results indicate that the plastic casing does not affect the measured resistivities of the formation, and that the probe would therefore be suitable for use in such situations. Holes drilled for environmental studies frequently have plastic casing.

CONCLUSIONS

In all the field tests, the agreement between the galvanic and the capacitive resistivity logs was excellent. Observed differences between galvanically and capacitively acquired resistivity data are to be expected, primarily because of differences in the mode of measurement and also in the electrode geometry. Within the sedimentary environment, it is interesting to note that there is excellent correlation between the capacitive and porosity logs recorded using the neutron absorption technique. This observation suggests that porosity estimates derived from the capacitive resistivity logs would be comparable to those derived from the neutron log. More field tests are underway to evaluate the probe in air-filled, uncased, and plastic cased boreholes.

ACKNOWLEDGMENTS

The authors would like to thank V.M. Timofeev for the use of the prototype capacitive resistivity logging equipment, and J. McLatchy for providing access to holes at the New Calumet deposit. Thanks are due to J. Parker, W. Hyatt and Y. Blanchard of the Borehole Geophysics group and to two summer students, C. Slater and M. Prince, for the acquisition and processing of the field data.

REFERENCES

Schlumberger, C.
1930: Étude sur la prospection electrique du sous sol; Gauthier-Villars, Paris, France (revised edition).

Timofeev, V.M., Rogozinski, A.W., Hunter, J.A., and Douma, M.
1994: A new ground resistivity method for engineering and environmental geophysics; in Proceedings of the Symposium on the Application of Geophysics to Engineering and Environmental Problems, 1994.

Taylor, K.C., Hess, J.W., and Mazzela, A.
1989: Field evaluation of a slim-hole borehole induction tool; Groundwater Monitoring Revue, Winter Issue 1989, p. 100-104.

Geological Survey of Canada Project 880030-ZZ

Aeromagnetic Survey Program of the Geological Survey of Canada, 1997-1998

R. Dumont, F. Kiss, and J. Tod
Continental Geoscience Division, Ottawa

Dumont, R., Kiss, F., and Tod, J., 1998: Aeromagnetic Survey Program of the Geological Survey Canada, 1997-1998; in Current Research 1998-D; Geological Survey of Canada, p. 75-77.

Abstract: In 1997, four high-resolution, regional aeromagnetic surveys totalling 168 917 line kilometres were flown over Baffin Island, southern Saskatchewan, and northern British Columbia. One of these surveys was funded by private industry, the Geological Survey of Canada provided complete funding for two surveys, and one survey was cost-shared by the Geological Survey of Canada and partners. One detailed helicopter-borne electromagnetic/ magnetic/gamma-ray spectrometric survey totalling 10 632 line kilometres was flown in New Brunswick. This survey was funded by the Province of New Brunswick. The program to level the Canadian aeromagnetic profile data set, for the elimination of survey boundary effects, proceeded with drape computation and levelling of surveys flown at constant altitude in British Columbia and western Alberta. An aeromagnetic/gamma-ray spectrometric survey flown in Guinea West Africa has been supervised by the Geological Survey of Canada.

Résumé : En 1997, quatre levés aéromagnétiques régionaux à haute résolution totalisant 168 917 kilomètres linéaires ont été réalisés dans l'île de Baffin, en Saskatchewan méridionale et en Colombie-Britannique septentrionale. Un de ces levés a été financé par le secteur privée, deux autres l'ont été entièrement par la Commission géologique du Canada et le quatrième a été cofinancé par la CGC et ses partenaires. Un levé électromagnétique/magnétique/spectrométrique gamma détaillé totalisant 10 632 kilomètres linéaires a été réalisé par hélicoptère au Nouveau-Brunswick. Il a été financé par la province. Le programme de nivellement des ensembles de données sur les profils aéromagnétiques canadiens, qui vise à l'élimination des effets consécutifs à la délimitation des relevés, a permis de procéder aux calculs du drapage et au nivellement des levés réalisés à altitude constante en Colombie-Britannique et dans l'ouest de l'Alberta. Un levé aérien aéromagnétique/spectromagnétique gamma réalisé en Guinée, en Afrique occidentale, a été supervisé par la CGC.

INTRODUCTION

The 1997-1998 GSC aeromagnetic survey program included three regional aeromagnetic projects: one on Baffin Island, one in Saskatchewan, and one in British Columbia. Survey activity for 1997 is shown on Figure 1 and summarized in Table 1.

BRITISH COLUMBIA

An aeromagnetic survey totalling 33 682 line kilometres was flown in the Toodoggone River region and eastward across the Rocky Mountains and the Finlay River (Fig. 1, Table 1). The western portion is being actively explored for Au and Au-Cu, the eastern portion for sedex Zn-Pb-Ag deposits. Regional aeromagnetic data have not been previously available to the public. They will support detailed geological mapping and future mineral exploration programs. Funding was provided by the Geological Survey of Canada.

Draping (computing magnetic data to a draped surface) of the constant altitude surveys over the Rocky Mountains has been completed. Profile data have been extracted from a reference grid.

SASKATCHEWAN

Phase VII of the program to complete the regional aeromagnetic coverage of southern Saskatchewan (Fig. 1, Table 1) has been completed with the flying of a survey in the Swift Current area. The survey consisted of 44 040 line kilometres and was co-funded by the Geological Survey of Canada, Saskatchewan Energy and Mines (SEM), and one industry partner. Survey results will be useful for hydrocarbon and kimberlite exploration, as well as for detailed mapping of the sub-Phanerozoic basement. Consortium members receive one year exclusive use of the data, prior to release to the public.

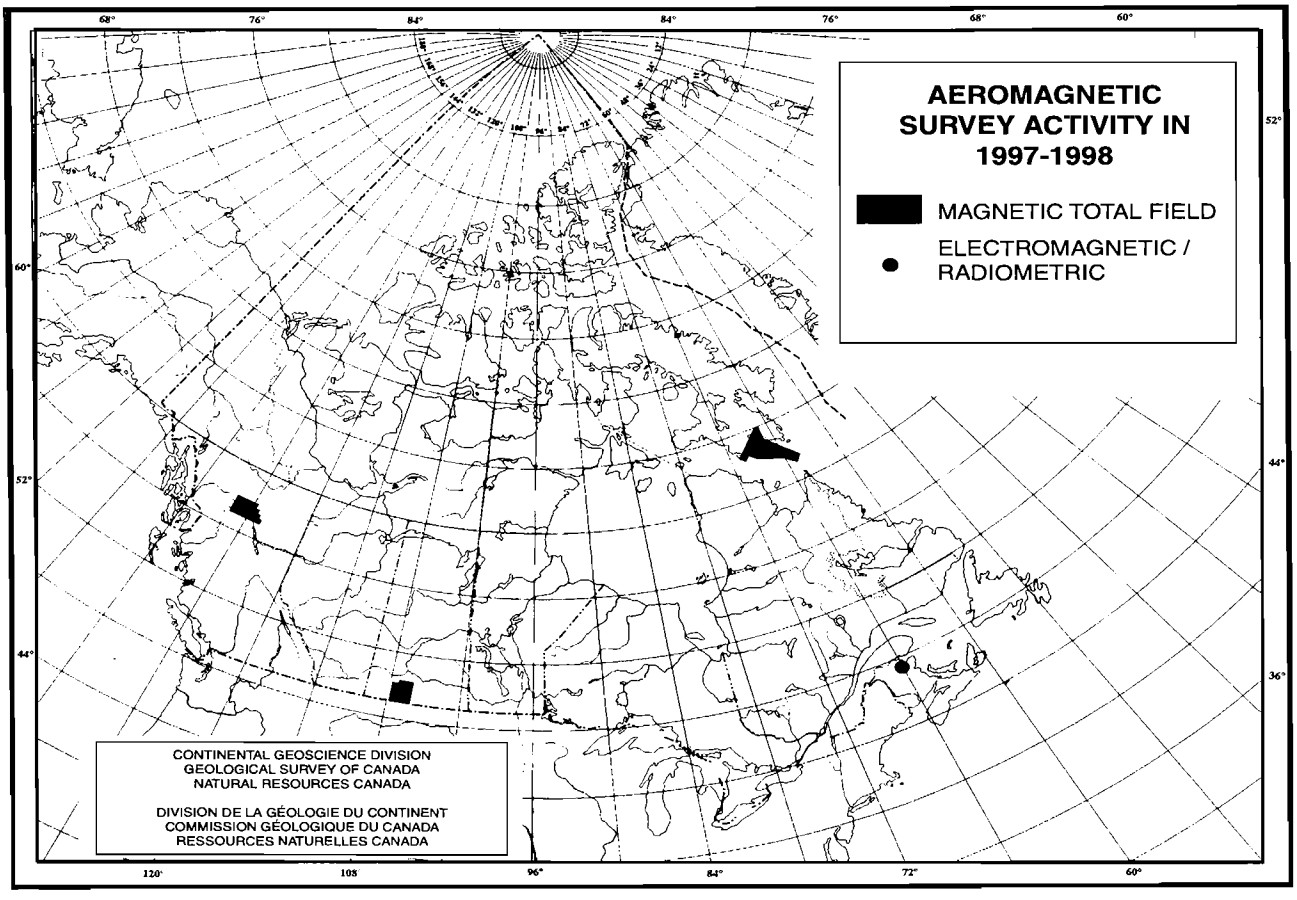

Figure 1. *Aeromagnetic survey activity in 1997-1998.*

Table 1. Aeromagnetic survey activity in 1997-1998.

Survey	Type	Line km	Line spacing	Altitude	Year of publication
Saskatchewan Phase VII (Swift Current) 1996-97	Aeromagnetic Total Field	44 040	800 m	150 m MTC	1998
Baffin Island, N.W.T. Phase II 1997	Aeromagnetic Total Field	59 951	800 m	150 m MTC	1998
British Columbia (Toodoggone) 1997	Aeromagnetic Total Field	33 682	800 m	300 m MTC	1998
New Brunswick (Restigouche) 1997	Magnetic Electromagnetic Spectrometric	10 632	200 m	60 m MTC	1998
Saskatchewan 1997	Aeromagnetic Total Field	31 244	800 m	150 m MTC	1999
Guinea 1997	Aeromagnetic Total Field Spectrometric	80 000	1000 m	120 m MTC	1998

The GSC supervised another aeromagnetic survey in southern Saskatchewan. Funding was provided by a company; the GSC will receive a copy of the digital data after a period of two years. The survey consisted of 31 244 line kilometres.

NEW BRUNSWICK

Publication of the digital data for the helicopter-borne/electromagnetic/magnetic/VLF-EM/gamma-ray spectrometric survey covering the Bathurst mining camp was completed over the last year. A new survey of the same type was initiated in the Restigouche area (Fig. 1, Table 1). It comprises 10 632 line kilometres and is being funded by the Province of New Brunswick. Survey objectives are to assist in mapping bedrock and surficial geology, locating structures and conductors, and outlying zones of hydrothermal alteration, which should lead to identification of new targets for base metal exploration. Results from this survey will be used to assess the validity of the different geophysical techniques in this environment; that assessment will determine the parameters for a larger survey.

BAFFIN ISLAND, NORTHWEST TERRITORIES

Phase II of a program to collect regional aeromagnetic data over Baffin Island continued with a survey totalling 60 000 line kilometres. (Fig. 1, Table 1). No regional public aeromagnetic coverage existed previously and the results will support the current GSC mapping initiative in the area. The private sector, engaged in base metal exploration, will have access to the data when it is released to the public in 1998. The funding was provided by the Geological Survey of Canada.

GUINEA

The GSC has supervised the field operation and compilation of an aeromagnetic/spectrometric survey totalling 80 000 line kilometres in the northeast region of Guinea in Western Africa. The World Bank is funding this project, as a means of improving the geological infrastructure of the country. Results of the survey will assist in geological mapping and future mining exploration projects.

Geological Survey of Canada Projects 910029, 920024, 930002, 940001, 960009, 960010

National Gravity Program of the Geodetic Survey of Canada, 1997-1998

D.B. Hearty[1] and R.A. Gibb[1]

Hearty, D.B. and Gibb, R.A., 1998: National Gravity Program of the Geodetic Survey of Canada, 1997-1998; in Current Research 1998-D; Geological Survey of Canada, p. 79-81.

Abstract: During the year, seven gravity surveys were planned under the National Gravity Program. Two are scheduled to commence in late October 1997 and five have been completed as follows: a reconnaissance survey of Rae Strait and Rasmussen Basin; three detailed surveys of geological targets including profiles across the Kaminak Lake greenstone belt, Churchill structural province, profiles across the Sleepy Dragon Complex and flanking Cameron River greenstone belt, Slave structural province, a road traverse near the Royal Oak's Colomac Mine, Slave structural province; and the second phase of a marine survey of the seaward extension of the Chicxulub crater, Mexico (completed in late 1996). Totals of 485 new gravity stations and 1300 line kilometres of marine gravity data were collected during these surveys. The remaining two surveys will be reported next year. The absolute gravity field program included three measurements completed in late 1996 and two measurements made in 1997.

Résumé : Au cours de l'année, sept levés gravimétriques ont été élaborés dans le cadre du Programme gravimétrique national. Deux d'entre eux devaient démarrer fin octobre 1997. Les cinq autres sont les suivants : un levé de reconnaissance du détroit de Rae et du bassin de Rasmussen; trois levés détaillés de cibles géologiques, notamment des profils à travers la ceinture de roches vertes de Kaminak Lake, dans la Province de Churchill, des profils à travers le complexe de Sleepy Dragon et la ceinture de roches vertes bordière de Cameron River, dans la Province des Esclaves, et une traverse routière près de la mine Colomac de la société Royal Oak, dans la Province des Esclaves; et enfin la seconde phase d'un levé marin du prolongement en mer du cratère de Chicxulub, au Mexique (complété fin 1996). En tout, 485 nouvelles stations gravimétriques ont été installées et 1 300 kilomètres linéaires de données gravimétriques marines ont été recueillis au cours de ces levés. Les deux derniers levés seront l'objet d'un rapport l'année prochaine. Le programme d'étude du champ gravimétrique absolu comprend trois mesures effectuées fin 1996 et deux mesures effectuées en 1997.

[1] Geodetic Survey Division, Geomatics Canada, 615 Booth Street, Ottawa, Ontario K1A 0E9

INTRODUCTION

In 1997-1998, the gravity survey component of the National Gravity Program comprised one reconnaissance survey sponsored by Geodetic Survey Division (GSD), four detailed surveys sponsored by GSC over geological targets, and two marine surveys sponsored by GSC. Two of these surveys scheduled for late in the year will be reported next year. These are (i) profiles along seven seismic reflection lines of the Western Superior LITHOPROBE transect and (ii) a multi-parameter marine survey off the west coast of Newfoundland.

RAE STRAIT AND RASMUSSEN BASIN

An on-ice gravity survey of Rae Strait and Rasmussen Basin from the western end of Simpson Strait to 94.5°W and north of 68°N latitude to the entrance of Roch Basin was completed in the period February 28 to March 10, 1997. The survey formed part of a long-term program of combined bathymetric and gravity surveys of the Canadian Arctic channels carried out in co-operation with the Canadian Hydrographic Service (CHS) and the Polar Continental Shelf Project on an annual basis. From a base camp established by CHS at Gjoa Haven, a total of 197 gravity and bathymetry observations were made at 6 km intervals on the sea-ice using a Bell 206L helicopter for transportation. Water depths were obtained using a Knudsen A350 Arctic sounder and gravity observations were made by hydrographers trained by GSD using a damped LaCoste and Romberg gravimeter. Magnavox MX300 DGPS receivers with radio links to base GPS receivers, located at Gjoa Haven and at the northern and southern extremities of the survey area, provided real-time differential positioning for all stations and eliminated the requirement for post-survey GPS processing. The data will be made available through the Canadian Gravity Database when final processing is completed in 1998.

KAMINAK LAKE GREENSTONE BELT, CHURCHILL STRUCTURAL PROVINCE

At the request of GSC's Continental Geoscience Division, a gravity survey was conducted in the vicinity of Kaminak Lake located 200 km southwest of Rankin Inlet in the Churchill structural province to investigate the deep structure of the Kaminak Lake greenstone belt. Seventy six stations were observed at intervals of 1 km on two profiles which were 36 and 40 km in length respectively, during the period August 7 to 12 using a Bell 206B helicopter for transportation. Gravity control was established at the GSC base camp with ties to Rankin Inlet and gravity traverse measurements were made using LaCoste and Romberg gravimeters. Horizontal and vertical positions were obtained from post-survey differential processing of GPS observations collected at a ten second sample rate using two TurboRogue receivers (Allan Osborne Associates, SNR- 8000). Elevations derived from altimeter measurements, made using two AIR digital barometers, were used in preliminary processing in the field to verify data quality. Final data will be made available to the user community through the Canadian Gravity Database.

SLEEPY DRAGON COMPLEX, SLAVE STRUCTURAL PROVINCE

In response to a request from GSC's Continental Geoscience Division, three gravity profiles were observed to investigate the deep structure of the Sleepy Dragon (basement) Complex and its flanking greenstone belts in the Yellowknife Domain of the Slave structural province from August 15 to 19 (for details see Bleeker et al., 1998). One hundred and fifty two stations were observed at intervals of 1 or 2 km on the three profiles, which were 65 km, 65 km, and 70 km in length, using a Hughes 500D helicopter for transportation. LaCoste and Romberg gravimeters were used for the gravity observations and TurboRogue GPS receivers in differential mode were used for horizontal and vertical positioning. A GPS base station was established 16.8 m east of GSD's Active Control Point 889201 at GSC's Seismic Observatory in Yellowknife to minimize base line lengths and provide good control for differential processing. Elevations derived from observations using two AIR digital barometers and uncorrected single point GPS positions were used for preliminary processing in the field. Final data will be made available to the user community through the Canadian Gravity Database.

ROYAL OAK'S COLOMAC MINE, SLAVE STRUCTURAL PROVINCE

At the request of GSC's Continental Geoscience Division two road traverses comprising 60 gravity stations, spaced at intervals of 500 m, were observed at the Royal Oak's Colomac mine located approximately 200 km north of Yellowknife in the Slave structural province in the period August 22 to 24. LaCoste and Romberg gravimeters were used for gravity observations and two TurboRogue GPS receivers in differential mode were used for horizontal and vertical positioning. A GPS base station was established at the Colomac mine site to minimize base line lengths and provide good control for differential processing.

CHICXULUB CRATER, MEXICO

The shallow-water phase of a gravity survey of the seaward extension of the Chicxulub crater, Yucatan Peninsula, Mexico was completed in October and November 1996 as part of a multi-parameter marine geophysical survey sponsored by the GSC's Continental Geoscience Division, Imperial College (London), the British Institutions Reflection Profiling Syndicate, the University of Texas, the Universidad Nacional Autonoma de Mexico, the National Science Foundation, the Pan American Institute of Geography and History, and the National Geographic Society. A total of 1300 line kilometres of gravity data was collected. These data were processed and

compiled along with 3809 line kilometres of data from the deep-water phase of the survey, previous marine data sets, and approximately 1100 stations observed by GSC on land during three surveys since 1994. The initial results of the geophysical interpretation of the gravity and co-located seismic results (deep-water phase) which define the seaward extension of the crater were presented at the Fall Meeting of the American Geophysical Union (Hildebrand et al., 1997).

ABSOLUTE GRAVIMETRY

Three absolute gravity stations observed in Quebec during the latter part 1996 are reported here. The stations were located at Lauzon, l'Acadie and Ste-Marthe-du-Cap along the St. Lawrence River. They form three of a series co-located with GPS stations established by the Canadian Coast Guard as an integral part of their On-The-Fly (OTF) project to aid shipping operations in the river. Two measurements were made in 1997. One measurement, part of a four station survey, was made at Pinawa in September before instrument problems curtailed the survey. A second measurement was made to establish an absolute gravity reference station in the new gravimetry laboratory in the basement of 615 Booth Street, Ottawa. After a two year period of repeat readings, the new station will replace the existing reference station in Room 8, 3 Observatory Crescent, Ottawa.

REFERENCES

Bleeker, W., Cooper, R.V., Berrigan, M.E., Roest, W., and Hendry, K.A.B.

1998: Detailed gravity profiles across the Sleepy Dragon Complex and adjacent parts of the Yellowknife Domain, Slave structural province: preliminary data; in Current Research 1998-D; Geological Survey of Canada.

Hildebrand, A.R., Pilkington, M., Halpenny, J.F., Cooper, R.V., Connors, M., Oritz-Aleman, C., Chavez, R.E., Urrutia-Fucuguachi, J., Graniel-Castro, E., Camara-Zi, A., and Buffler, R.T.

in press: Mapping Chicxulub Crater structure with gravity and seismic reflection data; Program and Abstracts, American Geophysical Union.

Ten things the textbooks don't tell you about processing and archiving airborne gamma-ray spectrometric data

John A. Grant
Mineral Resources Division, Ottawa

Grant, J.A., 1998: Ten things the textbooks don't tell you about processing and archiving airborne gamma-ray spectrometric data; in Current Research 1998-D; Geological Survey of Canada, p. 83-87.

Abstract: Techniques used for acquiring and processing (correcting) airborne gamma-ray spectrometry data are well documented. However, these publications have not addressed some of the more subjective aspects of this process, such as filtering, presentation, and archiving of the data. This paper discusses some of the often overlooked, but important issues related to the proper handling of airborne gamma-ray spectrometry data.

Résumé : Les techniques utilisées pour l'acquisition et le traitement (correction) des données dérivant des levés aéroportés de spectrométrie du rayonnement gamma ont fait l'objet de nombreuses publications. Toutefois, aucune d'entre elles ne décrit certains des aspects parmi les plus subjectifs de ce processus, notamment le filtrage, la présentation et l'archivage des données. Le présent article aborde quelques-uns de ces aspects souvent négligés mais importants relativement au traitement adéquat des données susmentionnées.

INTRODUCTION

Techniques used for acquiring and processing (correcting) airborne gamma-ray spectrometry (AGRS) data are well documented (IAEA, 1991; Grasty and Minty, 1995). However, these publications have not addressed some of the more subjective aspects of this process, such as filtering, presentation, and archiving of the data. Consequently, there are few standards in this area. On several occasions, on reviewing airborne gamma-ray spectrometry display products and digital data produced by other organizations, it has become apparent that some questionable procedures have been followed. The following discussion outlines the principles and preferred techniques followed by the Airborne Geophysics Section, Mineral Resources Division.

1. Use correct names for variables and units

The recommended short and long names and their corresponding units are listed in Table 1.

It is important to note that the term "equivalent" must be used for uranium and thorium, because these element concentrations are computed from counts collected in windows that measure radiation from ^{214}Bi and ^{208}Tl respectively, assuming that these daughter products are in radioactive equilibrium within the U and Th decay series. The term "equivalent" does not apply to the potassium window, because the recorded counts are a direct measurement of ^{40}K.

Note that the units label for eU/K and eTh/K is "X 10^{-4}", reflecting the fact that eU and eTh are both measured in parts per million and K is measured in per cent.

Occasionally, the term "background radiation" is encountered, presumably to represent some form of "exposure" or "natural air absorbed dose rate" measure of "normal" radioactivity. This is an ambiguous term. The word "background" should not be used unless it is fully qualified (i.e. "cosmic background", "aircraft background", "atmospheric background", etc.) because it can be confused with radon (it is quite reasonable to create a map of radon) or the backgrounds that are removed from the raw counts as a normal part of the data processing.

2. Noise level

All values of magnetic total field carry equal weight – there is no lower level that is treated as noise (any "noise" exists in the resolution of the measurement of the field). However, airborne gamma-ray spectrometry data has a "noise level" that is tied directly to the nature of the Poisson distribution of the counts in the statistical process being measured, in that the proportion of noise increases with decreasing count rates.

A "rainbow" spectrum of colours that might be suitable for displaying a magnetic total field or magnetic residual grid image might not be appropriate for use with airborne gamma-ray spectrometry data, particularly if low values are assigned a dominant colour. Low values of airborne gamma-ray spectrometry data should be displayed with colours that emphasize this "noise level" (i.e. grey, blue).

A variety of methods can be used to remap or convert grid data values to colours, two of which are linear and equal-area (histogram-equalized) mapping. An equal-area colour scheme is usually not appropriate for use with airborne gamma-ray spectrometry data because it gives undue emphasis to low "noise values". We prefer a linear mapping of colours within the range [0, max] where "max" is the maximum data value of about 90% of the data (i.e. excluding spurious or unusually high anomalous values).

3. Negative values are important – don't discard them

Gamma-ray spectrometry data is a measure of a statistical process characterized by a Poisson distribution (as opposed to a measurement of a potential field). Any statistical set of data will have values that lie outside the expected range of values. Although measured count rates will always be greater than or equal to zero, it is normal to see a few negative values in the computed K, eU, and eTh concentrations. Although this may not seem "reasonable", it is a perfectly valid representation of the statistical data set and is a natural reflection of the correction process that includes background subtraction and application of stripping corrections. Negative values must never be set to zero, or this information will be lost and will bias subsequent statistical analysis. The number and size of these negative values is a measure of the correctness of the calculations that have been applied to the count rates (backgrounds, stripping, and sensitivities). If a significant proportion of the data for the entire survey is negative, perhaps the calibration of the equipment is incorrect. Similar observations for a particular region of the survey or set of flight lines on a particular day might indicate anomalous radon concentrations or unsuitable conditions for collecting data.

The negative airborne gamma-ray spectrometry values must:

a) remain in the archival data set,

b) carry equal weight as positive values and be treated as legitimate values during gridding and computation of eU/eTh, eU/K, and eTh/K ratios, and

c) be drawn as negative values in stacked profile plots (see Fig. 1)

Table 1. The primary variables.

Short name	Long name	Units
K	Potassium (measures ^{40}K)	%
eU	Equivalent uranium (measures ^{214}Bi)	ppm
eTh	Equivalent thorium (measures ^{208}Tl)	ppm
Total count	Total count	μR/h
Exposure	Natural air absorbed dose rate from geological sources (13.08*K + 5.43*eU + 2.69*eTh)	nGy/h
eU/K	Equivalent uranium/potassium	X 10^{-4}
eTh/K	Equivalent thorium/potassium	X 10^{-4}
eU/eTh	Equivalent uranium/equivalent thorium	

4. The gridding algorithm should be tailored to the statistical nature of the data

Most map products require the data to be interpolated onto a regular grid. Many of the popular gridding algorithms (i.e. splining) are suitable for potential surface data (i.e. magnetic, gravity), but are not necessarily suited to airborne gamma-ray spectrometry data, because of the inherent statistical variations of the airborne gamma-ray spectrometry data. A suitable gridding algorithm is one which takes the average of all data points lying within a circular or elliptical area, weighted inversely by distance from the grid point. The data is implicitly filtered by this algorithm during the gridding process: it is not necessary to filter the data first (as is required for the splining technique).

5. Ratios must be calculated carefully

The diagnostic ratios of the three radioelements (eU/eTh, eU/K, and eTh/K) are frequently plotted as profiles. Due to statistical uncertainties in the individual radioelement measurements, some care should be taken in the calculation of these ratios to avoid dividing "noise" by "noise", resulting in very small and very large meaningless values.

Each airborne gamma-ray spectrometry reading is assumed to be a sample counted over a homogeneous half space that represents a "Poisson source". It is well known that the mean and variance of a Poisson population are equal, therefore the standard deviation is the square root of the mean value.

When computing ratios of stripped and corrected data it is necessary to ensure that both numerator and denominator are positive. In addition, some smoothing is necessary to prevent wild swings in the lowest concentration areas. The method of computing ratios is as follows:

a) In order to remove areas that could be expected to have a mean concentration of 0 in both the numerator and denominator, a test was devised to eliminate points sampled "over water". It was observed early in the development of the GSC's Skyvan system, that whenever the system passed over a "large" body of water, the measured concentration of potassium fell below 0.25%. This value is used in all ratio computations as an indication of a sample probably "over water"; all three ratio values are set to 0 if "over water".

b) Progressively sum the element concentrations of adjacent points on either side of the data point until the total accumulated concentration of both the numerator and denominator exceed a threshold or minimum value. Then calculate the ratio by dividing the accumulated sums. This imparts a measure of smoothing to the computed ratio, as well as ensuring that the two values are statistically significant.

After some examination of profiles of airborne gamma-ray spectrometry data obtained with the first Skyvan acquisition system, it was observed that areas that had concentrations less than 1% K, 1 ppm eU, and 4 ppm eTh had ratio profiles that varied wildly. A running average was applied to the numerator and denominator in an attempt to smooth each variable before computing the ratio, however this technique was rejected because it resulted in rather nondescript-looking ratio profiles. A better sort of "adaptive filtering" was required that would have the most effect on the low concentration areas while leaving the responses in higher concentration areas relatively unchanged. A somewhat heuristic decision was made that a ±10% error (66% of the time) in each of the numerator and denominator would be acceptable for computation of the ratios and would result in an error of ±20% (66% of the time) in the computed ratio. The 10% error is equivalent to 100 counts. For the first Skyvan acquisition system (sensitivities: 50 cps/% K, 9 cps/ppm eU, and 7 cps/ppm eTh), 100 cps is equivalent to 2% K, 10 ppm eU, and 15 ppm eTh, so those are the minimum threshold values required for the numerator and denominator from which the ratio is computed. This requirement ensures that the error associated with the calculated ratios is similar for all data points.

Grid ratios

The gridded eU/eTh, eU/K, and eTh/K ratios are not created by gridding the ratios computed from the line data. Instead, the eU, eTh, and K variables are gridded and the grid ratios are computed by dividing the grids of the individual variables. The numerator and denominator are accumulated by summing the values of each ring of cells that surround the grid cell for which the ratio is being computed. It is normal to insist on greater "smoothness" for grid images than is acceptable in profiles. Thus a similar heuristic decision was made for gridding the airborne gamma-ray spectrometry variables: the equivalent of at least 500 counts (5% error) needs to be accumulated in both numerator and denominator before dividing to obtain the ratio. This results in an error in the computed ratio of ±10% (66% of the time).

The threshold values used depend on the sensitivity of the acquisition system: for the Skyvan system, a 500 cps minimum value is equivalent to summed values of 10% K, 55 ppm eU, and 71 ppm eTh, so those are the minimum threshold values required for the numerator and denominator.

6. Decorrugation, microlevelling

A variety of techniques have been developed to try to remove streaks or lineations in grid images along flight lines (i.e. decorrugation, microlevelling). The "noise" in airborne gamma-ray spectrometry data is usually caused by fluctuating background values (changing weather, terrain, ground moisture content, radon pockets, etc.) between adjacent flight lines. These techniques are suitable for geophysical data types that are a measure of a single variable (i.e. magnetic data), but care must be taken when they are used with airborne gamma-ray spectrometry data.

The line data is the primary data set and the grids are just one of several views of that data. If techniques are applied to the grids to improve their appearance, there must be a corresponding mechanism to direct those corrections back to the set of line data from which the grid images were created. It

must always be possible to create a grid image from the primary archival line data set, simply by routinely gridding the archival line data. There is little value in creating a polished, smoothed "airbrushed" grid image if it can never be reproduced (i.e. with a different projection or cell size) without applying the (possibly iterative and subjective) process again.

Complicating matters is the cross-coupling that exists between the count rates of the K, eU, and eTh variables: in particular the ^{40}K potassium window includes significant scattered counts from uranium and thorium decay series. This coupling is removed by applying the stripping ratio corrections after the backgrounds have been subtracted. The decorrugation corrections that are applied to a single airborne gamma-ray spectrometry grid are in effect modifying the background values of that variable in order to level the data. But for airborne gamma-ray spectrometry line data, a change in the background count rate for one variable can result in changes in the computed concentrations of all three variables, the degree of which depends on the sensitivities. This interdependence makes it difficult to correct any of the K, eU, or eTh grid images individually without applying related corrections to the other two grid images.

7. Line data is the primary archival data set, not grid data

The primary archival data set is the line (point) data, to which the following processing has been applied:

- subtraction of backgrounds
- stripping corrections
- attenuation correction (for variations from survey flying height)
- conversion of counts to equivalent ground concentration using sensitivities

It is particularly important to note that the archival data set is never filtered, however it may be filtered on the fly for presentation purposes (stacked profiles) or implicitly by a gridding algorithm.

Grids are considered secondary and are merely one of several possible "views" of the archival set of data. We do not archive grids – they are generated on demand from the archival line data to suit the requirements of individual clients, i.e. region, projection, and cell size.

8. Never archive filtered data

Airborne gamma-ray spectrometry data represents a measure of a statistical process and is completely different from magnetic or gravity data that represents a relatively smooth potential surface. By its very nature, statistical data is not "smooth", therefore smoothing techniques that might be applied to potential field data should not necessarily be applied to airborne gamma-ray spectrometry data. That which is considered "noise" in potential field data is treated as "information" in airborne gamma-ray spectrometry data. Smoothing airborne gamma-ray spectrometry data reduces the resolution of the data and effectively discards potentially useful information. The stacked profile section shown in Figure 1 contrasts the normal "noisy" character of airborne gamma-ray spectrometry data (potassium, 1 sample/s) with the relatively smooth nature of magnetic total field data (5 sample/s).

Once a filter has been applied to a set of data, the effect can never be removed. Therefore, the primary archival line data set must consist only of unfiltered K, eU, eTh components. The filtering that is applied implicitly during the computation of the eU/K, eU/eTh, eTh/K ratios, is acceptable for the archival data set.

Filtering should be a dynamic process that is applied and removed subjectively to the data during interpretation or presentation (i.e. viewing or printing stacked profiles). But routine filtering to make the final archival digital data set "look nice" can destroy a significant part of the signal contained in the data, leaving it less useful for interpretation. Furthermore, subsequent gridding of this filtered line data results in a dual application of filters, because interpolation is essentially a low-pass filtering operation in itself. Filtering may be applied during the gridding process, either explicitly (if splining) or implicitly (inverse distance-weighted averaging), but any line data that is prefiltered for gridding should be treated as temporary data that exists only for that purpose and it should be discarded when the gridding process is complete.

9. Ternary radioelement map

The primary archival data set is considered to be the line data for the primary variables (K, eU, eTh), from which other variables (eU/K, eTh/K, eU/eTh, exposure) are derived. The primary grid products are considered to be individual images (maps) of the primary variables (K, eU, eTh) plus a ternary radioelement map.

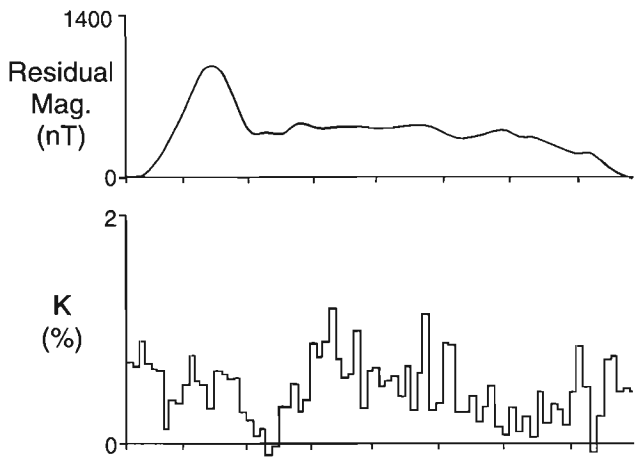

Figure 1. *Comparison of 'point-to-point' plotting method for non-airborne gamma-ray spectrometry data (5 sample/s) with the preferred "step" or "histogram" method for airborne gamma-ray spectrometry data (1 sample/s).*

The ternary radioelement map can not be created simply by assigning each of the K, eU, and eTh variables to a colour (i.e. red, green, blue or cyan, magenta, yellow). The values must be normalized to account for the natural relative abundance of potassium, uranium, and thorium. To ensure that the resultant map is not dark and muddy, a special equalization process is applied to limit the saturation of the colours (Broome et al., 1987). Furthermore, it has been found that, although the (red, green, blue) colour model might be appropriate for video display, it creates a relatively 'dark' image when printed. The Airborne Geophysics Section uses the CMY (cyan, magenta, yellow) colour model (for eU, K, and eTh respectively) for the printed map because the information is more visible.

The Airborne Geophysics Section creates a special 8-bit image file (TER.BIL –Ternary Band-Interleaved by Line), following the procedure described above. It can be displayed directly by ESRI ArcView and by SurView (Grant, 1992) and appears as a CMY image. Note that the file contains the RGB equivalents of the CMY values because ArcView uses only the RGB colour model.

10. Stacked profile presentation

Magnetic field, VLF, and EM data is acquired by taking an instantaneous measurement of each variable at each sample interval (typical sampling rates are 1, 2, 5, or 10 samples per second), therefore it is appropriate to plot the stacked profile trace as a simple point-to-point line. However, airborne gamma-ray spectrometry data is acquired by accumulating a sum of counts during the sample interval (typically 1 second). Therefore, it is recommended that the airborne gamma-ray spectrometry data be plotted using a "step" or "histogram" method, where each data value is represented by a horizontal line for the duration of the sample interval (see Fig. 1). This not only graphically illustrates the counting interval (in a spatial sense), it also portrays the statistical fluctuations in the data (even if a minimal presentation filter is applied).

ACKNOWLEDGMENT

I would like to thank John Carson for his valuable comments in the discussion of these issues.

REFERENCES

Broome, J., Carson, J.M., Grant, J.A. and Ford, K.L.
1987: A modified ternary radioelement mapping technique and its application to the south coast of Newfoundland; Geological Survey of Canada, Paper 87-14.

IAEA (International Atomic Energy Agency)
1991: Airborne Gamma Ray Spectrometer Surveying; IAEA Technical Report 323, International Atomic Energy Agency, Vienna.

Grant, J.A.
1992: SurView – A Microsoft Windows 3.x application to view geophysical survey data; Geological Survey of Canada, Open File 2661.

Grasty, R.L and Minty, B.R.S.
1995: A guide to the technical specifications for airborne gamma-ray surveys; Australian Geological Survey Organisation (AGSO) Record 1995/60.

Geological Survey of Canada Project 880029-ZZ

AUTHOR INDEX

NOTE TO CONTRIBUTORS

Submissions to the Discussion section of Current Research are welcome from both the staff of the Geological Survey of Canada and from the public. Discussions are limited to 6 double-spaced typewritten pages (about 1500 words) and are subject to review by the Chief Scientific Editor. Discussions are restricted to the scientific content of Geological Survey reports. General discussions concerning sector or government policy will not be accepted. All manuscripts must be computer word-processed on an IBM compatible system and must be submitted with a diskette using WordPerfect. Illustrations will be accepted only if, in the opinion of the editor, they are considered essential. In any case no redrafting will be undertaken and reproducible copy must accompany the original submissions. Discussion is limited to recent reports (not more than 2 years old) and may be in either English or French. Every effort is made to include both Discussion and Reply in the same issue. Current Research is published in January and July. Submissions should be sent to the Chief Scientific Editor, Geological Survey of Canada, 601 Booth Street, Ottawa K1A 0E8 Canada.

AVIS AUX AUTEURS D'ARTICLES

Nous encourageons tant le personnel de la Commission géologique que le grand public à nous faire parvenir des articles destinés à la section discussion de la publication Recherches en cours. Le texte doit comprendre au plus six pages dactylographiées à double interligne (environ 1500 mots), texte qui peut faire l'objet d'un réexamen par le rédacteur scientifique en chef. Les discussions doivent se limiter au contenu scientifique des rapports de la Commission géologique. Les discussions générales sur le Secteur ou les politiques gouvernementales ne seront pas acceptées. Le texte doit être soumis à un traitement de texte informatisé par un système IBM compatible et enregistré sur disquette WordPerfect. Les illustrations ne seront acceptées que dans la mesure où, selon l'opinion du rédacteur, elles seront considérées comme essentielles. Aucune retouche ne sera faite au texte et dans tous les cas, une copie qui puisse être reproduite doit accompagner le texte original. Les discussions en français ou en anglais doivent se limiter aux rapports récents (au plus de 2 ans). On s'efforcera de faire coïncider les articles destinés aux rubriques discussions et réponses dans le même numéro. La publication Recherches en cours paraît en janvier et en juillet. Les articles doivent être envoyés au rédacteur en chef scientifique, Commission géologique du Canada, 601, rue Booth, Ottawa K1A 0E8 Canada.

Geological Survey of Canada Current Research, is released twice a year, in January and July. The four parts published in January 1998 (Current Research 1998-A to D) are listed below.

Recherches en cours, une publication de la Commission géologique du Canada, est publiée deux fois par année, en janvier et en juillet. Les quatre parties publiées en janvier 1998 (Recherches en cours 1998-A à D) sont énumérées ci-dessous.

Part A:	Cordillera and Pacific Margin
Partie A :	Cordillère et marge du Pacifique
Part B:	Interior Plains and Arctic Canada
Partie B :	Plaines intérieures et région arctique du Canada
Part C:	Canadian Shield
Partie C :	Bouclier canadien
Part D:	Eastern Canada and national and general programs
Partie D :	Est du Canada et programmes nationaux et généraux